# New strategy for mechanistic studies of Chemical Vapor Deposition processes under UHV conditions

Dissertation
zur Erlangung des Doktorgrades
der Naturwissenschaften
- Dr. rer. nat. -

vorgelegt dem Promotionsausschuss
des Fachbereichs 2 (Biologie/Chemie)
der Universität Bremen

von
**Theodor Weiss**

Bremen 2015

Die hier vorliegende Arbeit wurde im Zeitraum zwischen April 2011 und November 2015 am Institut für Angewandte und Physikalische Chemie (IAPC) der Universität Bremen in der Arbeitsgruppe von Prof. Dr. Marcus Bäumer durchgeführt.

**Erstgutachter:** Prof. Dr. Marcus Bäumer (Universität Bremen)
**Zweitgutachter:** Prof. Dr. Katharina Kohse-Höinghaus (Universität Bielefeld)

**Disputation:** 15. Januar 2016

**Selbstständigkeitserklärung**

Hiermit erkläre ich, Theodor Weiss, dass ich die vorliegende Arbeit selbständig angefertigt und keine außer den angegebenen Hilfsmitteln verwendet habe. Diese Arbeit wurde nicht vorher an anderer Stelle eingereicht.

Bremen, den 13. November 2015

Th. Weiss

(Theodor Weiss)

**Einen herzlichen Dank möchte ich richten an...**

***Prof. Dr. Marcus Bäumer*** für deine gute Betreung und konstruktiven Fachgespräche. Deine Unterstützung und Anleitung in all den Jahren meiner Doktorandenzeit am IAPC war sehr hilfreich und vor allem lehrreich.

***Priv.-Doz. Dr. Volkmar Zielasek*** für die vielen Fachgespräche und dafür, dass du immer als Ansprechpartner da warst. Darüber hinaus danke ich dir für deine gründliche und engagierte Durchsicht und Korrektur aller Manuskripte.

***Prof. Dr. Katharina Kohse-Höinghaus*** für der Bereitstellung eines Laborplatzes und die Einführung in die CVD Welt. Darüber hinaus bedanke ich mich für die Bereitschaft diese Arbeit als Zweitgutachter zu lesen und zu beurteilen.

***Dr. Andreas Schaefer*** für die Unterstützung bei den Experimenten in UHV Labor und die geduldige Beantwortung vieler lästiger Fragen.

***Jin-Hao Jhang*** für das gute Büroklima und die grosse Hilfsbereitschaft wärend meiner gesamten Arbeit am IAPC.

***Dr. Lyudmila Moskaleva*** für den hilfreichen Erfahrungsaustausch und viele fundierte Fachdiskussionen.

***Dr. Jonas Warneke*** für den Ideenaustauch und nützliche Ratschläge in Organischen Chemie.

***Udo Mundloch*** für die herzliche Gastfreundlichkeit und die Hilfe mit den CVD Experimenten.

***Dr. Patrick Tchoua Ngamou*** für die nützliche Diskussionen über die Beschichtungsverfahren.

***Martin Nowak und Bogdan Tuschik*** für die technische Unterstützung, durch die das Projekt schnell zum Erfolg gebracht wurde.

***Petra Witte*** aus der AG Willems für die Messungen am Rasterelektronenmikroskop.

Alle übrigen Mitglieder der *AG Bäumer:* ***Simona Keil, Miriam Schubert, Imke Schrader, Anastasia Lackmann, Ingo Bardenhagen, Eva Morsbach, Andre Wichmann, Darius Arndt, Lena Altmann, Willian G. Menezes, Melanie Minnermann, Björn Neumann, Dr. Sebastian Kunz, Dr. Arne Wittstock, Jun-Jie Shi, Sarah Röhe, Ute Melville, Vera Suling, Brigitte Neimeier, Cornelia Rybarsch-Steinke*** und ***Dr. Günter Schnurpfeil*** für das angenehme Arbeitsumfeld.

**This cumulative doctoral thesis is based on the following publications (chronological order) focusing on investigation under UHV condition of metal thin films obtained via novel PSE-CVD technique. My work includes the apparatus construction, experiments performing, characterization and data analysis.**

I **Th. Weiss**, M. Nowak, U. Mundloch, V. Zielasek, K. Kohse-Höinghaus, M. Bäumer
*Design of a compact ultrahigh vacuum-compatible setup for the analysis of chemical vapor deposition processes*
Rev. Sci. Instrum., **2014**, 85(10), 104104, doi: 10.1063/1.4897620

II P. H. T. Ngamoua, A.E. Kasmi, **Th. Weiss**, H. Vieker, A. Beyer, A. Gölzhäuser, V. Zielasek, K. Kohse-Höinghaus, M. Bäumer
*Investigation of the growth behaviour of cobalt thin films from chemical vapour deposition, using directly coupled X-ray photoelectron spectroscopy*
Z. Phys. Chem., **2015**, 1-19, doi: 10.1515/zpch-2015-0602

III **Th. Weiss**, V. Zielasek, M. Bäumer
*Influence of Water on Chemical Vapor Deposition of Ni and Co thin films from ethanol solutions of acetylacetonate precursors*
Sci. Rep., **2015**, 5, 18194, doi: 10.1038/srep18194

IV **Th. Weiss**, J. Warneke, V. Zielasek, P. Swiderek, M. Bäumer
*XPS study of thermal and electron-induced decomposition of Ni and Co acetylacetonate thin films for metal deposition*
Surface Science, **2015** (submitted)

**In addition to my own PhD project, I was involved in additional research activities at the University of Bremen focusing on the theoretical investigation of Oxygen behavior in contact with Gold-Silver alloy.**

V L. V. Moskaleva, **Th. Weiss**, Th. Klüner, M. Bäumer
*Chemisorbed Oxygen on the Au(321) Surface Alloyed with Silver: A First-Principles Investigation*
J. Phys. Chem. C, **2015**, 119 (17), pp 9215–9226 DOI: 10.1021/jp511884k

## Conference contributions

**F. Strigunov (Th. Weiss)**, V. Zielasek, M. Bäumer
*Pulsed spray evaporation CVD of metal thin films: Role of reactor and precursor conditions*
Deutsche Physikalische Gesellschaft, 2013, Regensburg, Deutschland

**F. Strigunov (Th. Weiss)**, V. Zielasek, M. Bäumer
*UHV-compatible setup for alcohol-assisted chemical vapor deposition of metals*
Deutsche Physikalische Gesellschaft, 2012, Berlin, Deutschland

**Statement regarding my contribution to the publications:**

All stated publications are based on the collaboration of several researchers. My specific contributions are described in the following:

I I was responsible for the design, development, and construction of the UHV compatible PSE-CVD reactor. Furthermore, I was in charge of the samples preparation and their characterization (except for SEM measurements which were performed by Petra Witte at the Geosciences Department of the University of Bremen) and was responsible for the preparation of the figures and manuscript.

II I prepared and characterized the samples (except SEM measurements, were performed by Petra Witte at the Geosciences Department of the University of Bremen) and was responsible for the data analysis, figures preparation, and writing the manuscript text.

III I partly prepared and characterized the samples (another part of the data was collected at the University of Bielefeld under the supervision of Prof. Dr. Katharina Kohse-Höinghaus) and contributed to the discussion of the data as well as to the writing the part of the manuscript and approving the final text.

IV I performed all experiments and data analysis, prepared all figures and was responsible for the writing of the manuscript.

V I was involved in the discussion of the data and their presentation, especially in the preparation of the figures. I also read and approved the final manuscript.

## Zusammenfasung

Diese Arbeit widmet sich neuen Strategien für mechanistische Studien zu Prozessen der Chemischen Gasphasenabscheidung (CVD) unter Ultrahochvakuum (UHV). Das Ziel der vorliegenden Dissertation ist das mechanistische Verständnis der Wachstumsbedingungen von Metallfilmen, die mit der Technik der gepulsten Sprühverdampfung bei der Chemischen Gasphasenabscheidung (PSE-CVD) synthetisiert wurden. Die Metalle Nickel und Kobalt wurden als Beispiel ausgewählt, um die Verbindung zwischen den makroskopischen Abscheidungsbedingungen und den mikroskopischen Prozessen unter Einbeziehung eines Precursors, der Oberflächeneigenschaften und dem Wachstum eines dünnen Filmes aufzuzeigen.

Um die makroskopischen und mikroskopischen Ansätze zu kombinieren, wurde eine neue Anlage konzipiert und konstruiert. Dabei wurden die Material- und Abscheidungseigenschaften unter Wachstumsbedingungen berücksichtigt. Ein neuer, kompakter und modularer Beschichtungsreaktor wurde erfolgreich gebaut, der es insbesondere erlaubt, die Oberflächendiagnose quasi *in situ*, also während des laufenden PSE-CVD, durchzuführen. Neben Kompaktheit, Schnelligkeit und Einfachheit erlaubt die Anlage außerdem einen sauberen Probentransfer zwischen dem Reaktor und UHV, der eines der wichtigsten Ziele war. Der Reaktor mit einem Transfermechanismus wurde direkt an eine UHV-Kammer angebracht, sodass eine zuverlässige und systematische Untersuchung in jeder Phase des Filmwachstums möglich ist. Dies erlaubt eine detaillierte Charakterisierung der einflussnehmenden Parameter bei der PSE-CVD durchzuführen.

Die vorliegende Arbeit behandelt wichtige Eigenschaften des Wachstumsprozesses einschließlich des Einflusses verschiedener Parameter auf die CVD Wachstumskinetik, solche wie die Beschaffenheit des Metallzentrums, die Temperaturempfindlichkeit der Kohlenstoffverunreinigungen, die Funktion von Ethanol, sowohl als Lösungsmittel als auch als Katalysator, den Einfluss von Nickel als Keimschicht für verschiedene Kombinationen von Rahmenbedingungen und die Rolle des Wassers aus der Ethanol-Lösung während des PSE-CVD von Ni und Co-Dünnschichten. Ferner wird eine detaillierte Untersuchung der Mechanismen bei der PSE-CVD mit Acetylacetonat-Precursoren in Ethanol vorgestellt, sowie ein Vergleich von thermischer und elektronenstrahlinduzierter Zersetzung von lösemittelfreien Schichten vom intaktem Ni(acac)$_2$ und Co(acac)$_2$.

# Table of Contents

## Abbreviations

ALD - atomic layer deposition
CVD - chemical vapor deposition
PECVD - plasma-enhanced chemical vapor deposition
PSE - pulsed spray evaporation
EBID - electron beam-induced deposition
MO - metal-organic (precursor)
OM - organometallic (precursor)
UHV - ultrahigh vacuum
XPS - X-ray photoelectron spectroscopy
SEM - scanning electron microscope
LEED - low energy electron diffraction
acac - acetylacetone

## 1. Introduction

Thin metal and metal-oxide films are multifunctional key for technological progress in many areas, including catalysis, optics and microelectronics. To date, especially vacuum-based techniques are widely used for producing active materials for catalysis and sensors, protective and decorative coatings, optical and magnetic elements, or electrical conductors in microelectronic devices [1-4]. Besides physical thin film deposition techniques such as, for example, evaporation or sputter deposition, the chemical vapor deposition (CVD) can be used to produce monoliths, fibers, foams, and powders of pure metals or alloys with free variation of the composition, excellent reproducibility, and conformal coverage of three-dimensional structures [2,3,5]. Currently, a variety of the CVD techniques are consistently used in industry, because they fit production requirements in terms of demonstrated reliability and ease of use [4]. Generally, in the CVD processes a solid film is deposited from the gas phase of precursor molecules by chemical reactions taking place on or in the neighborhood of a substrate surface, which is usually preheated to thermally initiate the reaction. Therefore in industry most often employed are thermal CVD where deposition is activated by heating, plasma-enhanced CVD (PECVD) with plasma-initiated reaction, and, as CVD-derivative, atomic layer deposition (ALD) which produces films in sequential, self-limiting layer-by-layer manner, using various reaction activation methods.

The deposition process development is not standing still and new deposition techniques with innovative approaches are proposed regularly. For instance a recently developed hydrogen-free approach to thin film CVD is based on pulsed spray evaporation delivery (PSE-CVD) of commercially available metal-organic (MO) precursors, in particular metal β-diketonates such as acetylacetonates [6-9]. It is a low vacuum deposition technique that uses alcohols as both, solvent and reducing agent, and permits deposition of metal films without employing gaseous hydrogen for precursor reduction. Compared to standard gas phase CVD, PSE-CVD poses less demand on the precursor in terms of volatility and thermal stability. The metal-containing precursors can be spray-evaporated from liquid solution at room temperature and do not need to be heated [6,10-13]. Another good example of a recently developed deposition approach is electron beam-induced deposition (EBID) where a focused electron beam is used to produce three-dimensional micro- and nanometer sized deposits by decomposing precursor molecules (also the volatile metal acetylacetonate) from a feedstock gas adsorbed on the substrate surface [14-18].

The metal-containing precursors used in CVD can be divided in three classes. The first class is inorganic precursors represented mainly by halides [3]. Unfortunately, when these precursors are used, the pure metallic films can be obtained only for a narrow range of metals. Very often, halide contaminations are present or technical and security problems have to be faced, such as a tendency towards particle formation or corrosive byproducts. As second and major class of precursors, the organometallic (OM) precursors cover a wider range of metals. OM precursors represent molecules with metal-carbon bonds with such ligands as cyclopentadienyl or carbonyl, as well as methyl derivatives [3,19,20]. Metal centers in these precursors are mostly in their elemental oxidation state, assisting the formation of a metallic film without strong reducing agents. However, the strong metal-carbon bonds may lead to the co-deposition of metal carbides and graphitic carbon. Furthermore, OM precursors are usually expensive, very toxic, and highly sensitive to air, moisture, or temperature which requires handling and deposition in dry inert gases and glove boxes [19-21]. Mentioned above MO precursors, as a third class, are represented, e.g. by the family of β-diketones [3]. They avoid many major disadvantages of OM precursors but also have their own. For instance, the metal center is bound to O, N, or S in a high-valence state so that strong reducing agents, such as a $H_2$ flow or electron irradiation (plasma), are required which, in turn, pose safety or technology problems. Here the film contamination by carbon impurities may be observed as well. Nevertheless, using MO precursors is generally seen as promising CVD method if reducing agent safety and technology as well as carbon contamination problems can be solved.

Shedding light upon the CVD reaction mechanisms for the metal containing precursors in the full scale and in detail is essential requirement for the deposition process optimization and beneficial for the selection and synthesis of new precursors. In this respect, the boundary conditions of the deposition parameters may play important roles as well. For thin film analysis in order to understand the mechanisms and the resulting film properties, to characterize the film quality and for optimizing process parameters, the surface-sensitive analytical tools in ultrahigh vacuum (UHV) are optimally suited [22-30]. Unfortunately, only a narrow range of CVD processes can be used for operation directly in an UHV chamber. For example, in high temperature (500 - 950 °C) deposition of the Si, SiGe or SiC films from disilane $Si_2H_6$, germane $GeH_4$, or methylsilane $CH_3SiH_3$ is not only the variety of precursors, but also the choice of deposition parameters applicable in an UHV setup that is limited and typically different from industrially profitable [31-35]. The employment of the organic precursors in the UHV setup is also known to cause chamber contaminations [36-38]. Therefore, in general, CVD, ALD, and EBID with large organic precursor molecules and, moreover, PSE-CVD with precursors in liquid solution are incompatible with UHV conditions where gaseous precursors and reaction residues are required that can be easily pumped. Consequently, sample transfer between a CVD reactor and an UHV chamber for thin film analysis can usually not be avoided. But there are no commercially available solutions for CVD reactors directly linked to UHV chambers via gate valves that are opened only for sample transfer [39-41]. This approach is most promising for clean, fast and effortless transfer if UHV chamber contaminations due to precursor adsorption on the sample holder, transfer rods or gate valves can be avoided and if restrictions due to limited space can be met. Therefore, in this work, such a homebuilt CVD reactor was designed, successfully constructed and directly attached to a commercial UHV system used for thin film analysis. The next chapters of this framework article will present the design of the developed transfer system and thereby direct coupling of the CVD reactor to the UHV chamber for mechanistic studies and deposition process optimization. Furthermore, my own contributions to the studies of CVD processes via analytical tools under UHV conditions will be discussed.

In general:
- basic design ideas, construction details, highlights and capabilities of the PSE-CVD Reactor,
- investigation of the growth behavior of cobalt thin films from PSE-CVD,
- systematical study of the water influence on the composition and growth kinetic of PSE-CVD nickel and cobalt metal films,
- preparation of undecomposed Ni(acac)$_2$ and Co(acac)$_2$ layers via PSE, and
- comparison of thermally initiated and electron-induced precursor decomposition with CVD,

will be summarized and discussed as product of my PhD work.

Ongoing experiments are focused on systematic studies of the influence of various CVD parameters on the growth kinetics of transition metal films and aimed at a fundamental understanding of the reaction mechanisms of the metal deposition process. Elucidating the CVD reaction mechanisms comprehensively and in detail is prerequisite for process optimization and beneficial for the selection and synthesis of new precursors. In this respect, also boundary conditions may play important roles but often they lack systematic studies. The compact and modular reactor for quasi *in situ* UHV surface science studies is adaptable to most UHV systems, its versatility makes it a valuable and promising tool for any fundamental studies of CVD-based techniques such as, *e.g.* ALD. The design for the direct coupling of the thin film deposition process with the surface analysis and facile transfer under UHV conditions will facilitate the systematic study of such experiments and enable a more reliable, detailed characterization of the pertinent parameters of influence that are a prerequisite for progress in deposition engineering.

# 2. Experimental Part

## 2.1. PSE-CVD Reactor and its place in UHV System

The CVD reactor presented in this work was designed [PI] to be directly attached to the load-locks of any of the two Multiprobe UHV systems by Omicron Nanotechnology available in the IAPC laboratory for thin film analysis. The UHV systems contain temperature-programmed desorption (TPD) spectroscopy, low-energy electron diffraction (LEED), scanning tunneling microscopy (STM), Fourier-transform infrared spectroscopy (FTIR), and x-ray photoelectron spectroscopy (XPS) as surface science tools. For XPS, non-monochromatized Al Kα radiation was used for photoelectron generation and a Leybold EA 10 Plus hemispherical energy analyzer with single-channeltron detector was employed. The obtained XP spectra were normalized and then fitted using Igor Pro (from Wave Metrics) and FITT (Seoul National University) software. For the fit a Shirley-type background was taken into account. The morphology of the deposited films was assessed *ex situ* using a Carl Zeiss Ultra Plus Field Emission scanning electron microscope operated at 15.0 keV electron energy.

The reactor design is multifunctional – easy to use in PSE-CVD as well as in classical thermal CVD or ALD regimes. While some parts and geometry of the reactor are based on previous developments [6,7], the design of sample holder, deposition area, and transfer mechanism are completely new, resulting in thin film deposition reactor setup of very compact size which is based on many commercially available components, is relatively easy to assemble, and may be used with widespread UHV-compatible Omicron-type sample holders. The CVD setup accomplishes short pathways for transfer but maintains well separated individual pressure regimes of CVD reactor and UHV chamber. After any stage of a CVD or ALD growth process in the reactor, samples can be transferred easily, quickly and cleanly without contaminating the sample surface or compromising UHV conditions to the UHV chamber for thin film analysis, allowing us to perform systematic studies on the influence of various CVD parameters on the growth kinetics. Thereby, a fundamental understanding of the reaction mechanisms of the chemical vapor deposition process gets within reach.

A drawing to scale of the fully assembled CVD reactor is shown in Figure 1. The reactor, connected to the load lock of the UHV chamber via a CF 38 gate valve, has a small lateral footprint, i.e., there are no protruding parts which could complicate positioning and connection to the Omicron Multiprobe system. The deposition area of the reactor is designed close to previous developments [6,7] and comprises a carrier gas supply and preheating zone

(I), and a spray injection, evaporation and delivery zone (II) (see Figure 1). Carrier gas preheating in zone (I) avoids spray condensation in zone (II) where the precursor is injected by a piezo-driven spray nozzle, operated by low-voltage direct current pulses. The tube size (diameter 40 mm, length 250 mm) of the evaporation and delivery zone (II) provides homogeneous distribution of precursor spray in the carrier gas and uniformity of the precursor mixture in case of multicomponent systems. Preheating of this zone as well as the vacuum line (III) prevents precursor adsorption on the walls of reactor or vacuum line. Almost all components of the deposition area are commercially available. More technical details can be found in PI.

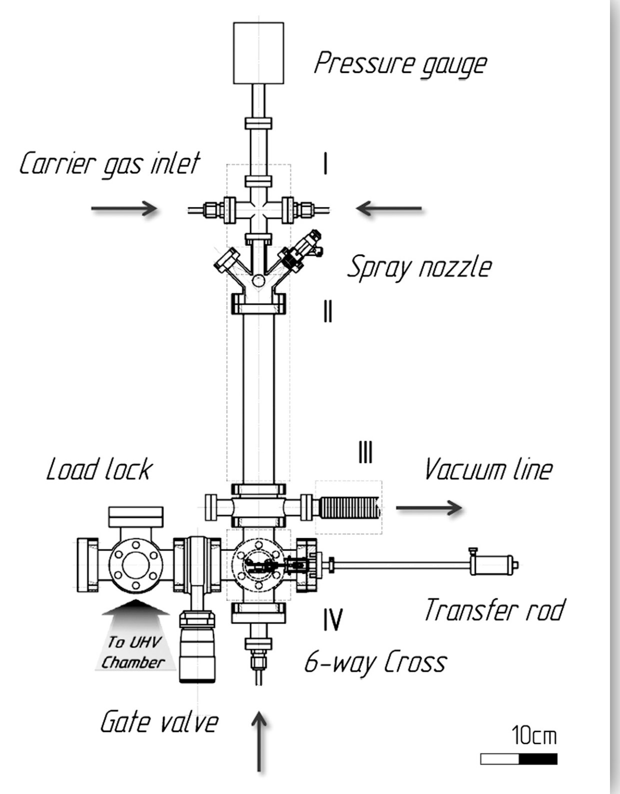

*Fig.1. Drawing to scale of the assembled CVD reactor attached to the UHV chamber. I – Carrier gas preheating zone, II – Spray evaporation zone, III – Vacuum line, IV – Sample manipulation area with parts for sample transfer and gate valve to the UHV chamber load lock.*

The homebuilt sample manipulation area (IV) (see Figure 1) which is described in detail in the PI as well, comprises the sample holder, the transfer mechanism, and the shutter between deposition and sample manipulation area, all placed inside the CF 38 six-way cross. The sample is mounted on an Omicron-type sample holder which slides into a mobile platform for transfer (shuttle) with heater and thermocouple contacts. The reactor is completed by a support system including gas supply, pressure control, temperature control, and precursor delivery systems [PI]. Overall, the designed reactor has a very compact size, is relatively easy to assemble, and should be attachable to any UHV chamber after manageable adaptations.

As it was mentioned before the direct connection allows for quick and contamination-free sample transfer without interrupting vacuum between the CVD reactor and XPS. For the explanation of the transfer procedure the Figure 2 could be used.

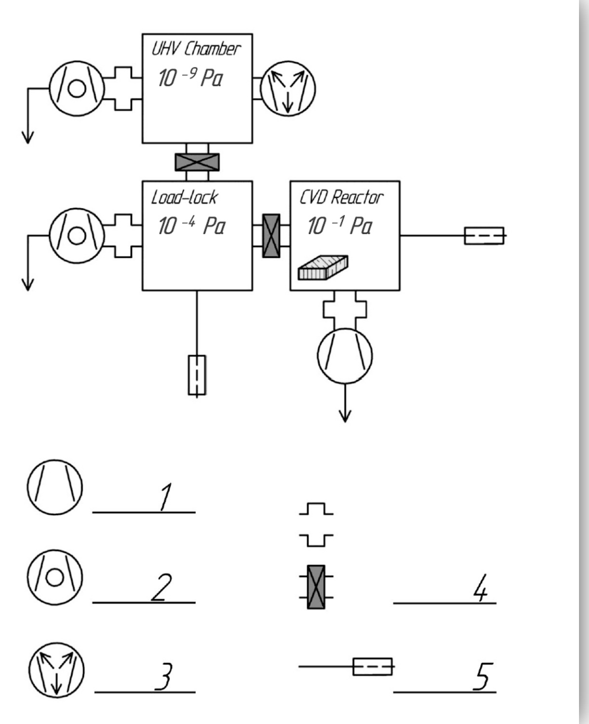

*Fig.2. Scheme illustrating major parts of the vacuum system. 1) Scroll pump, 2) Turbo pump, 3) Ion getter pump, 4) Gate valves, 5) Linear-rotary drives.*

After finishing a deposition or any stage of the deposition process, the reactor is pumped by an oil-free scroll pump attached to the vacuum line of the deposition area, reaching a lowest pressure in the range $10^{-1}$ Pa. Then the sample is transferred from the CVD reactor to the load lock of the UHV chamber. Being now pumped by the turbo molecular pump of the load lock, the reactor pressure typically drops to $\sim10^{-4}$ Pa. In the load lock, the sample is then picked up, and the gate valve between CVD reactor and load lock is closed. After further pumping of the load lock, the sample is transferred into UHV chamber which has a base pressure of $\sim10^{-9}$ Pa maintained by a turbomolecular pump and an ion getter pump. During this last transfer step the pressure in the UHV chamber typically remains below $10^{-6}$ Pa even without bake-out of the load lock. The pressure conditions have been well maintained over more than hundred PSE-CVD and transfer cycles, meanwhile, providing evidence for the cleanness of the entire procedure.

The UHV chamber contamination problem was solved in the way that the CVD reactor is separated in two areas. The first is "deposition area" (Figure 3 (1)), where the precursors spray is produced and carried by a carrier gas to the sample surface. In the second "sample manipulation area" (Figure 3 (2)) the sample temperature is controlled and all parts for sample transfer into the UHV load lock are located. In order to avoid MO precursor adsorption on the reactor walls preheating of all parts is required. In fact any contamination of the sample manipulation area can potentially reach the UHV chamber. Therefore, both deposition and sample manipulation areas must be well isolated from each other during deposition so that only the sample surface but not the sample holder or any part of the transfer mechanism is exposed to the CVD precursors. Making the sample quickly and easily movable for transfer and provide isolation of the sample surface from all transfer parts during deposition is the major technical challenge. It was solved by a uniquely designed movable shutter (Figure 3 (3)) for separation of the deposition area from the sample manipulation area.

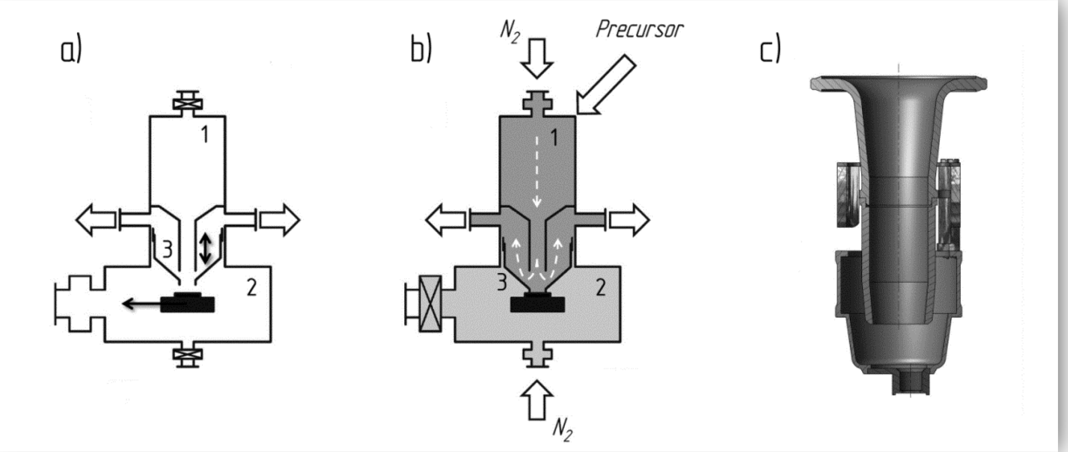

*Fig.3. Schematic diagram of the CVD reactor depicting (1) deposition area (carrier gas preheating, spray evaporation, vacuum line), (2) sample manipulation area, and (3) movable shutter during (a) sample transfer (gate valve to load lock (not shown) on the left is open) and (b) deposition (gate valve to load lock closed, deposition and sample manipulation areas purged independently); (c) shows a cross-sectional drawing of the shutter.*

A short overview of the movable shutter function can be given at this point as well. The shutter (Figure 3 c) consists of a stationary nozzle fixed between flanges on top of the six-ways cross and a similarly shaped part acting as movable mask which is suspended below the nozzle. The stationary nozzle centers and holds the mask which has an aperture in the size of the sample surface area to be exposed to the CVD precursor. The motion of the mask is driven by magnets from the outside. For that purpose, all shutter components are made of nonmagnetic stainless steel except for two magnetic steel parts mounted on top of the mask. It can be lifted upwards and rotated by 55° into a locked position (transfer regime), or rotated back and moved downwards to rest on the sample holder (deposition regime). In deposition regime leaks between sample manipulation and deposition areas are as small as possible, sample surface directly underneath the mask's aperture. For further details on the shutter design see in the PI.

The principle of CVD reactor operation using the movable shutter is as follows. In transfer regime (Figure 3 a) the shutter is fixed in upper position and the gate valve to the load lock is open. With the shutter in upper position, there is enough space available to move the sample holder (mounted on a transport shuttle) out of the CVD position into the load lock and vice versa. The pressure in the CVD reactor, being now additionally pumped via the load lock, is typically as low as $10^{-4}$ Pa during transfer. In deposition regime (Figure 3 b) the shutter is kept in a lower position so that its aperture is slightly pressed to the sample surface and openings between (1) and (2) are as small as possible. The deposition area and the sample manipulation area (the gate valve to the UHV load lock being closed) are pressurized individually by $N_2$ in such way that the pressure in (2) is somewhat higher than in (1) in order to prevent gas flow from the deposition to the sample manipulation zone through rest leaks. Then the precursor mixture passes the deposition area - where pressure is kept in the range required for CVD - and reaches through the aperture of the shutter the sample surface which is kept at the required deposition temperature. Residue of precursor, solvent, and reaction byproducts are pumped off via outlets of the deposition area to a vacuum line. Overall it was found that the shutter maintains the sample manipulation area clean and contamination of load lock or UHV chamber during transfer is negligible. The design of the sample manipulation area combines small size and modularity, allowing for quick repair with contamination-free operation. Details on the design of the rector parts for sample manipulation area as well as construction of a modified Omicron-type sample holder can be found in the PI.

The pressure conditions have been well maintained over more than hundred PSE-CVD and transfer cycles, meanwhile, providing evidence for the cleanness of the entire procedure. It should be noted that separation of deposition and sample manipulation areas within the CVD reactor by means of the movable shutter, as described above, is crucial for the cleanness of sample transfer. Without the shutter the creeping contamination such as, e.g., precursor condensation at the gate valve or metal deposition on all insulating parts have been observed.

## 2.2. Sample Preparation

The deposition experiments were performed in a home-built CVD reactor employing a pulsed-spray evaporation unit for delivery of the precursor liquid feedstock. The experimental deposition parameters, like deposition area pressure, carrier $N_2$ gas flow rate, spray pulse width and frequency, substrate temperature, and total depositions duration were optimized and discussed in the published articles [PI-PIV],[6,7,13,25]. Commercially available anhydrous $Ni(acac)_2$ and $Co(acac)_2$ were dissolved in absolute ethanol at a concentration of 2.5, 5.0, and 7.5 mM. The solution was ultrasonically shaken to achieve complete dissolution. All feedstock solutions were freshly prepared directly before PSE deposition. The purity of the absolute ethanol (>99.9 vol%) was confirmed by an analytical hydrometer. For a systematic study of the water influence on the PSE-CVD process [PII], distilled water was added to the precursor solution to adjust the $H_2O$ concentration from 0.0 to 15.0 vol% (where 1.0 vol% corresponds to 0.555 mol/l).

A 1.5 x 0.5 cm piece of a Si(100) wafer was cut as substrate, cleaned with isopropanol in an ultrasonic bath, and dried in air, so that Ni or Co films were deposited on top of the native or thermal silicon oxide layer. For Co deposition [PIII] also Si substrates with Ni interlayer were used. In case of the Ni and Co precursor adsorption experiments [PIV], the silicon substrates annealed under UHV conditions at 700 °C and transferred *in vacuo* into CVD reactor. In general the photoelectron spectroscopy analysis showed that the mild cleaning procedure left very reproducibly, a level of 9 atom% (~5 atom% after *in vacuo* thermal treatments) residual carbon contaminations on the substrate surface. The thickness of the films obtained by PSE-CVD was varied from few nm to several hundred nm by varying deposition time and precursor concentration in the liquid feedstock. The thermal and electron-induced decomposition experiments [PIV] of the PSE deposited, undecomposed, thin precursor films were performed in the UHV chamber. For electron-induced precursor decomposition experiments the electron gun of a conventional electron diffraction system was used.

For some further details concerning sample preparation and deposition system handling, as well as sample analysis see the attached publication [PI–PIV].

## 2.3. Benefit of the direct sample transfer

The importance of sample transfer from the CVD reactor to surface analysis tools without interrupting vacuum, in order to obtain reliable results on the CVD process can be demonstrated with the following example. A thin Ni film was freshly prepared by PSE-CVD on the Si substrate and transferred into the UHV chamber for XPS analysis under high vacuum conditions directly afterwards. The obtained XP spectrum within the region of Ni 2p emissions is shown in the upper panel of Figure 4.

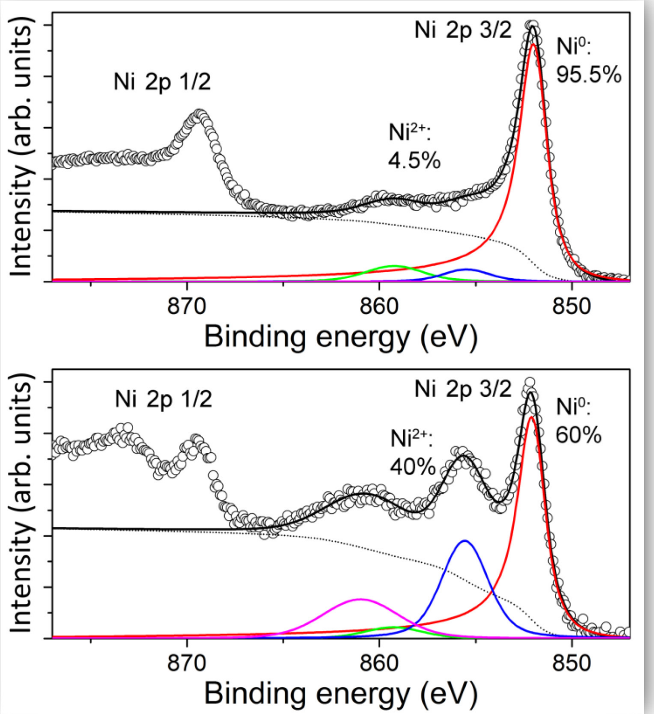

*Fig.4. Ni 2p XPS signal of a thin Ni film deposited on $SiO_x$/Si(100) substrate. Upper panel: freshly prepared film directly transferred into UHV; Bottom panel: after resting in ambient conditions (in air) for 1 hour.*

The red and green curves in Figure 4 represent emissions from reduced Ni ($Ni^0$) with binding energies 852.0 and 859.2 eV. The blue and purple curves represent emission from oxidized Ni ($Ni^{2+}$) (binding energies 855.6 and 861.0 eV). Obviously, the freshly prepared Ni film was almost completely reduced as it comprises more than 95 % metallic Ni. Thereafter the sample was transferred out of the UHV chamber, let rest in the air atmosphere for one hour, and transferred back into UHV. A subsequent XP spectrum (bottom panel in Figure 4) revealed that only 60 % of the surface Ni had remained metallic after this treatment. It can be concluded that even short sample transfers within minutes through air would significantly deteriorate the CVD-grown Ni film surface and that contamination-free transfer is a prerequisite for reliably estimating the influence of deposition parameters in the CVD reactor.

## 3. Summary of the results

Recent works [13,25,26,42] have demonstrated the new approach to deposition of some metals (Ru, Pt, Ag, Cu, Ni, Co) and their alloys using ethanol as unique reducing agent. This CVD technique is characterized by the liquid delivery of commercial MO precursors into the CVD reactor via a pulsed-spray evaporation system. Bahlawane et al. [13,26] studied the reaction mechanisms involved in the PSE-CVD of nickel and copper thin films from an ethanol solution of $Cu(acac)_2$ and $Ni(acac)_2$. The catalytic chemical reduction of the acetylacetonate precursor by ethanol, as shown in Equation 1, was identified as the summarized reaction pathway that enables the deposition of high quality films of transition metals:

$$2\ M(acac)_n + n\ C_2H_5OH \rightarrow 2\ M + 2n\ Hacac + n\ CH_3CHO \qquad (1)$$

Where the first step, the metal acetylacetonate precursor adsorption on silica substrates can be suggested to proceed via ligand exchange reactions:

$$M(acac)_2 + OH\text{-}silica \rightarrow (acac)\text{-}M\text{-}O\text{-}silica + Hacac \qquad (2)$$

While the metal (Ni or Co) catalyzed dehydrogenation of ethanol to acetaldehyde, i.e.

$$C_2H_5OH \rightarrow C_2H_5O + \tfrac{1}{2}\ H_2 \qquad (3)$$

can be proposed as promoter for the decomposition of the adsorbed precursor and reduction of metal:

$$(acac)\text{-}M\text{-}O\text{-}silica + H_2 \rightarrow M + OH\text{-}silica + Hacac \qquad (4)$$

There it has been reported several studies on the interaction of water vapor with Ni surfaces [43-47]. Oxidation of the Ni surface in presence of water vapor was observed at temperatures as low as 300 °C and even in UHV environment with the oxidation rate increasing as the temperature or the $H_2O$ dose are increased [43,48]. Therefore, as the most probable explanation for the metal oxidation at water presence can be suggested as the second decomposition channel of the precursor (where water serves as an oxygen source) [49], initiated by excessive amounts of water:

$$(acac)\text{-}M\text{-}O\text{-}silica + H_2O \rightarrow MO + OH\text{-}silica + Hacac \qquad (5)$$

This pathway leads to the formation of metal oxide and will compete with the precursor decomposition by hydrogen which, as previously shown [13,50], is produced by dehydrogenation of ethanol to acetaldehyde and leads to reduction of metal.

In order to obtain more information on precursor decomposition on the substrate surface and stimulated by the current interest in the electron-beam induced deposition processes, the preparation of solvent-free layers of intact Co(acac)$_2$ and Ni(acac)$_2$ can be achieved by PSE of the precursor onto SiO$_x$/Si substrates at 115 °C. In UHV, these films were than heated to the typical temperature for PSE-CVD or irradiated by electrons in order to induce precursor decomposition.

## 3.1. CVD process optimization (Paper I)

Successful deposition of thin metal films by CVD needs control over a number of physical and chemical parameters, such as precursor and substrate selection, delivery, flow, pressure and temperature conditions. Using the unique UHV-compatible CVD reactor directly attached to an XPS containing UHV chamber gives us opportunity to identify an optimal deposition temperature and hoped to thereby better understand the influence of temperature on the deposition process [PI]. Previous work with β-diketonates [6,7,13] found 230 - 310 °C as deposition temperature range for growing Ni metal films of good quality, i.e., with metallic conductivity and a low degree of contaminations.

In the present study the Ni films were deposited on SiO$_x$/Si(100) substrate samples as described before at various sample temperatures in the range 230 to 310 °C (at steps of 20 °) and transferred under high vacuum conditions into the UHV chamber for XPS analysis. The Ni$^{2+}$/Ni$^0$ intensities ratio determined from the integral Ni 2p peak intensities is shown in the left panel of Figure 5 as a function of the sample temperature during deposition.

Obviously, the highest concentration of Ni$^{2+}$ is observed at the lowest deposition temperature. With increasing deposition temperature, the content of reduced Ni$^0$ increases, until at 270 °C and above the film contains almost only metallic Ni. The right panel of Figure 5 provides information on the amount of carbon contamination at the surface and in the film. It shows the ratio of the integral C 1s and Ni 2p peak intensities (C$_{SUMM}$/Ni$_{SUMM}$ ). While C$_{SUMM}$/Ni$_{SUMM}$ varies only in the range ~1.0 - 1.3 within the deposition temperature range 230 - 310 °C, the XPS analysis indicates the lowest carbon concentration for 270 °C.

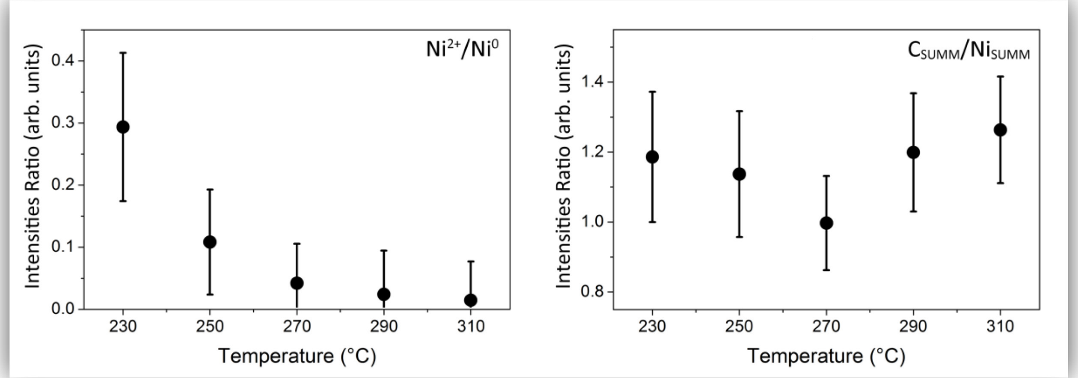

*Fig.5. Changing the intensities ratio of the Ni 2p XPS signals for* $Ni^{2+}/Ni^{0}$ *(left) and* $C_{SUMM}/Ni_{SUMM}$ *(right) at various deposition temperatures.*

These results can be interpreted as follows: Below 270 °C, precursor decomposition is probably incomplete, i.e., undecomposed precursor remains at the surface and contributes to the detected amount of carbon contamination and oxidized Ni. The increase of the carbon signal at sample temperatures above 270 °C during deposition may indicate that the precursor is already overheated, i.e., the residues from its decomposition do not completely desorb but are fragmented, producing carbon black in the film. Overall, within the range 230 to 310 °C proposed before [6,7] the 270 °C was identified as optimal temperature for PSE-CVD with $Ni(acac)_2$ precursor on $SiO_x/Si(100)$ surfaces.

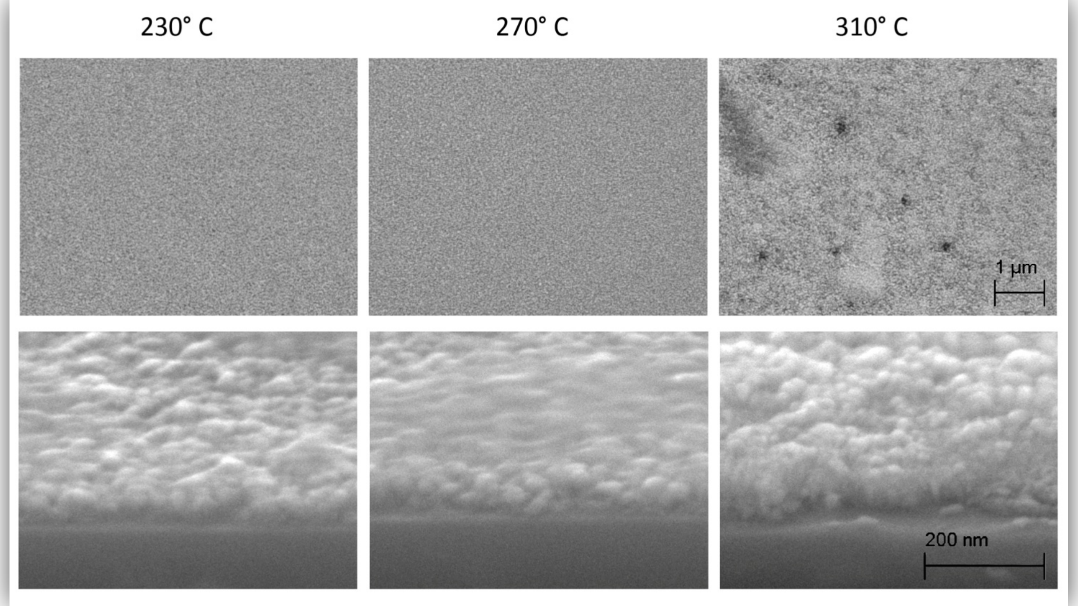

*Fig.6. SEM of* $SiO_x/Si(100)$ *substrate coated with Ni films at 230, 270, and 310 °C. Upper row: plane view on the Ni-covered substrate surface (scale bar 1 µm); bottom row: enlarged view (scale bar 200 nm, viewing angle ~60° with respect to surface normal) of cleaved sample edge showing substrate (bottom) and Ni deposits on top.*

The morphology of the deposited films was assessed as well. The samples prepared at 230, 270, and 310 °C were selected for SEM analysis, the results are shown in Figure 6. The nickel films deposited at 230 or 270 °C appear to be closed and composed of grains with diameters on the order of some ten nanometers (The surface of the film deposited at 270 °C appears to be somewhat smoother than of that deposited at 230 °C). Films obtained at 310 °C present a coarser morphology with smaller, more heterogeneously sized grains. Furthermore, SEM of the film deposited at 310 °C reveals pronounced defects (see upper panel of Figure 6) which may represent gaps in the metal film.

## 3.2. Cobalt films growth on $SiO_x$ and Ni/$SiO_x$ (Paper II, Own contribution)

In contrast to Cu and Ni acetylacetonates, the PSE-CVD of cobalt films from $Co(acac)_2$ was found to be highly sensitive to the nature of the underlying substrate and the deposition temperature. For example, a transition from cobalt carbide to metallic cobalt was observed upon increasing the substrate temperature from 240 to 280 °C, while an improvement of the growth rate and a decrease of the required deposition temperature were observed when coating a 5 nm thick nickel interlayer on bare glass [25]. Despite these observations, the role of the nickel sub layer during the film growth is not well understood.

In the presented work [PII], to monitor the effect of the nickel interlayer on the resulting films, both $SiO_x$/Si(100) and Ni-deposited substrates, with a nickel film thickness of ~5 nm, were used for ultrathin $Co^0$ films (of thickness 2 - 6 nm, representing an early stage of the nucleation) deposition in the UHV-compatible PSE-CVD reactor directly attached to an UHV system. Therefore any post-deposition contamination or metal oxidation during sample transfer from the reactor to XPS can be neglected. The Co films deposited on $SiO_x$/Si(100) substrate at various temperatures in the range 250 - 370 °C and characterized by XPS are shown in Figure 7 (left). Where at sample temperatures up to 270 °C during deposition, the film surface is composed of carbon, oxygen and oxidized $Co^{2+}$, represented, probably, by Co oxide or $Co(OH)_2$. For deposition temperatures of 310 °C and higher, metallic $Co^0$ was also found, where the ratio of metallic and oxidised Co increased with temperature. Only at the highest deposition temperature of 370 °C, the Co signal was found to be entirely metallic. At this deposition temperature, however, carbon contamination, which increased with deposition temperature, has a highest level. Probably due to fragments of decomposed precursor or alcohol, which result from pyrolysis of the precursor solution at the hot sample surface. Below 270 °C deposition temperature, presence of carbon may be attributed to undecomposed precursor at the surface. Compared to the XPS data obtained from 250 nm-thick films deposited from Co(acac)$_2$ precursor at 250 °C, where only metallic Co and some Co carbide were detected, these findings indicate that the growth mode changes as more and more Co is deposited. Probably, the initially deposited cobalt oxide acts as a seed layer and promotes the catalytic decomposition of the precursor at later stages of film growth.

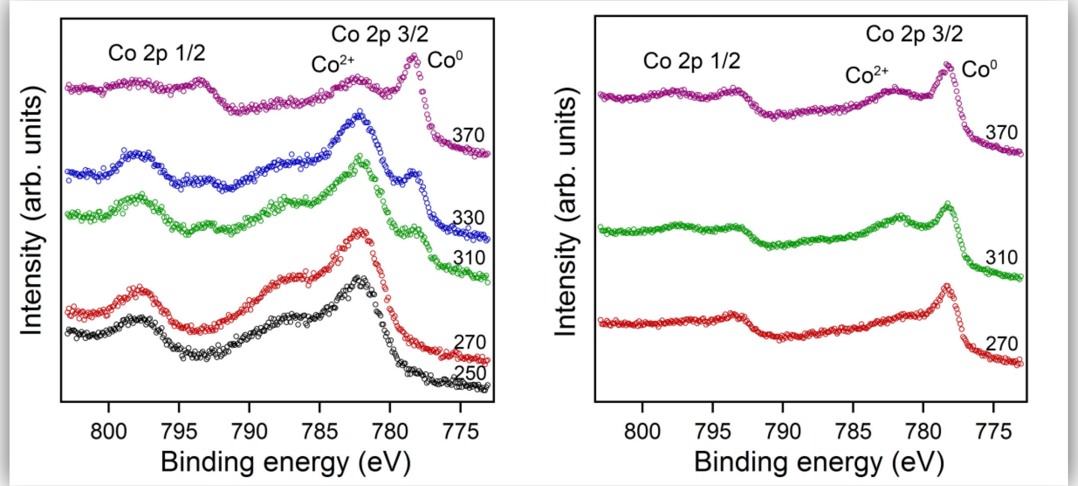

*Fig.7. Co 2p XPS signal of a thin PSE-CVD cobalt films deposited at various temperatures on* $SiO_x$ *(left) and* $Ni/SiO_x$ *(right) substrates using ethanol solution of* Co(acac)$_2$.

When a nickel interlayer was deposited on the $SiO_x$/Si(100) substrates before depositing Co in the UHV-compatible PSE-CVD reactor, the XPS revealed (Figure 7 (right)) that thin films were composed of entirely metallic cobalt even at temperatures as low as 270 °C. It seems that, nickel, as more efficient catalyst for dehydrogenation of ethanol to acetaldehyde and thus, via hydrogen, the decomposition of the adsorbed precursor, promotes the reduction of Co(acac)$_2$ during the initial stage of deposition.

In general using the nickel interlayer for Co(acac)$_2$ precursor decreases the deposition temperature window and improves the growth rate until a critical temperature of 360 °C. Enhancement of the growth when using a nickel seed layer can be ascribed to the improved dehydrogenation of ethanol to acetaldehyde, a process that enables the reduction of the acetylacetonate precursor. However, this effect was limited to temperatures below 360 °C, above which the thermal decomposition of the precursor is predominant. With and without Ni interlayer, carbon contamination at the film surface appears to be inherently connected to the formation of metallic Co and increases with deposition temperature as a consequence of the thermal decomposition of the precursor.

## 3.3. Influence of Water on deposition process (Paper III)

One of the big problems with solid organic precursors in metal CVD is their sensitivity to air and moisture [19-21]. Commonly, the hygroscopic nature of many OM and MO precursors promotes the formation of hydrates which leads to significant configuration changes within the precursor depending on the water content [19,51-53]. These changes may induce strong dependencies of the precursor volatility and thermal stability on the water concentration [19,49,53]. Additionally, water may influence the precursor adsorption selectivity by formation of OH groups on the substrate surface and affect reaction mechanisms thereon [3,52,54-56]. Overall, the sensitivity of the precursor to moisture may render the control of parameters such as nucleation rate, growth rate, or precursor fragmentation difficult and thus affect quality (morphology) and purity (carbon incorporation) of the CV deposits. However, water may even have beneficial effects on the composition or growth rate of the deposit [57-63]. In practice, controlling water contamination in the entire CVD process is harder than just to care for pure precursor feedstock. As pointed out by Pierson [2], a pure reactant can become contaminated in the distribution system to the reactor by, amongst others, moisture even if gas-tight metal lines are used. Therefore, in order to limit costs it is essential to know what grades of purity of precursors, feed gases and reactor lines have to be maintained for good results. Consequently, in order to make use of these effects purposefully and reach optimal growth conditions with reasonable efforts, systematic studies on the influence of water on CVD processes are, as also noted by others [64], a prerequisite.

In the current work [PIII] a comprehensive study of the influence of water on metal film formation exemplarily in a special field of CVD - the pulsed-spray evaporation CVD will be presented [PI],[6]. By varying systematically and in a broad range the water content in Ni and Co acetylacetonate precursors for PSE-CVD of Ni and Co, it was found both, beneficial and detrimental effects of water on the metal film growth, strongly depending on the concentration of water and the β-diketonate in the precursor solution. The first part of this section will discuss a full account of the observed effects of water concentration variation in the precursor solution on composition and morphology of the deposited Ni films. The second part of this section will demonstrate the influence of water on films deposited from 7.5 mM $Co(acac)_2$ precursor solution. In contrast to PSE-CVD of Cu or Ni, finding parameters for deposition of pure metal Co films from $Co(acac)_2$ has been reported as difficult because cobalt precipitates mainly unreduced as carbide or oxide [42]. Moisture may play a key role here.

Figure 7 provides selected SEM data of films deposited from 2.5 mM Ni(acac)$_2$ with 0.0, 0.5, 5.0, and 10.0 vol% water in the precursor feedstock, respectively. Within the SEM resolution, all films appear to be continuous or percolated but composed of grains with diameters on the order of some nanometers in the case of 0.0 and 0.5 vol%. Films obtained from precursor solution with 5.0 vol% water show somewhat bigger grains and those deposited from Ni(acac)$_2$ solution with 10.0 vol% water show an even coarser morphology with more heterogeneously sized grains in the diameter range of some 10 nanometers. The measured thickness values of the deposited films are 30, 40, 40, and 50 nm (± 5 nm), for films deposited from solutions with 0.0, 0.5, 5.0, and 10.0 vol% water, respectively.

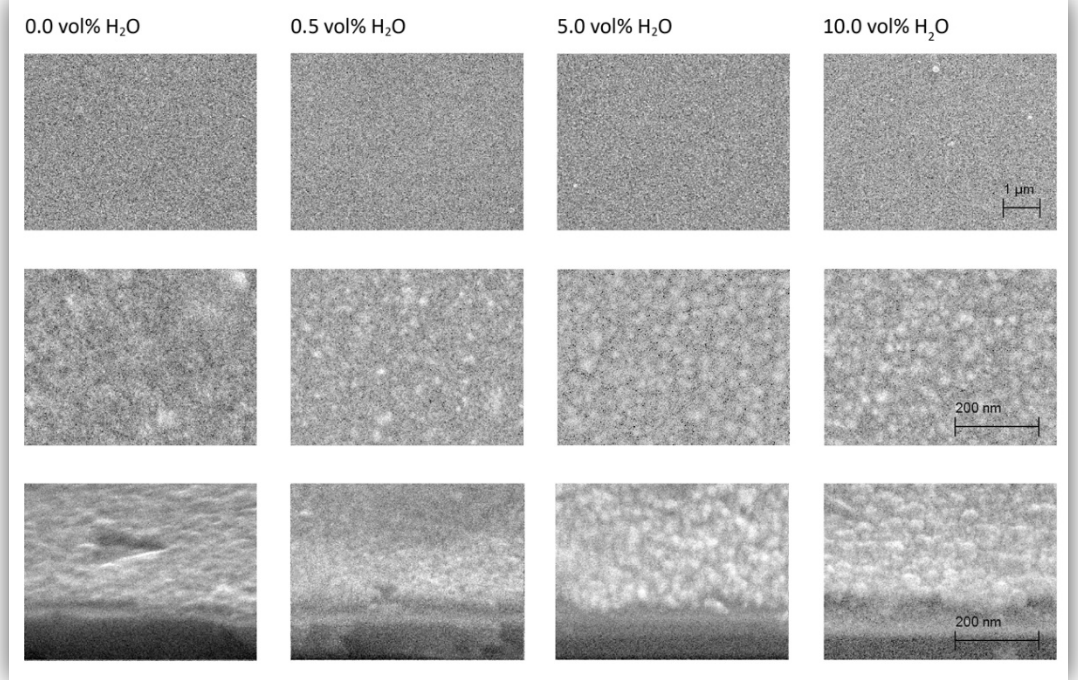

*Fig.7. SEM of films deposited on a SiO$_x$/Si(100) substrate from 2.5 mM Ni(acac)$_2$ in ethanol with 0.0, 0.5, 5.0, and 10.0 vol% water, respectively. First row: plane view on the substrate surface (scale bar 1 µm); second row: enlarged plane view on substrate surface (scale bar 200 nm); third row: enlarged view (scale bar 200 nm) at a viewing angle of ~60° with respect to surface normal, showing a cleaved sample edge with the substrate (bottom) and deposits on top. Film thicknesses estimated by SEM: 30, 40, 40, and 50 nm for films obtained from solutions with 0.0, 0.5, 5.0, and 10.0 vol% of water, respectively.*

Figure 8 shows a comprehensive overview of the XPS data in the binding energy regions of a) Ni 2p, b) O 1s, and c) C 1s obtained for films deposited from 2.5 mM Ni(acac)$_2$ for various water concentrations in the liquid precursor feedstock mixture. Results of a quantitative analysis of these spectra based on the standard fitting routine are compiled in panels d), e), and f). They are show the intensities of major signal contributions depending on the water concentration and allow us to pinpoint trends for the composition of the deposited films.

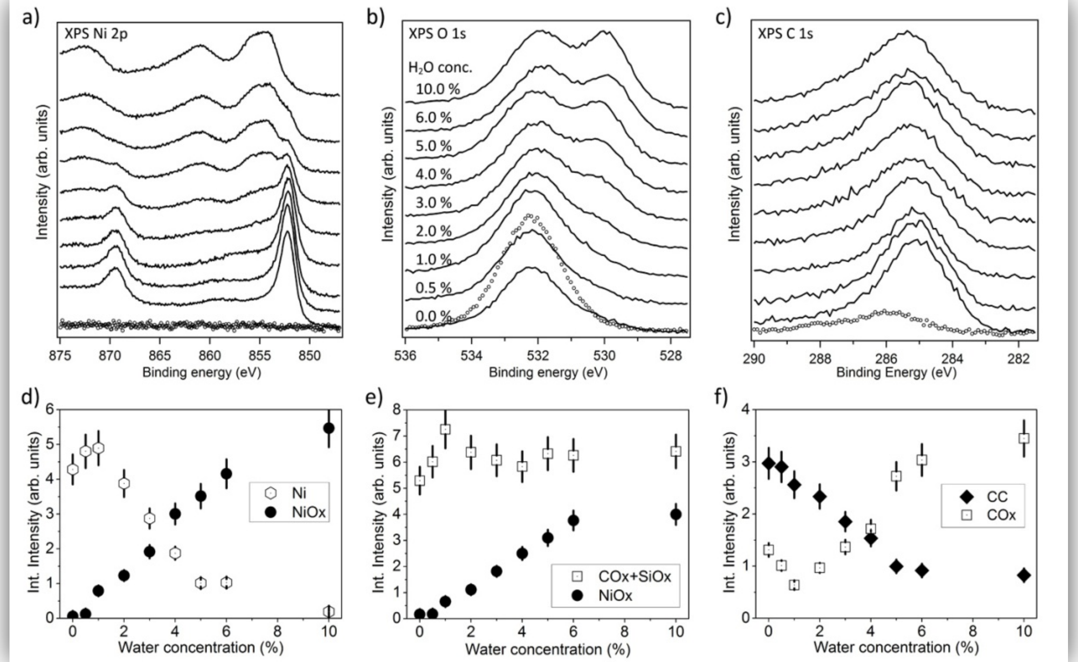

*Fig.8. Top panels: XPS spectra in the binding energy range of a) Ni 2p, b) O 1s, and c) C 1s emissions obtained from the $SiO_x$/Si(100) substrate (dotted curves) and from Ni/$NiO_x$ films (thickness 30-50 nm) grown ontop by PSE-CVD from 2.5 mM precursor solution with various water concentrations (from 0.0 to 10.0 vol%) at a substrate temperature of 270 °C (solid lines). Bottom panels: Integral peak intensities determined from fits to the XPS data.*

For water concentrations in the range 0.0 - 1.0 vol% the following trends were observed: water in the liquid precursor feedstock promotes the growth of metallic Ni and reduces carbon contamination of the deposited films. Ni oxide starts to grow only at water concentrations above 0.5 vol%, so that 0.5 vol% water is optimal for the deposition of fully reduced Ni films, i.e., water at that concentration has a positive influence on PSE-CVD of Ni films from 2.5 mM Ni(acac)$_2$ precursor dissolved in ethanol. While more than 1.0 vol% water in the liquid 2.5 mM Ni(acac)$_2$/ethanol feedstock is detrimental for the deposition of Ni films, as it leads to oxidation of the deposited metal, small amounts of water (between 0.0 and 1.0 vol%) have positive effects, such as a lower level of carbon contamination and, apparently, an denser and smoother morphology. An improved growth rate may be linked to a promotion of precursor adsorption on the substrate surface by OH-groups forming at the surface upon adsorption of water, as previously reported for various precursors deposited on alumina, soda-lime glass, and $SiO_2$ substrates [52,54,56,65]. On $SiO_2$, surface hydroxyl groups have been demonstrated to be stable up to 800 °C and above [54,66-68]. At the first nucleation steps of the deposited Ni film, OH-groups on the substrate surface may serve as preferable bonding sites for the precursor [54-56]. Enhancing the initial precursor adsorption rate may be very important in the case of relatively low (2.5 mM) precursor concentrations in the liquid feedstock.

Several studies on the interaction of water vapor with Ni surfaces have been reported [43-47]. Oxidation of the Ni surface in presence of water vapor was observed at temperatures as low as 300 °C, and even in UHV environment, with the oxidation rate increasing as the temperature or the $H_2O$ dose are increased [43,48]. Therefore, as the most probable explanation for the onset of Ni oxidation at water concentrations of 1.0 vol% and above, can be suggested the second decomposition channel of the precursor (where water serves as an oxygen source) [49], initiated by excessive amounts of water (>3 mol% $H_2O$ in ~97 mol% $C_2H_5OH$ with only 0.01 mol% $Ni(acac)_2$ present). This pathway (Equation 5) leads to the formation of Ni oxide and will compete with the precursor decomposition by hydrogen which, as previously shown [13,50], is produced by dehydrogenation of ethanol to acetaldehyde (Equation 3) and leads to metallic Ni (Equation 4). In summary, there are no positive effects of water on the growth rate or carbon impurity levels of metallic Ni films for 5.0 and 7.5 mM $Ni(acac)_2$ feedstock, in contrast to deposition from 2.5 mM precursor solutions that were observed. Very likely that any promotional effect of surface OH-groups for the precursor adsorption should be most efficient at the lowest precursor concentrations whereas at for 5.0 and 7.5 mM precursor concentration in the deposited gas phase (spray) the precursor molecule density on the surface may be so high that there is no need to promote adsorption.

Overall, the results show that by tuning the concentrations of $Ni(acac)_2$ and water in the precursor solution, the fraction of Ni metal and Ni oxide in the film or the film morphology can be adjusted. At low (2.5 mM) precursor concentration in the feedstock smoothest morphologies (with grains from 5 to 10 nm) are obtained and the fraction of Ni oxide in the deposit is adjustable from 0 to 100 % by varying the water concentration. At high $Ni(acac)_2$ concentrations (5.0 and 7.5 mM) excessive amounts of water strongly affect the film morphology and grain sizes can be varied from 10 to 150 nm. The carbon contamination in deposited films can be minimized to less than 10 % when the precursor solution is adjusted to 2.5 mM $Ni(acac)_2$ concentration and 0.5 % - 1.0 vol% water content.

In contrast to nickel, the deposits from $Co(acac)_2$ contained mainly $CoO_x$, even when waterless precursor solutions were used. With increasing precursor concentration from 2.5 mM (data not shown) to 7.5 mM the Co metal fraction significantly increased, but accounted for only 42 % of the Co 2p signal (Figure 9 d). Thus, in contrast to PSE-CVD from $Ni(acac)_2$ even small amounts (1.0 vol%) of water in the 7.5 mM $CO(acac)_2$ precursor feedstock lead to complete oxidation of the deposited Co. A significant fraction of metallic $Co^0$ can be detected in the Co

2p signal only in deposits obtained without water. As well known from recent reports, cobalt is not as good catalyst for ethanol dehydrogenation as nickel is [25,50]. Therefore, even small amounts of water in the feedstock probably lead to a high water/hydrogen ratio at the substrate surface, rendering the precursor decomposition and $CoO_x$ formation according to Equation 5 as dominant pathway [49] because Co reduction by hydrogen is expected to be much slower. In accordance with observations made for Ni deposition, it was found the water-induced oxidation of carbon impurities when the reaction mechanism changed from M to $MO_x$ formation. A significant metallic fraction of deposited Co is observed only for the waterless precursor solution, the observed maximum ratio of Co:$CoO_x$ is ~40:60.

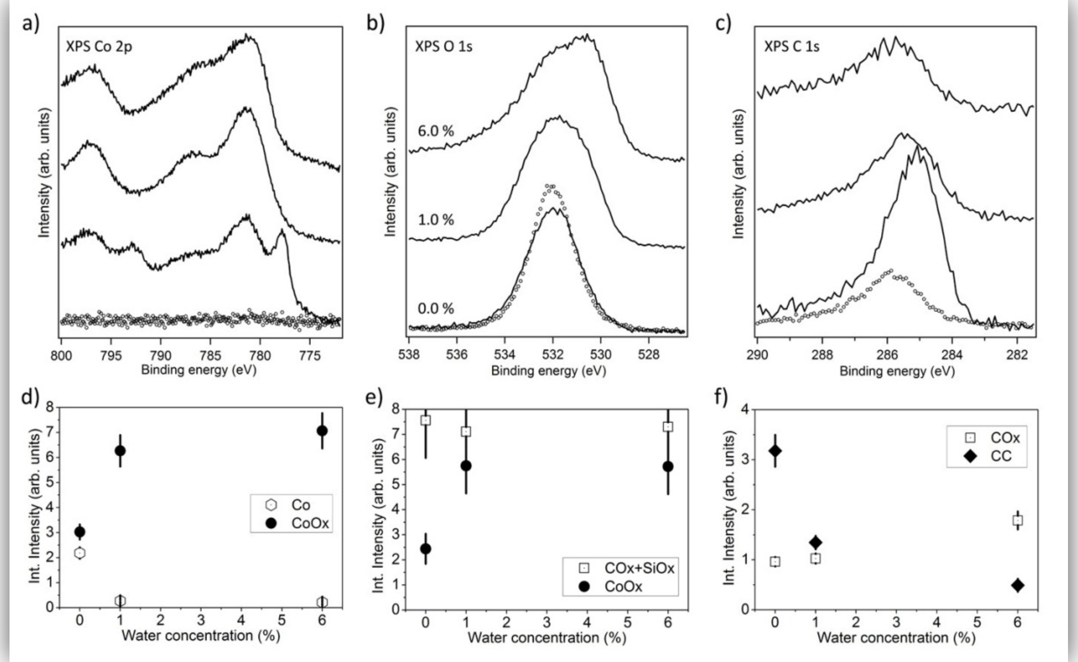

*Fig.9. Top panels: XPS spectra in the binding energy range of a) Co 2p, b) O 1s, and c) C 1s emissions obtained from the $SiO_x$/Si(100) substrate (dotted curves) and from Co/$CoO_x$ films (thickness 100 - 150 nm) grown ontop by PSE-CVD from 7.5 mM precursor solution with various water concentrations (from 0.0 to 6.0 vol%) at a substrate temperature of 310 °C (solid lines). Bottom panels: Integral peak intensities determined from fits to the XPS data.*

Because previous studies demonstrated that a Ni interlayer on the $SiO_x$/Si substrate may drastically improve the quality of films deposited from $Co(acac)_2$ on top (almost completely metallic Co, only small amount of $CoO_x$) [25,50], the PSE-CVD from 7.5 mM $Co(acac)_2$ on a 40 nm thick Ni layer on $SiO_x$/Si(100) was also included in actual study. It was suggested [25,50] that the benefit of a Ni seed layer is catalysis of ethanol dehydrogenation for the formation of hydrogen as reducing agent. Co and in particular $CoO_x$ are worse catalysts in this respect. Consequently, while a Ni layer helps to catalyse the formation of an initial metallic Co layer which then may sustain the $Co^0$ formation on top by catalyzing ethanol dehydrogenation, the balance quickly shifts to the precursor decomposition pathway depicted in Equation 5 as soon as water is present because water oxidizes deposited Co which, in turn, is not available to catalyze ethanol dehydrogenation.

In summary, both, beneficial and detrimental effects of water on the growth of metallic films, strongly depending on the concentration of water and the β-diketonate in the precursor solution, were observed. The smoothest morphologies (with grains from 5 to 10 nm) were obtained for metallic Ni films grown from 2.5 mM Ni(acac)$_2$ precursor solution. The film growth could be optimized and the carbon contamination of the deposited Ni films minimized to less than 10 % when the water concentration in the precursor solution was adjusted to 0.5 vol%. Only at concentrations of 1.0 vol% and higher water induced significant oxidation of the Ni deposit. From precursor solutions with higher Ni(acac)$_2$ concentrations (5.0 and 7.5 mM), purely metallic films were only obtained when any water in the feedstock was eliminated. Here, the film morphology strongly depended on the water concentration, indicating inhibition of nucleation on the Si/SiO$_x$ substrate by excessive amounts of water which lead to the growth of relatively large grains and a coarse film morphology. Overall, the gathered detailed overview over water-induced effects on the PSE-CVD with Ni acetylacetonate precursors dissolved in ethanol shows that by carefully tuning the precursor and water concentration in the feedstock, e.g., the degree of Ni oxidation can be adjusted from 0 to 100 % or the size of the films grains can be varied from less than 10 to 150 nm.

Compared to Ni(acac)$_2$, an even higher sensitivity for water in the feedstock was observed in the case of Co(acac)$_2$ as precursor. Significant metallic Co fractions within the deposited films on SiO$_x$/Si(100) as well as on Ni/SiO$_x$/Si(100) were obtained only from waterless solutions. The relative sensitivities of Ni- and Co-based precursor solutions on water indicate a strong competition between two precursor decomposition pathways, one probably involving the Ni- or Co-catalyzed dehydrogenation of ethanol and H$_2$-induced reduction of the precursor metal center, the other involving H$_2$O-induced Ni or Co(acac)$_2$ decomposition which leads to Ni or Co oxidation.

## 3.4. Comparison of thermal and electron-induced decomposition of metal acetylacetonate thin films (Paper IV)

Having available PSE-CVD reactor directly connected to UHV system with surface science tools such as XPS and LEED, the solvent-free layers of undecomposed Ni or Co(acac)$_2$ precursor were generated for fundamental surface science studies of the EBID process in UHV. The precursor layers obtained by this approach were used for a qualitative comparison of thermally initiated and electron-induced precursor decomposition and metal reduction, based on XPS data. Thermal treatments in connection with EBID are particularly interesting because they have demonstrated the ability to improve the EBID purity [69,70]. The focus on Ni and Co precursors was concentrated, taking into account wide applicability and permanent industrial interest in deposits of Ni, Co and their alloys [3,71-74], as well as previous experience with PSE-CVD of Ni and Co [PI-PIII].

To obtain a solvent-free layer of undecomposed Ni or Co acetylacetonate precursor molecules via PSE of the liquid feedstock, the substrate temperature should be kept higher than the ethanol desorption temperature from silica surfaces (peak at ~90 °C) [75] and below the desorption temperature of M(acac)$_2$ (thermogravimetric studies[49] indicated that M(acac)$_2$ precursors volatilized completely between 150 and 200 °C). To test that concept, the first pure solvent was spray-evaporated on the surface at three different temperatures (Figure 10): at 30 °C for reference, at 115 °C, i.e., somewhat above the reported desorption temperature of ethanol, and at 270 °C, i.e., at that temperature at which the CVD process is initiated.

Figure 10 a) reveals reduction of the level of carbon contamination as the benefit of annealing the freshly prepared $SiO_x/Si$ substrate to 700 °C in vacuum. While clear indication of ethanol adsorption was observed only at 30 °C. Overall, any residues from ethanol at 115 and 270 °C substrate temperature are negligibly small, i.e., a deposition temperature of 115 °C is high enough to safely get rid of the solvent. When Ni(acac)$_2$ precursor solution is injected at 270 °C sample temperature (Figure 10 b), the acetylacetonate decomposes and a film containing only metallic Ni (100 % $Ni^0$) and some carbon inclusions are formed (CVD process [PIII],[6]). In contrast, during injection of Ni(acac)$_2$ precursor solution at 115 °C substrate temperature adsorption of intact Ni(acac)$_2$ molecules predominates. There is only $Ni^{2+}$ present on the sample surface, similar to deposition at 30 °C. Overall, it could be concluded that a solvent-free layer of intact Ni(acac)$_2$ precursor molecules forms during deposition at 115 °C. After injection of Ni(acac)$_2$ precursor solution at 30 °C, the joint adsorption of ethanol and Ni(acac)$_2$ was found.

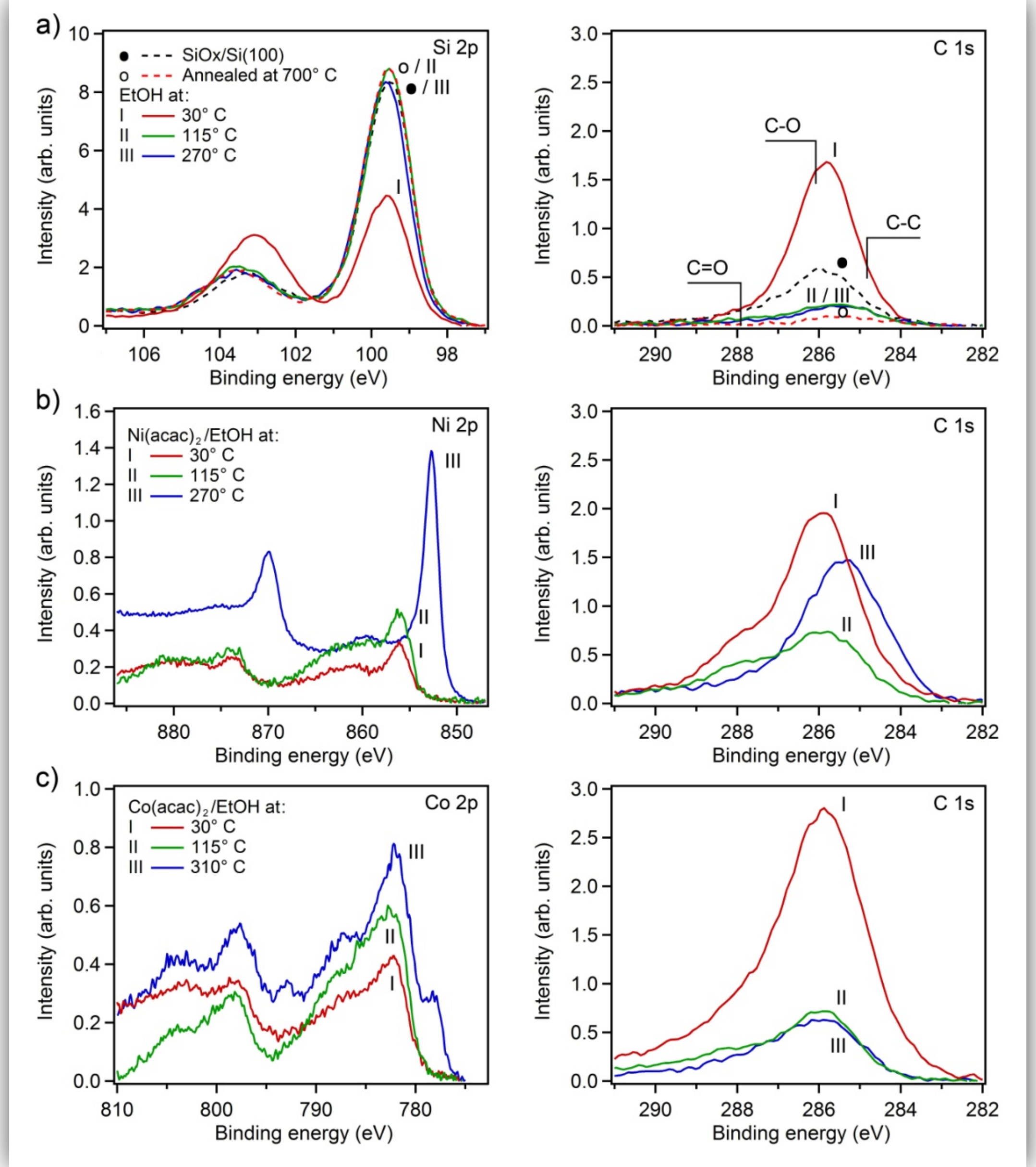

*Fig.10. XP spectra obtained from the $SiO_x/Si(100)$ substrate before and after precursors deposition by PSE.*

*a) (top row): XP spectra in the binding energy range of Si 2p (left) and C 1s (right) emissions obtained from the native $SiO_x/Si(100)$ substrate (●), annealed at ~700 °C (○), and after ethanol deposition on the substrate at 30 (I), 115 (II), and 270 (III). b) (center row): XP spectra in the binding energy range of Ni 2p (left) and C 1s (right) emissions obtained after deposition of $Ni(acac)_2$/ethanol by PSE on annealed $SiO_x/Si(100)$ substrate from 5.0 mM precursor at a substrate temperature of 30 (I), 115 (II), and 270 °C (III). c) (bottom row): XP spectra in the binding energy range of Co 2p (left) and C 1s (right) emissions obtained after deposition of $Co(acac)_2$/ethanol by PSE on annealed $SiO_x/Si(100)$ substrate from 5.0 mM precursor at a substrate temperatures of 30 (I), 115 (II), and 310 °C (III).*

Similar to nickel, injection of $Co(acac)_2$ precursor solution at 30 °C leads to joint adsorption of ethanol and $Co(acac)_2$, while at 310 °C substrate temperature the Co precursor decomposes on the surface and forms a deposit of Co oxide and metallic Co, with some carbon inclusions (CVD process [PIII]). Notably, in contrast to CVD from Ni(acac)$_2$, the acetylacetonate ligands are not fragmented during precursor decomposition. Also the smaller amount of carbon impurities as compared to the Ni PSE-CVD indicates that, during Co-PSE CVD, the Co precursor decomposes more easily into the metal center and volatile acetylacetone, which is in accordance with the observation that Co(acac)$_2$ is less stable than Ni(acac)$_2$ [76-78]. After injection of Co(acac)$_2$ dissolved in ethanol at 115 °C substrate temperature the XPS data indicate that, similar to Ni(acac)$_2$ injection at that temperature, adsorption of intact Co(acac)$_2$ precursor molecules are predominated. Thus the selected substrate temperature of 115 °C during PSE of metal acetylacetonate precursors is well suited for the preparation of solvent-free layers of undecomposed M(acac)$_x$ precursor.

Precursor layers produced by PSE onto an annealed SiO$_x$/Si substrate at 115 °C and then either irradiated by electrons at room temperature or heated up to 270 or 310 °C. The data obtained after electron irradiation of Ni(acac)$_2$ layers are shown that irradiation in the low-energy electron exposure regime (at $E_0$=25 eV) for 15 min and 375 min did not lead to any significant changes. Only after switching to the high-energy electron exposure regime (at $E_0$=500 eV) electron induced reduction of the metal from Ni$^{2+}$ to Ni$^0$ can be observed after 15 min. After 90 min irradiation the final film contained 59 % of Ni$^0$ (Table 1) with some carbon inclusions shown in Table 2. Table 1 also shows that after a Ni precursor layer was heated up to 270 °C for 1 min, the 86 % of the metal ions reduced to Ni$^0$. The level of residual carbon contamination (Table 2) was even ~30 % lower than after ethanol-assisted CVD.

Tab. 1. Percentage amount of metallic Ni or Co (of all deposited Ni or Co) in treated films.
The Data were obtained by PSE-CVD or by thermal treatment or electron irradiation of Ni and Co acetylacetonate precursor layers.

| | Ni precursor | Co precursor |
|---|---|---|
| **Ethanol assisted CVD** | 100 | 25 |
| **Thermal decomposition** | 86 | 41 |
| **Electron beam-induced decomposition** | 59 | 21 |

Similar to the Ni(acac)$_2$, also Co(acac)$_2$ layers did not show significant changes in XPS after electron irradiation at room temperature in the low-energy electron exposure regime ($E_0$=25 eV) for 15 min and 375 min. Unlike Ni(acac)$_2$, however, even the high-energy electron exposure regime ($E_0$=500 eV) for 15 min, 90 min, and 210 min did only reduce minor amounts of Co$^{2+}$ precursor ions to Co$^0$. Only 21 % of Co was metallic after irradiation (Table 1). Also heating a $Co(acac)_2$ film to 310 °C leads to precursor decomposition and fragmentation. Compared to electron irradiation and, in particular, the ethanol assisted CVD at 310 °C, after heating it was found an unexpectedly high fraction of metallic $Co^0$ (41 % of the entire Co) and preferably $CoO_x$ (Table 1) with some carbon inclusions (Table 2).

Tab. 2. Atomic ratio C to M in the films.
The Data were obtained by various ways from Ni and Co acetylacetonate precursors.

| | **Ni precursor** | **Co precursor** |
|---|---|---|
| **Ethanol assisted CVD** | 0.19 | 0.07 |
| **Thermal decomposition** | 0.13 | 0.11 |
| **Electron beam-induced decomposition** | 0.13 | 0.08 |

In the presented work, the level of carbon impurities (Table 2) compared to reports for continuous EBID processes is relatively low (for some MO precursors it may reach even 80 - 90 atom%) [14,18,27]. The relatively low level of carbon impurities may be explained as follows: In discussed experiments, post-deposition electron beam-induced decomposition of the precursor is performed in good vacuum conditions while usually in EBID electron irradiation is performed during exposure of the substrate to the precursor gas. Therefore, any accumulation of carbonaceous species from electron beam-induced decomposition of precursor in the gas phase and adsorption of the produced fragments is avoided, in contrast to “real” EBID. The temperature range of EBID is often so low that dissociation fragments remain adsorbed and immobile on the substrate [14] while classical CVD operates at temperatures above the precursor decomposition temperature in order to increase the probability of rapid desorption of ligands or other undesired precursor fragments.

The temperature difference results in different ways in which adsorbed metal-ligand species are processed by either electrons or thermal reactions. Under EBID deposition conditions, experimental evidence suggests that ligand *decomposition* rather than *desorption* dominates. In the CVD reaction pathway thermal reactions are often characterized by ligand *desorption* as opposed to ligand *decomposition* [17]. A comparison of the metal contents in the PSE-CVD films of Ni or $Co(acac)_2$ is achieved by thermal or electron-induced *post-deposition* decomposition of solvent-free Ni or $Co(acac)_2$ layers that is summarized in Table 1. As pointed out before, ethanol-assisted CVD of $Co(acac)_2$ leads to a lower amount of metallic Co in the deposit than plain thermal treatment of a $Co(acac)_2$ layer at the same temperature. Possibly, the high sensitivity of cobalt to oxidizing agents plays a major role here. Ethanol is added for the CVD process because hydrogen is formed upon the decomposition of ethanol (Equation 3) and acts as a reducing agent. However, also water is a product of EtOH decomposition (and may be also be present as contamination in the precursor solution) and acts as oxidizing agent [PIII],[49,52]. The observation that thermal decomposition of the ethanol-free precursor layer produces higher metal contents than obtained during CVD indicates that oxidation reactions by the presence of water (Equation 5) dominate over the reduction of $Co^{2+}$ by protons (Equation 4) delivered by catalytic ethanol decomposition at Co (Equation 3) [PIII]. On $SiO_x$, reaction between surface OH-groups could lead to the formation of siloxane bonds and molecular water [79]:

$$H_2O + silica \rightarrow HOH\text{-}silica \qquad (6)$$

However, according to the study of L.T. Zhuravlev [79] there is neither physisorbed nor chemisorbed $H_2O$ on top of $SiO_x$ in vacuum at temperatures above 190 °C and only a low density of free single or geminal OH-groups is stable at and above 400 °C. Therefore, it could be assumed that in presented experiments at the temperature regime of precursor layer deposition (115 °C) and in particular when the substrate is heated to 310 °C in UHV for the thermal decomposition of the precursor film, the amount of water on the substrate surface is reduced to such low levels that oxidation of precursor metal centers is negligible.

In summary, the injection of liquid precursors using pulsed spray was successfully applied for preparation of solvent-free layers of undecomposed $M(acac)_2$ precursor. This method opens up acetylacetonates layers to qualitative and quantitative analysis by a variety of UHV-based surface science tools. A qualitative comparison of thermally initiated and electron beam-induced precursor decomposition and metal center reduction was carried out and shows that the level of carbon impurities in experiments of post-deposition electron-induced precursor decomposition was notably low compared to reports for continuous EBID processes. Therefore, it could be suggested that at least in the laboratory the metal acetylacetonate deposition followed by post-deposition irradiation with a focused electron beam and subsequent removal of intact precursor by dissolution in ethanol or by heating may constitute an interesting electron beam lithography technique for the production of the metal nanostructures.

## Concluding remarks

This PhD thesis based on the joint project between Universities Bremen and Bielefeld was aimed at contributing to the mechanistic understanding of the growth conditions of metallic films synthesized by the previously established technique of pulsed spray evaporation chemical vapor deposition (PSE-CVD). Nickel and cobalt were selected as an example to study links between the macroscopic deposition conditions and the microscopic processes involving the precursor, surface properties and the growing thin film.

To combine macroscopic and microscopic approaches, here it was a need to design and build up new apparatus, as a consequence of the joint studies, combining deposition and material characterization under growth conditions. In particular, novel, compact and modular deposition reactor was successfully constructed that permitted *in situ* surface diagnostics while performing PSE-CVD. This reactor was directly attached to a UHV chamber with a transfer mechanism that allowed to systematic study of the film growth at any stage of the deposition process without contamination, and enabled more reliable, detailed characterization of the pertinent parameters of influence. With this novel reactor established in Bremen, systematic investigations using surface analysis were conducted under growth conditions that had been identified in Bielefeld. Therefore I am particularly grateful to all collaborators providing this project.

The present work addressed important features of the growth process including the influence of various CVD parameters on the growth kinetics, such as the nature of the metal centre, the temperature sensitivity of carbon contamination, the function of ethanol, both as a solvent as well as a catalytic agent, influence of nickel as a seed layer for different combinations of boundary conditions, the role of water on CVD of Ni and Co thin films from ethanol solutions. Furthermore, investigation of the mechanisms of PSE-CVD from acetylacetonate metal precursors in ethanol, as well as thermal and electron beam-induced decomposition of solvent-free layers of intact $Co(acac)_2$ and $Ni(acac)_2$ was performed.

# References

[1] K. Wetzig, C.M. Schneider, Metal based thin films for electronics, Wiley-VCH, Weinheim, 2006.

[2] H.O. Pierson, H.O. Pierson, Handbook of chemical vapor deposition (CVD): principles, technology, and applications, Noyes Publications/William Andrew Pub., Norwich, N.Y., 1999.

[3] T.T. Kodas, M.J. Hampden-Smith, The chemistry of Metal CVD, VCH, Weinheim; New York, 1994.

[4] P.M. Martin, Handbook of deposition technologies for films and coatings: science, applications and technology, Elsevier, Amsterdam; Boston, 2010.

[5] J. Lee, H.J. Yang, J.H. Lee, J.Y. Kim, W.J. Nam, H.J. Shin, Y.K. Ko, J.G. Lee, E.G. Lee, C.S. Kim, J Electrochem Soc 153 (2006) G539.

[6] P.A. Premkumar, N. Bahlawane, K. Kohse-Höinghaus, Chemical Vapor Deposition 13 (2007) 219.

[7] P.A. Premkumar, N. Bahlawane, G. Reiss, K. Kohse-Höinghaus, Chemical Vapor Deposition 13 (2007) 227.

[8] M. Oshima, A. Komeda, K. Tominaga, M. Nakao, T. Shimizu, J. Senda, K. Ishida, Heat Transfer-Asian Research 38 (2009) 284.

[9] L. Gao, P. Härter, C. Linsmeier, J. Gstöttner, R. Emling, D. Schmitt-Landsiedel, Materials Science in Semiconductor Processing 7 (2004) 331.

[10] M.J. Crosbie, P.A. Lane, P.J. Wright, D.J. Williams, A.C. Jones, T.J. Leedham, C.L. Reeves, J. Jones, Journal of Crystal Growth 219 (2000) 390.

[11] S. Krumdieck, R. Raj, Surf Coat Tech 141 (2001) 7.

[12] S. Pasko, A. Abrutis, L.G. Hubert-Pfalzgraf, V. Kubilius, Journal of Crystal Growth 262 (2004) 653.

[13] N. Bahlawane, P.A. Premkumar, Z. Tian, X. Hong, F. Qi, K. Kohse-Höinghaus, Chem Mater 22 (2009) 92.

[14] I. Utke, P. Hoffmann, J. Melngailis, J Vac Sci Technol B 26 (2008) 1197.

[15] W.F. van Dorp, T.W. Hansen, J.B. Wagner, J.T.M. De Hosson, Beilstein Journal of Nanotechnology 4 (2013) 474.

[16] N. Silvis-Cividjian, C.W. Hagen, P. Kruit, M.A.J. v.d. Stam, H.B. Groen, Appl Phys Lett 82 (2003) 3514.

[17] J. Spencer, S. Rosenberg, M. Barclay, Y.-C. Wu, L. McElwee-White, D. Howard Fairbrother, Appl. Phys. A 117 (2014) 1631.

[18] J. Warneke, W.F. Van Dorp, P. Rudolf, M. Stano, P. Papp, S. Matejcik, T. Borrmann, P. Swiderek, Phys Chem Chem Phys 17 (2015) 1204.

[19] L. Brissonneau, C. Vahlas, Ann Chim-Sci Mat 25 (2000) 81.

[20] E.P. Boyd, D.R. Ketchum, H. Deng, S.G. Shore, Chem Mater 9 (1997) 1154.

[21] L.G. Hubert-Pfalzgraf, H. Guillon, Applied Organometallic Chemistry 12 (1998) 221.

[22] M. Kawase, Y. Ishikawa, T. Fukui, Appl Surf Sci 130 (1998) 457.

[23] L. Li, B.K. Han, Q. Fu, R.F. Hicks, Phys Rev Lett 82 (1999) 1879.

[24] K. Lüdge, P. Vogt, O. Pulci, N. Esser, F. Bechstedt, W. Richter, Phys Rev B 62 (2000) 11046.

[25] P.A. Premkumar, A. Turchanin, N. Bahlawane, Chem Mater 19 (2007) 6206.

[26] N. Bahlawane, P.A. Premkumar, F. Reilmann, K. Kohse-Höinghaus, J. Wang, F. Qi, B. Gehl, M. Baumer, J Electrochem Soc 156 (2009) D452.

[27] J.D. Wnuk, S.G. Rosenberg, J.M. Gorham, W.F. van Dorp, C.W. Hagen, D.H. Fairbrother, Surf Sci 605 (2011) 257.

[28] A. Lafosse, M. Bertin, R. Azria, Progress in Surface Science 84 (2009) 177.

[29] C.R. Arumainayagam, H.-L. Lee, R.B. Nelson, D.R. Haines, R.P. Gunawardane, Surface Science Reports 65 (2010) 1.

[30] E. Bohler, J. Warneke, P. Swiderek, Chemical Society Reviews 42 (2013) 9219.
[31] B.S. Meyerson, Appl Phys Lett 48 (1986) 797.
[32] B.S. Meyerson, P Ieee 80 (1992) 1592.
[33] M. Racanelli, D.W. Greve, Appl Phys Lett 56 (1990) 2524.
[34] T.N. Adam, S. Bedell, A. Reznicek, D.K. Sadana, A. Venkateshan, T. Tsunoda, T. Seino, J. Nakatsuru, S.R. Shinde, Journal of Crystal Growth 312 (2010) 3473.
[35] T.N. Adam, S. Bedell, A. Reznicek, D.K. Sadana, R.J. Murphy, A. Venkateshan, T. Tsunoda, T. Seino, J. Nakatsuru, S.R. Shinde, Ecs Transactions 33 (2010) 149.
[36] J.-P. Lu, R. Raj, A. Wernberg, Thin Solid Films 205 (1991) 236.
[37] N. Pütz, H. Heinecke, M. Heyen, P. Balk, M. Weyers, H. Lüth, Journal of Crystal Growth 74 (1986) 292.
[38] E. Tokumitsu, Y. Kudou, M. Konagai, K. Takahashi, J Appl Phys 55 (1984) 3163.
[39] S. Yoshiki, K. Kunihiko, O. Masashi, Jpn J Appl Phys 27 (1988) L2189.
[40] M. Kasu, N. Kobayashi, J Appl Phys 78 (1995) 3026.
[41] L. Li, B. Han, S. Gan, H. Qi, R.F. Hicks, Surf Sci 398 (1998) 386.
[42] N. Bahlawane, P. Antony Premkumar, K. Onwuka, K. Rott, G. Reiss, K. Kohse-Höinghaus, Surface and Coatings Technology 201 (2007) 8914.
[43] P.R. Norton, R.L. Tapping, J.W. Goodale, Surf Sci 65 (1977) 13.
[44] C. Benndorf, C. Nöbl, F. Thieme, Surf Sci 121 (1982) 249.
[45] A.F. Carley, S. Rassias, M.W. Roberts, Surf Sci 135 (1983) 35.
[46] J.M. Heras, E.V. Albano, Applications of Surface Science 17 (1983) 207.
[47] J.M. Heras, E.V. Albano, Applications of Surface Science 17 (1983) 220.
[48] B.P. Payne, M.C. Biesinger, N.S. McIntyre, Journal of Electron Spectroscopy and Related Phenomena 175 (2009) 55.
[49] M. Utriainen, M. Kröger-Laukkanen, L.-S. Johansson, L. Niinistö, Appl Surf Sci 157 (2000) 151.
[50] N. Bahlawane, K. Kohse-Höinghaus, P.A. Premkumar, D. Lenoble, Chemical Science 3 (2012) 929.
[51] G.J. Bullen, R. Mason, P. Pauling, Inorganic Chemistry 4 (1965) 456.
[52] M. Utriainen, M. Kröger-Laukkanen, L. Niinistö, Materials Science and Engineering: B 54 (1998) 98.
[53] E. Lindahl, M. Ottosson, J.-O. Carlsson, Chemical Vapor Deposition 15 (2009) 186.
[54] S. Haukka, E.L. Lakomaa, A. Root, The Journal of Physical Chemistry 97 (1993) 5085.
[55] S. Takeda, M. Fukawa, Y. Hayashi, K. Matsumoto, Thin Solid Films 339 (1999) 220.
[56] K. Bernal Ramos, M.J. Saly, Y.J. Chabal, Coordination Chemistry Reviews 257 (2013) 3271.
[57] B. Lecohier, B. Calpini, J.M. Philippoz, H. van den Bergh, J Appl Phys 72 (1992) 2022.
[58] A. Nobuyoshi, A. Yoshinobu, Jpn J Appl Phys 32 (1993) 3915.
[59] A.V. Gelatos, R. Marsh, M. Kottke, C.J. Mogab, Appl Phys Lett 63 (1993) 2842.
[60] H.A. Marzouk, J.Y. Kim, J.S. Kim, P.J. Reucroft, R.J. Jacob, J.D. Robertson, C. Eloi, Thin Solid Films 249 (1994) 22.
[61] J.-Y. Kim, Y.-K. Lee, H.-S. Park, J.-W. Park, D.-K. Park, J.-H. Joo, W.-H. Lee, Y.-K. Ko, P.J. Reucroft, B.-R. Cho, Thin Solid Films 330 (1998) 190.
[62] J. Huo, R. Solanki, J. McAndrew, Journal of Materials Research 17 (2002) 2394.
[63] T. Törndahl, M. Ottosson, J.-O. Carlsson, J Electrochem Soc 153 (2006) C146.
[64] A. Jain, T.T. Kodas, T.S. Corbitt, M.J. Hampden-Smith, Chem Mater 8 (1996) 1119.
[65] D.J.H. Emslie, P. Chadha, J.S. Price, Coordination Chemistry Reviews 257 (2013) 3282.
[66] J. Farkas, M.J. Hampden-Smith, T.T. Kodas, The Journal of Physical Chemistry 98 (1994) 6753.
[67] J. Farkas, M.J. Hampden-Smith, T.T. Kodas, The Journal of Physical Chemistry 98 (1994) 6763.
[68] S. Haukka, T. Suntola, Interface Science 5 (1997) 119.

[69] N.A. Roberts, J.D. Fowlkes, G.A. Magel, P.D. Rack, Nanoscale 5 (2013) 408.

[70] S.G. Rosenberg, K. Landheer, C.W. Hagen, D.H. Fairbrother, Journal of Vacuum Science; Technology B 30 (2012) 051805.

[71] W.-Q. Deng, X. Xu, W.A. Goddard, Nano Letters 4 (2004) 2331.

[72] V.V. Bakovets, V.N. Mitkin, N.V. Gelfond, Chemical Vapor Deposition 11 (2005) 368.

[73] C. Elbuken, M. Yavuz, M.B. Khamesee, J Appl Phys 104 (2008) 044905.

[74] Z. Zhang, T.M. Nenoff, J.Y. Huang, D.T. Berry, P.P. Provencio, The Journal of Physical Chemistry C 113 (2009) 1155.

[75] H. Noller, G. Ritter, Journal of the Chemical Society, Faraday Transactions 1: Physical Chemistry in Condensed Phases 80 (1984) 275.

[76] P.S. Gentile, A. Dadgar, Journal of Chemical & Engineering Data 13 (1968) 236.

[77] V.A. Barabanov , S.L. Davydova, N.A. Plate, Zhur. Fiz. Khim. 42 (1968) 990.

[78] A.T. Pilipenko, L.I. Savransky, Talanta 34 (1987) 77.

[79] L.T. Zhuravlev, Colloids and Surfaces A: Physicochemical and Engineering Aspects 173 (2000) 1.

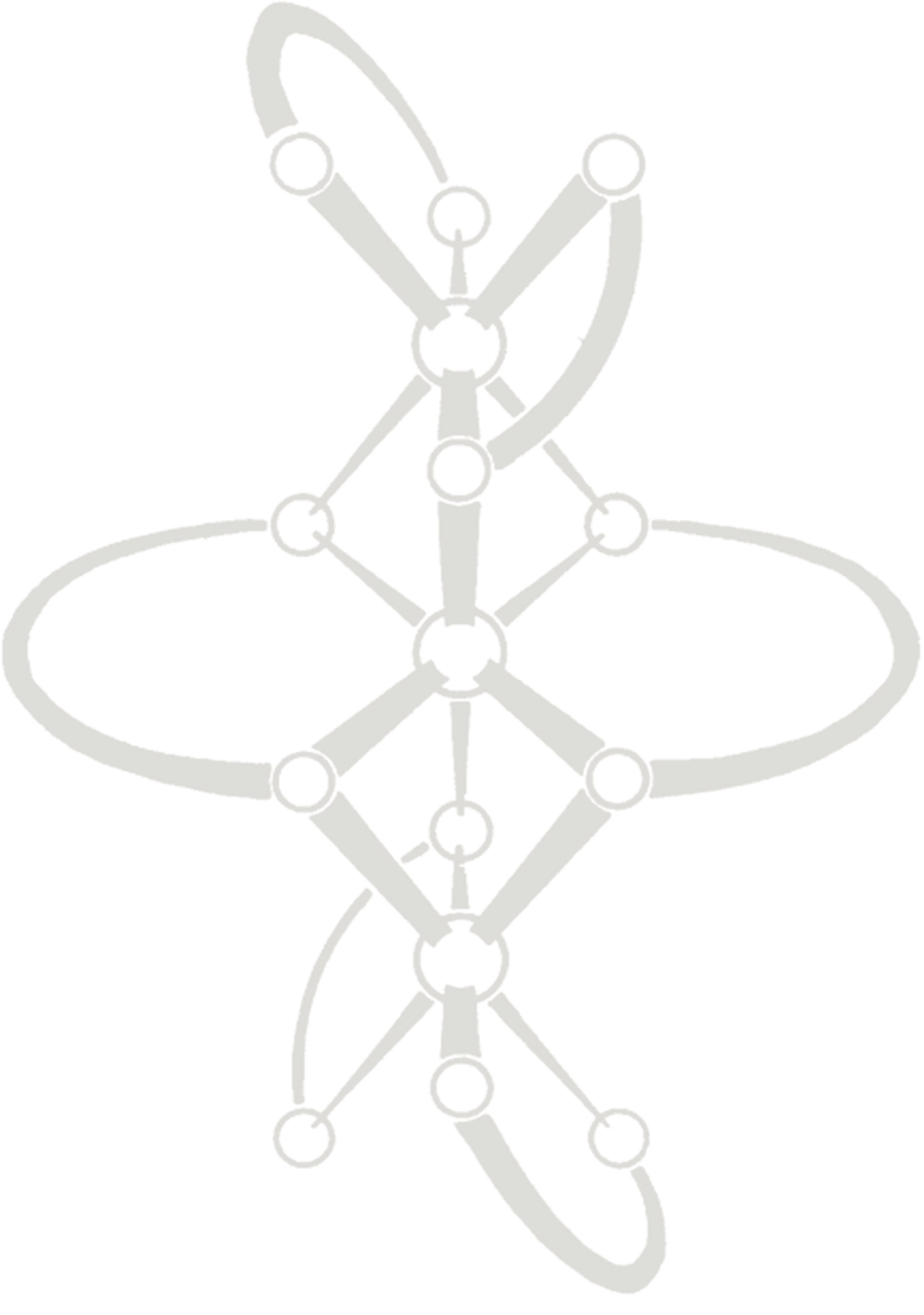

# Paper I

# Design of a compact UHV-compatible setup for the analysis of chemical vapor deposition processes

Theodor Weiss[1], Martin Nowak[1], Udo Mundloch[2,+], Volkmar Zielasek[1,*], Katharina Kohse-Höinghaus[2], Marcus Bäumer[1]
1. Institut für Angewandte und Physikalische Chemie, Universität Bremen, Leobener Straße UFT, D-28359 Bremen, Germany
2. Physikalische Chemie I, Fakultät für Chemie, Universität Bielefeld, Universitätsstraße 25, D-33615, Bielefeld, Germany

+) present address: ZMP, Friedrich Alexander Universität Erlangen-Nürnberg, Dr.-Mack-Straße 81, D-90762 Fürth, Germany
*) corresponding author

## Abstract

Optimizing thin film deposition techniques requires contamination-free transfer from the reactor into an ultrahigh vacuum (UHV) chamber for surface science analysis. A very compact, multifunctional Chemical Vapor deposition (CVD) reactor for direct attachment to any typical UHV system for thin film analysis was designed and built. Besides compactness, fast, easy, and at the same time ultimately clean sample transfer between reactor and UHV was a major goal. It was achieved by a combination of sample manipulation parts, sample heater, and a shutter mechanism designed to fit all into a NW38 Conflat six-ways cross. The present reactor design is versatile to be employed for all commonly employed variants of CVD, including Atomic Layer Deposition (ALD). A demonstration of the functionality of the system is provided. First results of the setup (attached to an Omicron Multiprobe XPS system) on the temperature dependence of Pulsed Spray Evaporation (PSE)-CVD deposition of Ni films from Ni acetylacetonate as the precursor demonstrate the reactor performance and illustrate the importance of clean sample transfer without breaking vacuum in order to obtain unambiguous results on the quality of CVD-grown thin Ni films. The widely applicable design holds promise for future systematic studies of the fundamental processes during chemical vapor deposition or atomic layer deposition.

**Keywords:** Chemical vapor deposition (CVD), Ultrahigh vacuum (UHV), Sample transfer, Pulsed spray evaporation (PSE), Metal acetylacetonates, Metal thin film, Nickel, XPS

## I. INTRODUCTION

Functional thin films are key for technological advances in many fields, including catalysis and microelectronics. For example, chemical vapor deposition (CVD) of thin metal films is widely used for producing protective and decorative coatings, active materials for sensors and catalysis, optical and magnetic elements, or electrical conductors in microelectronic devices.[1-5] Unlike other thin film deposition techniques such as, for example, evaporation or sputter deposition, metal CVD can be used to produce fibers, monoliths, foams, or powders of pure metals or alloys with free variation of the composition.[6] Using this method, coverage of three-dimensional structures with a conformal layer of metal and excellent reproducibility can be achieved as well.[7, 8] Furthermore, the metal CVD technique fits industry requirements of reliability and ease of use.[9] Nowadays, a variety of CVD methods are routinely used in industry. Most often employed are thermal CVD where precursor reaction or decomposition for metal deposition is activated by heating, plasma CVD with plasma-initiated reaction, and, as CVD-derivative, atomic layer deposition (ALD) which produces films in sequential, self-limiting layer-by-layer manner, using various reaction activation techniques.

The metal CVD precursors used in production can be divided in three classes. The first is inorganic precursors represented mainly by halides.[7] Unfortunately, metal films can be obtained only for a narrow range of metals from inorganic precursors. Often, halide contaminations are observed or technical and security problems have to be faced, such as corrosive byproducts or a tendency towards particle formation. Organometallic precursors (OM), as second and major class of precursors, cover a wider range of metals. OM precursors represent molecules with metal-carbon bonds with such ligands as carbonyl or cyclopentadienyl as well as methyl derivatives.[7, 10, 11] Metal centers in these precursors are mostly in their elemental oxidation state, facilitating the formation of a metallic film without strong reducing agents. However, the strength of the metal-carbon bonds may lead to the (co)deposition of metal carbides and graphitic carbon. Moreover, OM precursors are usually expensive, highly sensitive to air, moisture, or temperature and they are very toxic which requires handling and deposition in dry inert gases and glove boxes. Metal-organic precursors (MO) as a third class, mainly taken from the family of β-diketones[7], avoid many of the disadvantages of OM precursors but also present their own. For example, the metal center is bound to O, N, or S in a high-valence state so that strong reducing agents such as a $H_2$ stream or electron irradiation (plasma) are required which, in turn, pose safety or technology problems. Film contamination by carbon may be observed as well. Nevertheless, using MO precursors is generally seen as promising metallization CVD method if reducing agent safety and technology as well as carbon contamination problems can be solved.

A recently developed hydrogen-free approach to metal-CVD is based on pulsed spray evaporation delivery (PSE-CVD) of commercially available MO precursors, in particular acetylacetonates.[12-15] Alcohols are used as both, solvent and reducing agent, and permit deposition of metal films without employing gaseous hydrogen for precursor reduction. Compared to standard gas phase CVD, PSE-CVD poses less demand on the precursor in terms of volatility and stability because it can be spray-evaporated from liquid solution at room temperature and does not need to be heated for thermal evaporation. Any required stoichiometry can be adjusted easily in the solution if, for example, two different metal precursors need to be inserted for bimetallic depositions.[12, 16-19]

Surface science tools in ultrahigh vacuum (UHV) are indispensable for thin film analysis in research and laboratory in order to understand the deposition process and the resulting film properties, to characterize the film quality and for optimizing process parameters.[20-24] Ample publications on CVD-grown films, subsequently analyzed in UHV, show that the possibility of contamination-free sample transfer from the CVD reactor, typically at low vacuum, into a UHV chamber is an urgent need for unambiguous understanding of growth mechanisms and better control of film deposition. Only a narrow range of CVD processes, such as Si, SiGe or SiC film deposition at fairly high temperatures (500-950° C) from disilane $Si_2H_6$, germane $GeH_4$ or methylsilane $CH_3SiH_3$ or GaAs precipitation from trimethylgallium, is suitable for operation directly in an UHV chamber. Not only the range of precursors but also the range of deposition parameters applicable in an UHV setup is limited and typically different from industrially profitable.[25-29] Furthermore, organic precursors are prone to causing UHV chamber carbon contaminations.[30-32] Therefore, in general, CVD with large MO or OM precursor molecules and, moreover, PSE-CVD with precursors in liquid solution are incompatible with UHV conditions where gaseous precursors and reaction residues are required that can be easily pumped. Consequently, sample transfer between a CVD reactor and an UHV chamber for thin film analysis can usually not be avoided.

There are several approaches to avoid or alleviate the general problem of sample contamination during the transfer procedure. Capping of CVD-grown films for transfer by, for example, amorphous layers of As or As/P that can be removed by thermal treatment after transfer has been reported.[20, 21] However, contamination by diffusion of the capping material into the film as well as capping layer-induced surface modification cannot be excluded. In the case of As/P capping of InP(100) and GaP(100) surfaces it was observed that the surface reconstruction of the CVD-grown films is altered by capping.[33-35] An obvious way to minimize sample contamination is using an interim vacuum chamber for transfer between CVD reactor and UHV chamber.[36] There are no commercially available solutions so that a mobile UHV-compatible transport chamber with a pump and, typically, a battery for autonomous power supply as well as the gates and load locks of CVD reactor and UHV chamber have to be constructed individually. While it is a substantial advantage that CVD and UHV system may be completely separate units, transfer procedures via interim chambers tend to be time-consuming and elaborate for truly contamination-free operation. As an alternative approach, CVD reactors have been directly linked to UHV chambers via gate valves that are opened only for sample transfer.[37-39] Again, there are no commercial solutions available but this approach is most promising for clean, fast and effortless transfer if UHV chamber contaminations due to precursor adsorption on the sample holder, transfer rods or gate valves can be avoided and if restrictions due to limited space can be met.

In the following, we present the design of a transfer system that permits direct coupling of the deposition process to the UHV analysis, thus avoiding undesired post-process reactions. Such direct coupling is a prerequisite for mechanistic studies and potential process optimization. In a demonstration example we have coupled a homebuilt PSE-CVD reactor for direct attachment to a commercial UHV system used for thin film analysis. While parts and geometry of the deposition area of the reactor are based on previous developments,[12, 13] the design of sample holder and transfer mechanism is completely new, resulting in a thin film deposition reactor setup of very compact size which is based on many commercially available components, is relatively easy to assemble, and may be used with widespread UHV-compatible Omicron-type sample holders. The CVD setup accomplishes short pathways for transfer but maintains the individual pressure regimes of CVD reactor and UHV chamber well separated so that samples can be easily and quickly transferred without contaminating the sample surface or compromising UHV conditions. Furthermore, the reactor design is multifunctional – easy to use in PSE-CVD as well as in classical thermal CVD or ALD regimes. After any stage of a CVD or ALD growth process in the reactor, samples can be transferred quickly and cleanly to the UHV chamber for thin film analysis, allowing us to perform systematic studies on the influence of various CVD parameters on the growth kinetics. Thereby, a fundamental understanding of the reaction mechanisms of the chemical vapor deposition process gets within reach. In this article we focus on the general design ideas, construction details, highlights, and sketches of the reactor. The device capabilities are demonstrated by presenting experimental results on Ni films grown by PSE-CVD from $Ni(acac)_2$ precursor dissolved in ethanol.

## II. INSTRUMENTATION

The PSE-CVD reactor presented here was designed to be attached to the load-locks of two Multiprobe UHV systems by Omicron Nanotechnology available in our laboratory for thin film analysis which, in our case, comprise x-ray photoelectron spectroscopy (XPS), low-energy electron diffraction, scanning tunneling microscopy, Fourier-transform infrared spectroscopy, and temperature-programmed desorption spectroscopy as surface science tools. The design is not restricted to fit the Omicron instrumentation and permits facile adaptation to many other commercially available or homebuilt UHV systems. The following main design tasks were addressed and resolved in this project: The setup had to keep sample and UHV chamber clean and provide fast and effortless sample transfer between CVD and UHV environments. Compactness - sample holder and transfer to the load-lock had to fit into a Conflat (CF) 38 mm clear bore (NW 38 CF) six-way cross - was a critical parameter in view of restricted available space. Thereby, however, we did not allow for any compromise on the requirements of CVD and UHV pressure regimes, respectively.

### 1. Solving the contamination problem

In order to solve the contamination problem, we separated two areas within the CVD reactor: In the deposition area (Fig.1 (1)) the precursor spray is produced and carried by a carrier gas (typically $N_2$) to the sample surface. Preheating of all parts in this area avoids precursor adsorption on their walls. In the sample manipulation area (Fig.1 (2)) the sample temperature is controlled and all parts for sample transfer into the UHV load lock are located. Any contamination of the sample manipulation area can potentially reach the UHV chamber. Therefore, both areas must be well isolated from each other during deposition so that only the sample surface but not the sample holder or any part of the transfer mechanism is exposed to the CVD precursors. Rendering the sample quickly and easily movable for transfer despite isolation of the sample surface from all transfer parts during deposition is the major technical challenge. It was solved by a uniquely designed movable shutter (Fig.1 (3)) for separation of the deposition area from the sample manipulation area. First, an overview of its function is presented here.

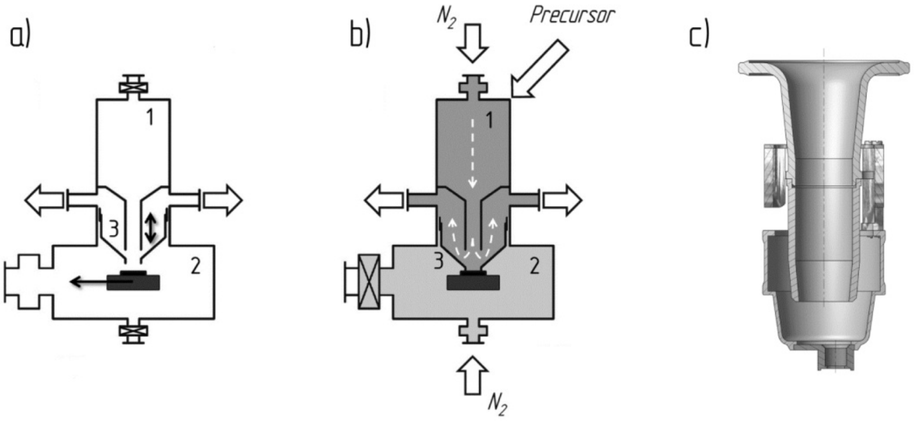

Fig.1. Schematic diagram of the CVD reactor depicting (1) deposition area (carrier gas preheating, spray evaporation, vacuum line), (2) sample manipulation area, and (3) movable shutter during (a) sample transfer (gate valve to load lock (not shown) on the left is open) and (b) deposition (gate valve to load lock closed, deposition and sample manipulation areas purged independently); (c) shows a cross-sectional drawing of the shutter (see also further details below and in the Supplement[40]).

The principle of CVD reactor operation using the movable shutter is as follows: For sample transfer (Fig. 1 (a)) the shutter is fixed in an upper position and the gate valve to the load lock (gate valve on the left side in Fig. 1(a), load lock is not shown) is open. With the shutter in upper position, there is enough space available to move the sample holder (mounted on a transport shuttle) out of the CVD position into the load lock and vice versa. The pressure in the CVD reactor, being now additionally pumped via the load lock, is typically as low as $10^{-4}$ Pa during transfer. During deposition (Fig. 1 (b)) the shutter is kept in a lower position so that its aperture is slightly pressed to the sample surface and openings between (1) and (2) are as small as possible. The deposition area and the sample manipulation area (the gate valve to the UHV load lock being closed) are pressurized individually by $N_2$ (or another carrier gas) in such way that the pressure in (2) is somewhat higher than in (1) in order to prevent gas flow from the deposition to the sample manipulation zone through rest leaks. The precursor mixture then passes the deposition area - where pressure is kept in the range required for CVD - and reaches through the aperture of the shutter the sample surface which is kept at the required deposition temperature. Unreacted precursor, solvent, and reaction byproducts are pumped off via outlets of the deposition area to a vacuum line. Details on the shutter construction as well as the transfer procedure from CVD to UHV will be given later. Overall we find that the shutter maintains the sample manipulation area clean and contamination of load lock or UHV chamber during transfer is negligible.

## 2. General arrangement

A drawing to scale of the fully assembled CVD reactor is shown in Fig. 2. The reactor, connected to the load lock of the UHV chamber via a CF 38 gate valve, has a small lateral footprint, i.e., there are no protruding parts which could complicate positioning and connection to the Omicron Multiprobe system.

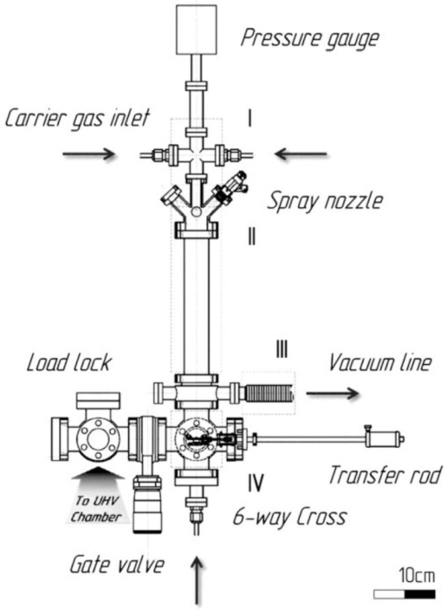

Fig.2 Drawing to scale of the assembled CVD reactor attached to the UHV chamber. I – Carrier gas preheating zone, II – Spray evaporation zone, III – Vacuum line, IV – Sample manipulation area with parts for sample transfer and gate valve to the UHV chamber load lock.

The deposition area of the reactor is designed close to previous developments[12, 13] and comprises a carrier gas supply and preheating zone (I), and a spray injection, evaporation and delivery zone (II). (see Fig.2). Carrier gas preheating in zone (I) avoids spray condensation in zone (II) where the precursor is injected by a piezo-driven spray nozzle, operated by low-voltage direct current pulses. The tube size (diameter 40 mm, length 250 mm) of the evaporation and delivery zone (II) provides homogeneous distribution of precursor spray in the carrier gas and uniformity of the precursor mixture in case of multicomponent systems. Preheating of this zone as well as the vacuum line (III) prevents precursor adsorption on the walls of reactor or vacuum line. Almost all components of the deposition area are commercially available. More technical details can be found in section A of the supplementary material.[40]

The homebuilt sample manipulation area (IV) (see Fig.2) which will be described in detail in the following sections, comprises the sample holder, the transfer mechanism, and the shutter between deposition and sample manipulation area, all placed inside the CF 38 six-way cross. The sample is mounted on an Omicron-type sample holder which slides into a mobile platform for transfer (shuttle) with heater and thermocouple contacts. The reactor is completed by a support system including gas supply, pressure control, temperature control, and precursor delivery systems which will be detailed in the section B of the supplementary material.[40] Overall, the designed reactor has a very compact size, is relatively easy to assemble, and should be attachable to any UHV chamber after manageable adaptations.

## **3. Design of the sample manipulation area including shutter and transfer mechanism**

As mentioned before, the entire sample manipulation area including the shuttle and all parts for transfer should be shielded from the sample surface as much as possible during the CVD process to avoid contamination with the precursor whereas, during sample transfer, the shield has to provide enough clear space for sample motion. Furthermore, sample holder and shuttle must provide sample heating and temperature measurement for sample temperature control during CVD. At the same time all components of this area have to fit into a CF 38 six-ways cross so that the reactor can be attached to the Omicron Multiprobe load-lock.

All these requirements have been implemented in the design of the parts for sample manipulation shown as perspective views in Fig. 3. Shown are the sample holder (1) the shuttle (2), a docking station for the shuttle (3), the homebuilt head of a mini linear-rotary drive for motion of the shuttle (4), electrical contacts for power supply to a ceramic heater (5), and the shutter separating the sample manipulation area from the deposition area (6). The functionality of these parts is indicated in Fig. 3 a) while Fig. 3 b) depicts their full assembly in a CF 38 six-ways cross.

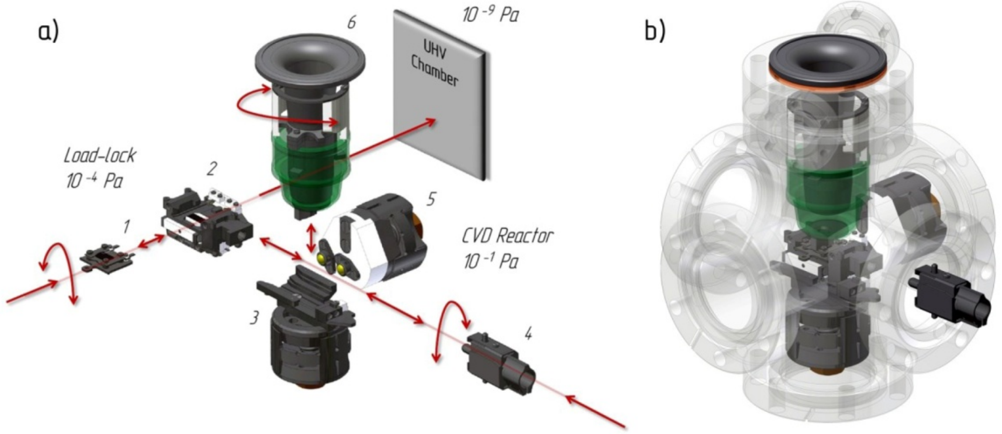

Fig.3. Perspective views of the sample manipulation parts, (a) indicating their functionality, (b) showing full assembly in a CF 38 six-ways cross. 1) sample holder, 2) mobile platform (shuttle), 3) docking station for shuttle with the contacts for the thermocouple, 4) head of a mini linear-rotary drive for motion of the shuttle, 5) electrical contacts for heater, 6) shutter between deposition and sample manipulation area.

The sample holder (1) is a modified Omicron-type sample holder. Details on the modifications will be given later. In the load lock, the sample holder can slide in and out of the shuttle (2) before release or after pickup by a linear-rotary motion drive (not shown in Fig. 3) which is used for transferring the sample holder into the UHV chamber. The shuttle has a homebuilt bayonet-type connector which enables its pickup by the mini linear-rotary drive (4) for transporting the shuttle from the load lock to the docking station (3) and vice versa. In the docking station, the shuttle provides sample heating and electrical contacts for a K type sample holder thermocouple. For that purpose a ceramic chip heater and 2-pin socket type connectors and conductors (Ni, NiCr, and 2 lines for the heater) are integrated in the shuttle. The docking station serves for automatic centering of the position of the shuttle with respect to the three spatial coordinates, provides contacts for the thermocouple, and has vents for pressurizing the sample manipulation area with $N_2$ gas. Electrical power for the heating element is supplied to the shuttle via two clamping ball contacts mounted on a glass-ceramic (Marcor) plate for electrical insulation from the reactor body (5). These clamping ball contacts are also used to fix the shuttle in position for CVD within the docking station. As remuneration of the elaborate design of such a relatively large number of reliable electrical contacts within the restricted space there is no need to connect the shuttle with flexible electrical wires. These would need more space and be prone to tangling problems during the transfer procedure.

The shutter (6) consists of a stationary nozzle fixed between flanges on top of the six-ways cross and a similarly shaped part acting as movable mask which is suspended below the nozzle. The stationary nozzle centers and holds the mask which has an aperture in the size of the sample surface area to be exposed to the CVD precursor. The motion of the mask is driven by magnets (two NdFeB N45 disc magnets) from the outside. For that purpose, all shutter components are made of nonmagnetic stainless steel except for two magnetic steel parts mounted on top of the mask. It can be lifted upwards and rotated by 55 degree into a locked position (transfer regime), or rotated back and moved downwards to rest on the sample holder (deposition regime - leaks between sample manipulation and deposition areas as small as possible, sample surface directly underneath the mask's aperture). For further details on the shutter design see in the section C of the supplementary material.[40]

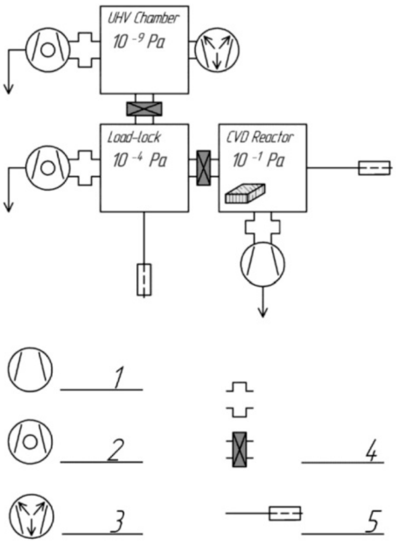

Fig.4. Scheme illustrating major parts of the vacuum system. 1) Scroll pump, 2) Turbo pump, 3) Ion getter pump, 4) Gate valves, 5) Linear-rotary drives.

Overall, we employ the following transfer procedure (c.f. Fig. 4): After finishing a deposition process, the reactor is pumped by a scroll pump (oil-free) attached to the vacuum line of the deposition area, reaching a lowest pressure in the range $10^{-1}$ Pa. Then the shuttle including the sample holder is transferred from the CVD reactor to the load lock of the UHV chamber (Operation of the shutter during this transfer has been described before, see section 1.). Being now pumped by the turbo molecular pump of the load lock, the reactor pressure typically drops to ~$10^{-4}$ Pa. In the load lock, the sample is then picked up from the shuttle, the shuttle is moved back to the docking station, and the gate valve between CVD reactor and load lock is closed. After further pumping and, optionally, bake-out of the load lock, the sample is transferred into UHV chamber which has a base pressure of ~$10^{-9}$ Pa maintained by a turbomolecular pump and an ion getter pump. During this last transfer step the pressure in the UHV chamber typically remains below $10^{-6}$ Pa even without bake-out of the load lock.

The pressure conditions have been well maintained over more than hundred PSE-CVD and transfer cycles, meanwhile, providing evidence for the cleanness of the entire procedure. We have found neither any impurity traces in the load-lock and the UHV chamber, nor any traces of metal deposition or condensed precursor on parts of the sample manipulation area (gate valve, linear rotary drive, docking station, shuttle, clamping ball contacts) of the reactor. The design of the sample manipulation area combines small size and modularity, allowing for quick repair with contamination-free operation. It should be noted that separation of deposition and sample manipulation areas within the CVD reactor by means of the movable shutter, as described above, is crucial for the cleanness of sample transfer. Without the shutter, we have observed creeping contamination such as, e.g., precursor condensation at the gate valve or metal deposition on all insulating parts.

## 5. Sample heating

There are various approaches to sample heating typically used in CVD reactors or in UHV environments. Some tools like infrared radiators, ceramic heaters, or plasma sources typically require significant amount of space and may heat up not only the sample but significant portions of surrounding parts. In view of application in the designed PSE-CVD reactor, unwanted metal film deposition on surrounding parts such as the shutter or the reactor walls may be the consequence. A hot filament for radiative or electron-beam heating can generate heat in a more localized fashion.

Being limited with space, we first tested radiative heating by a tungsten filament as frequently used in UHV setups. Aiming at a temperature range of ~150-350° C, however, we obtained only poor control of the heating rate and had difficulties maintaining and not overshooting a predetermined temperature. Obviously, the employed PID controller (Eurotherm 3504) lagged because of the large temperature gradient between the hot filament and the sample surface. Our requirements concerning compactness, cleanness, and good temperature control in the desired range were finally met by a ceramic chip heater (Model BACH-RC Chip heater, 24 V, 50 W). Critical for its use is good mechanical contact between heater surface and sample for heat transfer. For that purpose we modified the Omicron-type sample holder with several newly designed components. (c.f. Fig. 5): Through a center hole in the sample holder base plate a molybdenum plate carrying the sample is pushed downwards by four tiny springs in order to let the molybdenum carrier plate protrude below the base plate. At the same time, the springs are also used to press the sample via two Mo clamps onto the carrier plate.

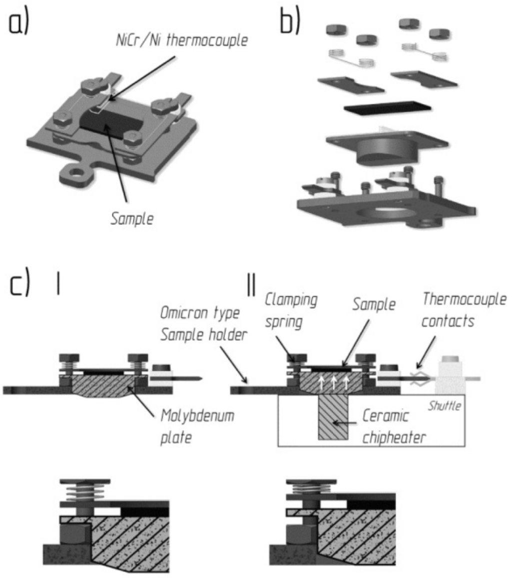

Fig.5. Drawings of the modified Omicron-type sample holder: (a) fully assembled, (b) exploded view, (c) sectional views and details showing the spring-suspended molybdenum sample carrier plate (I) protruding below the base plate and (II) being pressed against the heater surface when the sample holder is in the shuttle.

When the sample holder slides into the shuttle with the integrated ceramic heater, the molybdenum carrier plate is pushed upwards, further compressing the springs (see Fig. 5 c) which now provide the required direct mechanical contact between ceramic heater and sample. The sample holder does include 2-pin contacts for attaching a thermocouple Type K to the sample surface. Optimal sample geometry is 7 mm x 14 mm surface area and a thickness in the range of 0.3-1.5 mm. Despite the modifications, the total height of the sample holder is only 5 mm (maximum length of the springs 2 mm) which is fully compatible with our Omicron Multiprobe UHV systems. Thereby, the spring system allows fast and easy sample mounting and, in combination with the small and powerful ceramic chip heater, provides homogeneous sample heating and fast thermoregulation response.

Sample temperatures of up to 500° C can be achieved with the chip heater. If higher temperatures are required, a hot filament may be employed for sample heating in our setup. To ensure stability of the glass ceramic insulation of the shuttle, the sample temperature should then not continuously exceed 800°C. To complete information on the temperature range at which our CVD setup can be operated, it should be also noted that the parts of the spray evaporation zone will withstand temperatures up to 450° C. We tested the spray nozzle for PSE-CVD up to 250°C and found it fully operable. The periphery of the reactor's sample manipulation area such as the gate valve and the linear rotary drive should be kept below 150°C and 200°C, respectively.

## **III. EXPERIMENTAL TESTS**

In order to evaluate the performance of the CVD reactor and the cleanness of its operation, we deposited Ni on SiOx/Si(100) using pulsed spray evaporation of $Ni(acac)_2$ in ethanol as precursor. We chose this reaction as model reaction because first experiences with this CVD process have already been published [12, 13] so that information on the approximate range of optimal deposition parameters and the film quality to be expected is available [13, 19] and can be used as benchmark for our tests.

## 1. Experimental details for PSE-CVD of Ni films

All depositions were implemented in the PSE-CVD setup described above. Zones I and II of the reactor (c.f. Fig. 2) were heated up to 225° C to ensure fast and uniform heating of the carrier gas while zones III and IV were heated to 170° C which is the minimum temperature needed to avoid undesirable condensation of $Ni(acac)_2$ on the reactor walls. Decomposition of this precursor starts at much higher temperature.[1, 12, 41] All other experimental depositions parameters (see Table 1) were chosen on the basis of previous publications.[12, 13, 19]

Table 1. PSE-CVD reactor parameters for Ni metal film depositiom

| | |
|---|---|
| Precursor: | $Ni(acac)_2$ |
| Solvent: | Ethanol |
| Concentration of the precursor [mmol/l] | 2.5 |
| Spray pulse frequency [Hz] | 2 |
| Spray pulse width [ms] | 15 |
| Deposition area pressure [Pa] | $5 \cdot 10^3$ |
| Carrier gas flow rate [sml/min] | 500 |
| Substrate temperature [° C] | 270 |
| Total duration of deposition [min] | 30 |

For all depositions discussed in the following, 2.5 mM solution of the commercially available 95% $Ni(acac)_2$ (Sigma-Aldrich) in absolute ethanol (VWR Chemicals) was used. For precursor delivery via the spray nozzle a solenoid valve pulse frequency of 2 Hz and a spray injection phase of 15 ms were used, meaning that the solenoid valve opened two times per second for 15 ms, i.e., at a total deposition time of 30 min the net injection time was 54 s. The pressure in the deposition area was kept at the required level by controlling the pump capacity via a motorized butterfly valve in front of the pump. The sample surface temperature was adjusted and stabilized by an electronic controller as well.

Film deposition was carried out as follows: 160.6 mg of the Ni precursor was weighed and dissolved in 250 ml alcohol to provide the required 2.5 mM feedstock concentration. The solution was ultrasonically shaken to achieve complete dissolution. A piece from a Si(100) wafer was cut as substrate, cleaned with isopropanol in an ultrasonic bath, and dried in air. The CVD reactor was evacuated and the sample was transferred via the load-lock into the reactor. Then the reactor and the substrate were heated up to the desired temperatures and $N_2$ was let into the deposition area and the sample manipulation area as carrier and purging gas, respectively, using a calibrated mass flow controller. The required pressure was adjusted (see supplementary material (section B)[40] for details) and then deposition was started. After the deposition process was finished, the carrier gas flow was switched off so that pressure dropped. After it reached the $10^{-1}$ Pa regime, sample transfer to the load-lock and into UHV for XPS analysis was performed.

## 2. Benefit of direct transfer between CVD reactor and UHV chamber

The following set of experiments demonstrates the importance of sample transfer from the CVD reactor to surface analysis tools without interrupting vacuum, in order to obtain reliable results on the CVD process. A thin Ni film was freshly prepared by PSE-CVD on the Si wafer substrate (a native or thermal silicon oxide layer on Si(100)) and transferred into the UHV chamber for XPS analysis under high vacuum conditions directly afterwards. The obtained XP spectrum within the region of Ni2p emissions (shown in the upper panel of Fig. 6) was normalized and then fitted using the FITT software (Seoul National University). For the fit a Shirley-type background was taken into account. The red and green curves in Fig. 6 denote emissions from reduced Ni ($Ni^0$) with binding energies 852.0 and 859.2 eV. The blue and purple curves represent emission from oxidized Ni ($Ni^{2+}$) (binding energies 855.6 and 861.0 eV). Obviously, the freshly prepared Ni film was almost completely reduced as it comprises more than 95% metallic Ni. Thereafter the sample was transferred out of the UHV chamber, let rest in the air atmosphere for one hour, and transferred back into UHV. A subsequent XP spectrum (bottom panel in Fig. 6) revealed that only 60% of the surface Ni had remained metallic after this treatment. It can be concluded that even short sample transfers within minutes through air would significantly deteriorate the CVD-grown Ni film and that contamination-free transfer is a prerequisite for reliably estimating the influence of deposition parameters in the CVD reactor.

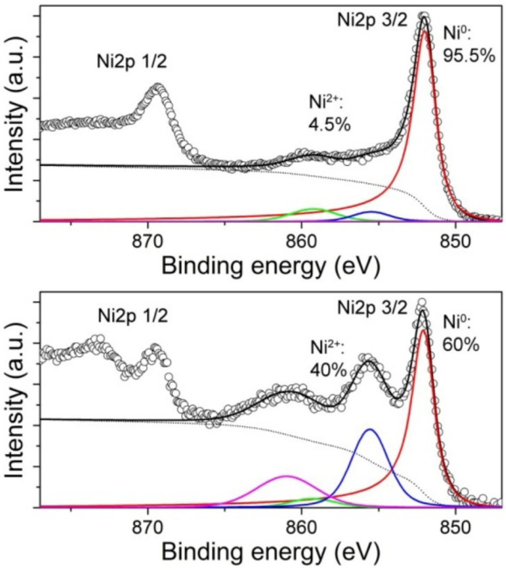

Fig.6. Ni2p XPS signal of a thin Ni film deposited on SiOx/Si(100). Upper panel: freshly prepared film directly transferred into UHV; bottom panel: after resting in ambient conditions (in air) for 1 hour.

In order to estimate the thickness of the deposited Ni film and determine a growth rate for our reactor, the attenuation of the Si 2p XPS signal from the Si substrate after Ni metal film deposition was determined. Based on the assumption that the metal film is homogeneously thick with bulk-like density and that it completely covers the Si substrate, the attenuated integral intensity $I_s$ of the Si 2p peaks should correspond to

$$I_s = I_s^0 exp\left(\frac{-t}{\lambda \cdot \cos\alpha}\right)$$

where $I_s^0$ is the Si 2p peak intensity of the clean substrate, $\lambda$ is the inelastic mean free path of the photoelectrons in Ni ($\lambda$ = 1.865 nm [42]), $\alpha$ = 0° is the angle of electron detection with respect to the surface normal, and $t$ is the film thickness. $I_s^0$ and $I_s$ were determined from the fitting routine which yielded $I_s/I_s^0$ as ~1/87. The calculated film thickness of 8.3±0.2 nm corresponds to a growth rate of ~9 nm/min. As deposition time we take here the net spray injection time, i.e., without purging phases in between. This value for the growth rate is in good agreement with previous results (~7-10 nm/min) obtained with a stand-alone PSE-CVD reactor of similar design.[12]

## 3. Effect of deposition temperature on growth process

Previous work [12, 13, 19] found 230-310° C as deposition temperature range for growing Ni metal films of good quality, i.e., with metallic conductivity and a low degree of contaminations. Using our setup we aimed at identifying an optimal deposition temperature within that range and hoped to thereby better understand the influence of temperature on the deposition process.

Ni was deposited on SiOx/Si(100) substrate samples as described before at various sample temperatures in the range 230 to 310° C (at steps of 20°) and transferred under high vacuum conditions into the UHV chamber for XPS analysis. The $Ni^{2+}/Ni^0$ intensities ratio determined from the integral Ni 2p peak intensities is shown in the left panel of Fig. 7 as a function of the sample temperature during deposition. Clearly, the highest concentration of $Ni^{2+}$ is observed at the lowest deposition temperature. With increasing deposition temperature, the content of reduced $Ni^0$ increases, until at 270° C and above the film contains almost only metallic Ni. The right panel of Fig. 7 provides information on the amount of carbon contamination at the surface and in the film. It shows the ratio of the integral C 1s and Ni 2p peak intensities ($C_{SUMM}/Ni_{SUMM}$ ). While $C_{SUMM}/Ni_{SUMM}$ varies only in the range ~1.0-1.3 within the deposition temperature range 230-310° C, the XPS analysis indicates the lowest carbon concentration for 270° C.

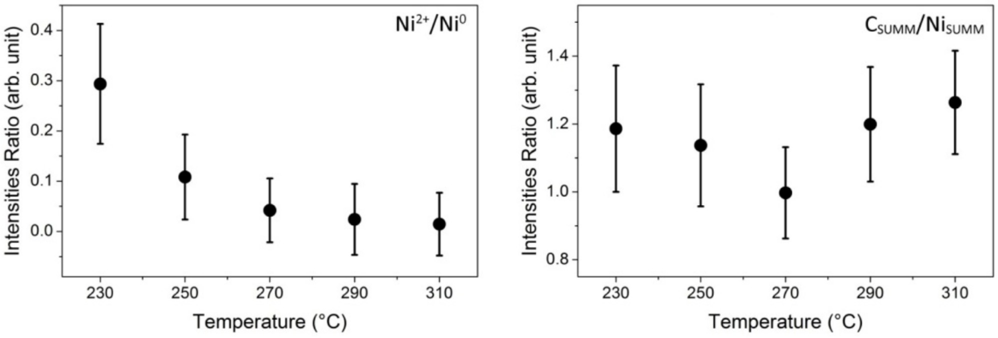

Fig.7. Changing the intensities ratio of the Ni2p XPS signals for $Ni^{2+}/Ni^0$ (left) and $C_{SUMM}/Ni_{SUMM}$ (right) at various deposition temperatures.

Tentatively, at this stage, we interpret the results as follows: Below 270° C, precursor decomposition is probably incomplete, i.e., undecomposed precursor remains at the surface and contributes to the detected amount of carbon contamination and oxidized Ni. The increase of the carbon signal at sample temperatures above 270° C during deposition may indicate that the precursor is already overheated, i.e., the residues from its decomposition do not completely desorb but are fragmented, producing carbon black in the film. Overall, within the range 230 to 310° C proposed before[12, 13] we identify 270° C as optimal temperature for PSE-CVD with Ni(acac)$_2$ precursor on SiOx/Si(100) surfaces.

The morphology of the deposited films was assessed using a Carl Zeiss Ultra Plus Field Emission scanning electron microscope (SEM). The samples prepared at 230° C, 270° C, and 310° C were selected for SEM analysis, the results are shown in Fig.8.

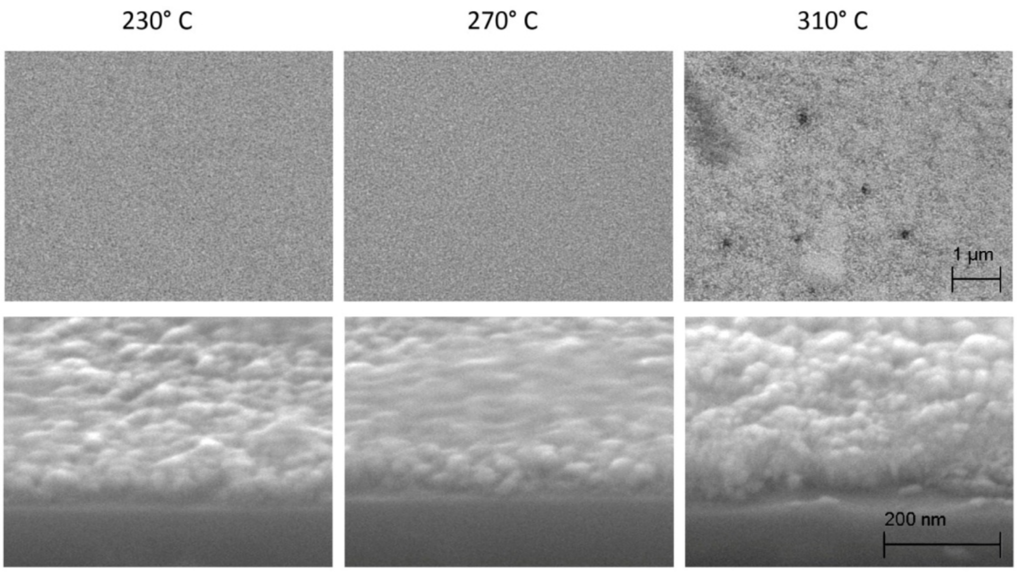

Fig. 8. SEM of SiOx/Si(100) substrate coated with Ni films at 230, 270, and 310° C. Upper row: plane view on the Ni-covered substrate surface (scale bar 1 µm); bottom row: enlarged view (scale bar 200 nm, viewing angle ~60° with respect to surface normal) of cleaved sample edge showing substrate (bottom) and Ni deposits on top.

The nickel films deposited at 230 or 270°C appear to be closed and composed of grains with diameters on the order of some ten nanometer (The surface of the film deposited at 270° appears to be somewhat smoother than of that deposited at 230° C). Films obtained at 310° C present a coarser morphology with smaller, more heterogeneously sized grains. Furthermore, SEM of the film deposited at 310°C reveals pronounced defects (see upper panel of Fig. 8) which may represent gaps in the metal film.

In addition to the morphology, the nickel layer thickness was estimated by means of SEM. The films were imaged in cross section at a cleaved substrate edge as shown in the lower panel of Fig. 8. In contrast to Fig. 8, however, the angle of sample rotation was adjusted in order to obtain a projection along the substrate surface plane so that the metal layer thickness could be directly measured in the

SE micrographs. The measured thickness values are 29 nm, 38 nm, and 25 nm for films deposited at 230° C, 270° C, and 310° C, respectively. These numbers are about four times higher than the values estimated from attenuation of the Si 2p XPS signal (6.7 nm, 8.3 nm, and 6.1 nm, resp.) which may be due to the granular structure of the Ni films and due to carbon contaminations, rendering the Ni films less dense than a perfectly epitaxial metal layer. Overall, however, also SEM confirms that the smoothest morphology and the highest growth rates are obtained at 270° C sample temperature during PSE-CVD of Ni films from Ni(acac)$_2$, in good agreement with the XPS results.

## IV. SUMMARY AND OUTLOOK

A very compact, UHV-compatible setup for pulsed spray evaporation-CVD of metals was designed and built to be directly attached to a commercial Omicron Multiprobe UHV system for surface and thin film analysis. In order to achieve full compatibility with the UHV system, the sample was kept on a small Omicron-type sample holder throughout the entire setup. Fast and at the same time contamination-free sample transfer between the CVD reactor part and UHV could be achieved by a uniquely designed shutter mechanism, separating a deposition area from an area for sample manipulation within the reactor housing. Shutter, sample manipulation parts, and a ceramic chip heater for the sample fit all into a Conflat 38 six-ways cross. In order to achieve good thermal contact between chip heater and sample, a spring-suspended sample base plate was added to the Omicron-type sample holder without compromising compatibility with the UHV system. Apart from parts for sample manipulation and transfer, many commercially available components were used for the reactor. Its modular design should be easily adaptable to any typical commercial or non-commercial UHV system.

Attached to an Omicron Multiprobe system equipped with XPS, the setup was tested by PSE-CVD deposition of Ni films from Ni acetylacetonate on 4 mm x 7 mm sized pieces of Si wafer as substrate. From the attenuation of the Si 2p XPS signal, a Ni deposition rate of 9 nm / min was determined for the reactor, in good agreement with stand-alone PSE-CVD reactors of similar type. The possibility of direct transfer between the reactor and the UHV system, i.e., without breaking vacuum, allowed for a refined systematic study on the influence of sample temperature on film composition and rendered 270° C as optimal for the growth of Ni metal films with lowest carbon contamination. XPS also showed that even a reasonably quick transfer of Ni films through air from, e.g, a stand-alone CVD reactor would quickly alter the film by significant Ni oxidation.

Ongoing experiments focus on systematic studies of the influence of various PSE-CVD parameters on the growth kinetics of transition metal films and aim at a fundamental understanding of the reaction mechanisms of the metal deposition process. In planned experiments the reactor will be employed also for similar studies on classical thermal CVD or Atomic Layer Deposition processes for which it is suited as well. The design for the direct coupling of the thin film deposition process with the surface analysis and facile transfer under UHV conditions presented here will facilitate the systematic study of such experiments and enable a more reliable, detailed characterization of the pertinent parameters of influence that are a prerequisite for optimization.

## ACKNOWLEDGMENTS

Assistance with scanning electron microscopy by Petra Witte (Geosciences department of the University of Bremen) and with setting up electronics for the support systems by Bogdan Tuschik is gratefully acknowledged. The project has been funded by the German Research Foundation (joint project BA 1710/20-1 and BA 2307/3-1)

## REFERENCES

1. M. Utriainen, M. Kröger-Laukkanen, L.-S. Johansson and L. Niinistö, Appl Surf Sci **157** (3), 151-158 (2000).
2. P. A. Lane, P. E. Oliver, P. J. Wright, C. L. Reeves, A. D. Pitt and B. Cockayne, Chemical Vapor Deposition **4** (5), 183 (1998).
3. V. V. Bakovets, V. N. Mitkin and N. V. Gelfond, Chemical Vapor Deposition **11** (8-9), 368-374 (2005).
4. T. Kada, M. Ishikawa, H. Machida, A. Ogura, Y. Ohshita and K. Soai, Journal of Crystal Growth **275** (1-2), E1115-E1119 (2005).
5. K. Wetzig and C. M. Schneider, *Metal based thin films for electronics*, 2nd, rev. and enl. ed. (Wiley-VCH, Weinheim, 2006).
6. H. O. Pierson and H. O. Pierson, *Handbook of chemical vapor deposition (CVD) : principles, technology, and applications*, 2nd ed. (Noyes Publications/William Andrew Pub., Norwich, N.Y., 1999).
7. T. T. Kodas and M. J. Hampden-Smith, *The chemistry of Metal CVD*. (VCH, Weinheim ; New York, 1994).
8. J. Lee, H. J. Yang, J. H. Lee, J. Y. Kim, W. J. Nam, H. J. Shin, Y. K. Ko, J. G. Lee, E. G. Lee and C. S. Kim, J Electrochem Soc **153** (6), G539-G542 (2006).
9. P. M. Martin, *Handbook of deposition technologies for films and coatings : science, applications and technology*, 3rd ed. (Elsevier, Amsterdam ; Boston, 2010).
10. L. Brissonneau and C. Vahlas, Ann Chim-Sci Mat **25** (2), 81-90 (2000).
11. E. P. Boyd, D. R. Ketchum, H. Deng and S. G. Shore, Chem Mater **9** (5), 1154-1158 (1997).
12. P. A. Premkumar, N. Bahlawane and K. Kohse-Hoinghaus, Chemical Vapor Deposition **13** (5), 219-226 (2007).
13. P. A. Premkumar, N. Bahlawane, G. Reiss and K. Kohse-Hoinghaus, Chemical Vapor Deposition **13** (5), 227-231 (2007).
14. M. Oshima, A. Komeda, K. Tominaga, M. Nakao, T. Shimizu, J. Senda and K. Ishida, Heat Transfer-Asian Research **38** (5), 284-296 (2009).
15. L. Gao, P. Härter, C. Linsmeier, J. Gstöttner, R. Emling and D. Schmitt-Landsiedel, Materials Science in Semiconductor Processing **7** (4–6), 331-335 (2004).
16. M. J. Crosbie, P. A. Lane, P. J. Wright, D. J. Williams, A. C. Jones, T. J. Leedham, C. L. Reeves and J. Jones, Journal of Crystal Growth **219** (4), 390-396 (2000).
17. S. Krumdieck and R. Raj, Surf Coat Tech **141** (1), 7-14 (2001).
18. S. Pasko, A. Abrutis, L. G. Hubert-Pfalzgraf and V. Kubilius, Journal of Crystal Growth **262** (1-4), 653-657 (2004).
19. N. Bahlawane, P. A. Premkumar, Z. Tian, X. Hong, F. Qi and K. Kohse-Höinghaus, Chem Mater **22** (1), 92-100 (2009).
20. M. Kawase, Y. Ishikawa and T. Fukui, Appl Surf Sci **130**, 457-463 (1998).
21. L. Li, B. K. Han, Q. Fu and R. F. Hicks, Phys Rev Lett **82** (9), 1879-1882 (1999).
22. K. Lüdge, P. Vogt, O. Pulci, N. Esser, F. Bechstedt and W. Richter, Phys Rev B **62** (16), 11046-11049 (2000).
23. P. A. Premkumar, A. Turchanin and N. Bahlawane, Chem Mater **19** (25), 6206-6211 (2007).
24. N. Bahlawane, P. A. Premkumar, F. Reilmann, K. Kohse-Hoinghaus, J. Wang, F. Qi, B. Gehl and M. Baumer, J Electrochem Soc **156** (10), D452-D455 (2009).
25. B. S. Meyerson, Appl Phys Lett **48** (12), 797-799 (1986).
26. B. S. Meyerson, P Ieee **80** (10), 1592-1608 (1992).
27. M. Racanelli and D. W. Greve, Appl Phys Lett **56** (25), 2524-2526 (1990).
28. T. N. Adam, S. Bedell, A. Reznicek, D. K. Sadana, A. Venkateshan, T. Tsunoda, T. Seino, J. Nakatsuru and S. R. Shinde, Journal of Crystal Growth **312** (23), 3473-3478 (2010).
29. T. N. Adam, S. Bedell, A. Reznicek, D. K. Sadana, R. J. Murphy, A. Venkateshan, T. Tsunoda, T. Seino, J. Nakatsuru and S. R. Shinde, Ecs Transactions **33** (6), 149-154 (2010).
30. J.-P. Lu, R. Raj and A. Wernberg, Thin Solid Films **205** (2), 236-240 (1991).
31. N. Pütz, H. Heinecke, M. Heyen, P. Balk, M. Weyers and H. Lüth, Journal of Crystal Growth **74** (2), 292-300 (1986).
32. E. Tokumitsu, Y. Kudou, M. Konagai and K. Takahashi, J Appl Phys **55** (8), 3163-3165 (1984).
33. P. Vogt, T. Hannappel, S. Visbeck, K. Knorr, N. Esser and W. Richter, Phys Rev B **60** (8), R5117-R5120 (1999).

34. L. Töben, T. Hannappel, K. Möller, H. J. Crawack, C. Pettenkofer and F. Willig, Surf Sci **494** (1), L755-L760 (2001).
35. W. G. Schmidt, F. Bechstedt, N. Esser, M. Pristovsek, C. Schultz and W. Richter, Phys Rev B **57** (23), 14596-14599 (1998).
36. T. Hannappel, S. Visbeck, L. Töben and F. Willig, Review of Scientific Instruments **75** (5), 1297-1304 (2004).
37. S. Yoshiki, K. Kunihiko and O. Masashi, Jpn J Appl Phys **27** (11A), L2189 (1988).
38. M. Kasu and N. Kobayashi, J Appl Phys **78** (5), 3026-3035 (1995).
39. L. Li, B. Han, S. Gan, H. Qi and R. F. Hicks, Surf Sci **398** (3), 386-394 (1998).
40. See supplemental material at [URL will be inserted by AIP] for CVD reactor construction details.
41. M. A. Siddiqi, R. A. Siddiqui and B. Atakan, Surface and Coatings Technology **201** (22–23), 9055-9059 (2007).
42. C. J. Powell and A. Jablonski, National Institute of Standards and Technology, Gaithersburg, MD (2011).

# Design of a compact UHV-compatible setup for the analysis of chemical vapor deposition processes

Theodor Weiss[1], Martin Nowak[1], Udo Mundloch[2,+], Volkmar Zielasek[1,*], Katharina Kohse-Höinghaus[2], Marcus Bäumer[1]

## - Supplementary Material -

**A) CVD reactor construction details**

Intentionally, design and construction of the PSE-CVD setup have been based on many commercially available parts, in order to allow for quick assembly of the reactor. Here we first provide a list of the vacuum parts, ordered top-down according to the four sections I-IV denoted in Fig.2 of the main text:

I) Carrier gas supply zone:

- MKS Baratron Capacitance Manometer
- DN16CF tube, 76 mm length (serves as spacer between the capacitance manometer and the precursor spray inlet. Moreover it prevents overheating of the pressure gauge)
- 4-ways DN16CF cross, 76 mm length, with two DN16CF flange adaptors to Swagelok ¼” gas inlet lines

II) Spray evaporation and gas delivery zone:

- Multi-mini flange DN38CF to 5xDN16CF
- Home-made DN16CF flange adaptor to Bosch Injector
- Removable Bosch injector (fuel injector for automotive applications)
- 250 mm length tube DN38CF

Optionally, a second Bosch injector may be installed, e.g., for simultaneous or subsequent deposition of a second liquid precursor which may be interesting for ALD.

III) Vacuum line:

- Flexible DN16CF metal hose, 750 mm length and hydraulically formed, connected to a Liquid $N_2$ trap. (see pressure control system described in Part B of the supplementary material)

IV) Sample manipulation area:

- DN38CF distance flange (25 mm length) with a DN16CF flange sideways, to which the vacuum line is connected.
- Six-ways DN38CF cross (with rotatable flanges)
- DN 38CF flange with electrical feedthroughs (two contacts for thermocouple type K (chromel/alumel) and two nickel conductors (Max current 16.5 A))
- Linear-Rotary Ferrovac MD16-150mm feedthrough - most compact commercially available design
- Viewport DN38CF
- DN38CF adaptor leading to DN16CF flange to the Swagelok ¼” gas inlet
- Mini UHV VAT gate valve DN40CF

Apart from these commercially available parts, the sample manipulation area houses several homebuilt components which are described in the main text.

**B) Deposition parameters control and precursor delivery**

Besides the vacuum parts, the PSE-CVD setup comprises several important support systems, such as carrier gas supply, pressure control, temperature control, and precursor delivery. A schematic diagram of these systems attached to the reactor is shown in Fig.S1. These systems are based on commercially available parts and their functions and components will be listed in the following:

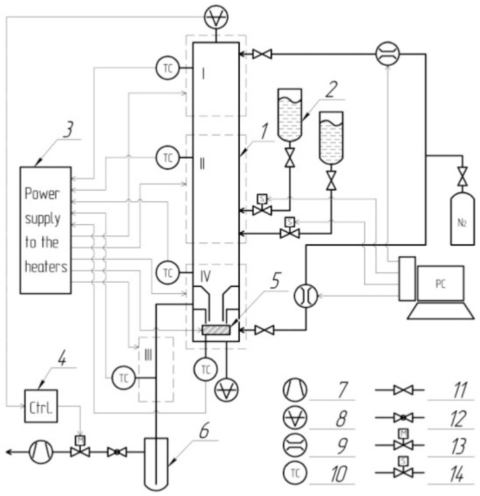

Fig.S1. Schematic diagram of the pump, gas supply, and injection systems as well as power control lines connected to the PSE-CVD setup. 1 – carrier gas preheating zone (I), spray evaporation and delivery zone (II), vacuum line (III), sample manipulation area (IV), 2 – precursor reservoir, 3 – power supply to the heaters, 4 – pressure controller, 5 – heater, 6 – liquid nitrogen trap, 7 – scroll pump, 8 – capacitance manometer, 9 – mass flow controller, 10 – thermocouple, 11 – shut-off valve, 12 – ball valve, 13 – motorized valve, 14 – solenoid valve (spray injector).

*Gas supply system*

The gas supply system is needed for transporting the precursor spray to the sample surface and purging the sample in-between spray injections. It generates the required operating pressure. The system comprises:

- Linde $N_2$ reservoir (Nitrogen 5.0 in 50 l gas cylinder)
- Swagelok gas lines
- Bronkhorst HI-TEC digital mass flow controllers (9)
- Shut-off valves (11)

*Pressure control system*

The pressure is controlled by a butterfly valve in the vacuum line which adjusts the pumping speed according to the pressure signal from the Capacitance Manometer in the deposition area. The control system comprises:

- MKS Baratron Capacitance Manometer (8)

- MKS pressure controller (4)
- MKS motorized butterfly valve (13)
- Oerlikon Scroll Pump SC 15 D (7)
- Liquid $N_2$ trap 4“ DN16KF (maximal condensate capacity is 300 ml) (6)

*Temperature control system*

All parts as well as the carrier gas have to be heated up to the evaporation temperature of the used precursors in order to avoid undesirable condensation of precursor molecules on the reactor walls. For example, zones I and II were heated up to 225° C to ensure uniform heating of the carrier gas while zones III and IV were heated to 170° C which is the needed precursor evaporation temperature. The temperature control system comprises:

- Horst multichannel temperature controller with modified power supply, providing 4 outputs 220 V AC for heating tapes and one output 24 V DC for the ceramic heater (3)
- Horst heating tapes
- Bach RC ceramic sample heater 24 V, 50 W (5)
- Thermocouples Type K (10)

*Precursor delivery and injection system*

The precursor for PSE-CVD, dissolved in alcohol, is delivered via a solenoid valve (Bosch spray nozzle Part No. 0-280-155-965), has the lowest commercially available flow rate (95.7 cc/min), built for automotive applications). It is operated by 12 V direct current pulses which are generated by a National Instruments I/O card (5 V output amplified to 12 V) and controlled by LabView Code.

Apart for PSE-CVD, the setup can be also used for classical, thermally activated CVD with, e.g., gaseous precursors, or be operated in the ALD regime by sequential delivery of different types of precursors or reactants. For such a multifunctional use, the precursor delivery technique and support system has to be adapted. Fig.S2. provides an overview over several precursor delivery techniques used in CVD applications which can be implemented in the UHV-compatible CVD reactor setup presented here.

Gaseous, solid or liquid precursors can be fed into the reactor via the carrier gas inlet (c.f. Fig.S2, showing a) a cylinder with mass flow controller for gaseous precursors, b) an evaporator with leak valve for solid precursors, and c) glass flask with solenoid valve or d) bottle with bubbler controlled by leak valve/mass flow controller for liquid precursors . In case of liquid precursors, deposition via the solenoid valve (Fig.S2.c) is more preferable than the bubbling technique when good control of precursor dosage and uniformity of the deposition rate are essential. The solenoid valves or digital shut-off valves are particularly promising for applications in ALD.

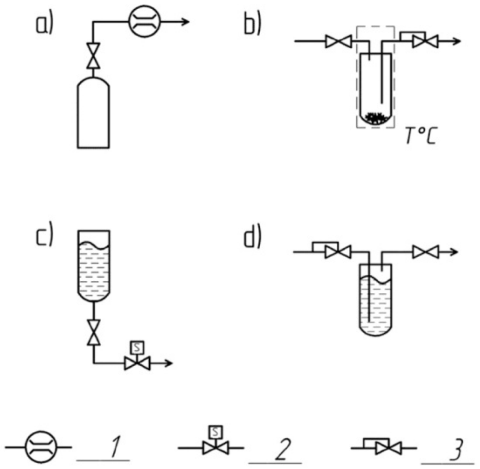

Fig.S2. Schematic diagrams of the delivery techniques used in CVD systems for various types of precursors: a) – gas, b) – solid c) – liquid injection via solenoid valve d) – conventional bubbler for liquid precursor. (1 – Mass flow controller, 2 – Solenoid valve (Injector), 3 – Leak valve.)

## C) Shutter design

For cleanness of the sample transfer procedure and for solving the contamination problem a shutter system between deposition area and sample manipulation area of the CVD reactor was developed and constructed as described in the main text. Its main parts are shown in Fig. S3: a stationary nozzle (upper part in Figs. S3 a)-c) ) centers and suspends a second, tapered part acting as movable mask with an aperture to the sample surface (lower part in Figs. S3 a-c, aperture at the bottom). In order to provide a uniform, unhindered gas flow, the stationary nozzle is tapered and has a smooth surface finish.

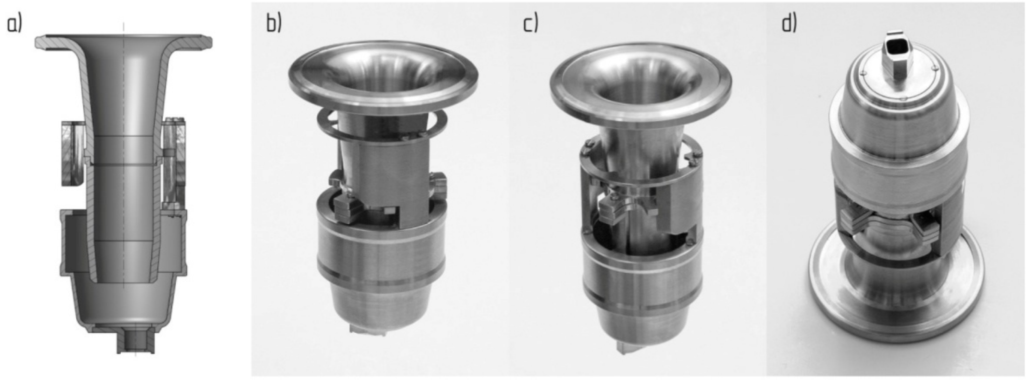

Fig.S3. Drawing (a) and photographs of the shutter: b) and c) movable mask locked in position for sample transfer and for deposition, respectively; d) upside down view showing the aperture of the mask.

Figs. S3 b) and c) show the movable mask locked in upper position for sample transfer and in lower position for deposition, respectively. Some details of the locking mechanism can be discerned in Fig. S3. It involves pins protruding from the nozzle and two L-shaped parts mounted on top of the movable mask which slide on and off the pins upon rotation of the mask (The thin ring visible in Figs. S3 b) and c) connects both L-shaped parts in order to keep them in place). These L-shaped latches are made of steel with high magnetic susceptibility and thereby provide the force closure to magnets outside the reactor which are used to drive the shutter motion.

The movable mask, shown upside down in Fig. S3 d), has a recess for the sample (square-shaped, 5 mm x 5 mm), which is placed off-center. Therefore, when the mask is lifted upwards and rotated by 55 degree into the locked position for sample transfer, the aperture does not expose the sample surface to the deposition area via direct line of sight. Consequently, precursor molecules or fragments which may still desorb from the reactor walls after deposition are less likely to reach and contaminate the sample surface.

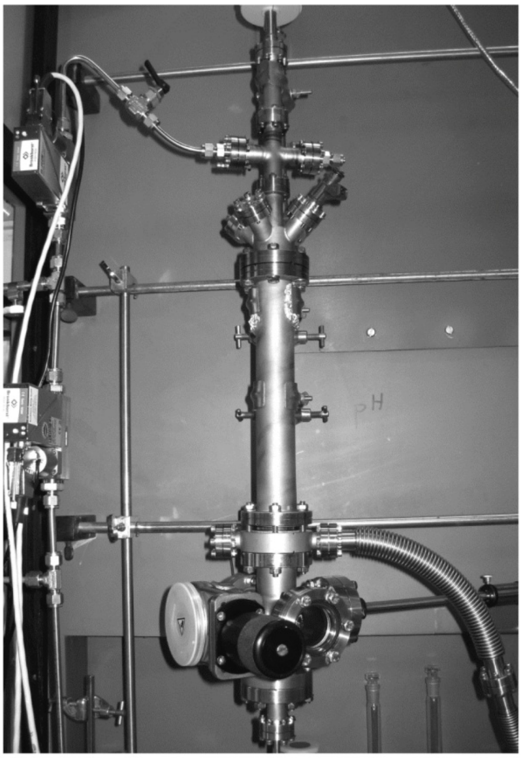

Fig.S4. Photograph of the reactor assembly showing (from top to bottom) carrier gas inlet, spray nozzle, tube of the evaporation and delivery zone, vacuum line, gate valve and six-way cross (c.f. Fig.2)

**Paper II**

# Investigation of the growth behaviour of cobalt thin films from chemical vapour deposition, using directly coupled X-ray photoelectron spectroscopy

P. H. Tchoua Ngamou[a,1,*], A. El Kasmi[a,b], Th. Weiss[c], H. Vieker[d,2] , A. Beyer[d], V. Zielasek[c], K. Kohse-Höinghaus[a], M. Bäumer[c,*]

[a] Department of Chemistry, Bielefeld University, Universitätsstraße 25, D-33615 Bielefeld, Germany

[b] Laboratory LGCVR, Faculty of Sciences and Techniques, University Abdelmalek Essaadi, B.P. 416 Tangier, Morocco

[c] Institute of Applied and Physical Chemistry, University of Bremen, Leobener Straße UFT, D-28359 Bremen, Germany

[d] Department of Physics, Bielefeld University, Universitätsstraße 25, D-33615 Bielefeld, Germany

* Corresponding authors:

| Dr. Patrick Hervé Tchoua Ngamou | Prof. Dr. Marcus Bäumer |
|---|---|
| Tel: +49 2461 61 6665 | Tel.: +49 421 218 63170 |
| E-mail: p.tchoua@fz-juelich.de | E-mail: mbaeumer@uni-bremen.de |

This paper includes Supplementary Material.

---

[1] Now at: Forschungszentrum Jülich GmbH, Institute of Energy and Climate Research, Wilhelm-Johnen-Straße, D-52428 Jülich, Germany

[2] Now at: CNM Technologies GmbH, Herforder Straße 155a, D-33602 Bielefeld, Germany

## Abstract

Thin films and coatings are a basis for many technological processes, including microelectronics, electrochemistry and catalysis. The successful deposition of metal films and nanoparticles by chemical vapour deposition (CVD) needs control over a number of physico-chemical processes such as precursor and substrate selection, delivery, temperature, pressure and flow conditions. Here, cobalt thin films were deposited by means of pulsed-spray evaporation chemical vapour deposition (PSE-CVD) from ethanol solutions of Co(acac)$_2$ and Co(acac)$_3$ on bare glass and silicon substrates. The physico-chemical properties of the grown films were characterised by XRD (X-ray diffraction), XPS (X-ray photoelectron spectroscopy) and HIM (helium ion microscopy). Co(acac)$_2$ enabled the growth of cobalt metal at lower temperatures than Co(acac)$_3$. The difference in deposition temperature was attributed to the ability of ethanol to reduce Co(acac)$_2$ better than Co(acac)$_3$. In addition, the film deposited from Co(acac)$_2$ exhibited a higher metal content and a less porous structure than that deposited from Co(acac)$_3$. Increasing the substrate temperature enhanced the carbon content because of the thermal decomposition of both precursors. Using a nickel seed layer improved the growth rate until a critical temperature of 360°C, at which the thermal decomposition of the precursor becomes predominant. A decrease in the deposition temperature when using the nickel seed layer was only observed with Co(acac)$_2$ precursor; the growth behaviour under these conditions was monitored with a unique UHV-compatible PSE-CVD reactor directly attached to an XPS system and ascribed to an enhancement of its catalytic reduction by ethanol.

Keywords: cobalt thin films, chemical vapour deposition, cobalt acetylacetonate, nickel seed layer, *in-situ* XPS

## 1. Introduction

Thin films and coatings of a variety of materials are of widespread use today because of their significant potential to drive important technological advances in fields including microelectronics, photovoltaics, catalysis and corrosion protection. To understand the relations between desired properties of the materials and the boundary conditions of their formation, highly interdisciplinary knowledge is desired, typically involving – besides material science – fluid dynamics and, in particular, physical chemistry that can address thermodynamic and kinetic properties of such complex systems and may make use of spectroscopic methods for their characterisation. As often on the way from elementary processes to application, mechanistic considerations based on fundamental knowledge from kinetics and thermodynamics as well as on advanced techniques to analyse important properties, have been instrumental to understand complex reactive systems such as in atmospheric chemistry, combustion or astrochemistry [1-3]. Such approaches have often pertained to the gas phase, and respective concepts for gas-solid systems are an active area of research [4]. Here, the successful deposition of metal films and nanoparticles by chemical vapour deposition (CVD), one of the most common techniques providing access to materials with desired properties, must again enable control over a number of physico-chemical processes. These include, but are not limited to properties of precursors and substrates, process temperature, pressure and flow conditions. Systematic characterisation of conditions in the extensive parameter space comprising gas- or liquid-phase delivery, precursor decomposition and reactions towards reactive intermediates, interactions of such species with substrate surface, seed layer or incipient thin films in nucleation and growth reactions, formation of specific phases, morphologies and surface properties, as well as tendencies to form undesired contaminations contribute to an overall understanding that can enable more detailed investigation of specific aspects of the process. Here, we focus on the deposition of cobalt metal and on the role of the valence state of the metal centre in the cobalt precursor as well as on the effects of a nickel seed layer.

Cobalt and cobalt-based thin films have attracted considerable interest for various technological applications because of their electrical, magnetic and catalytic properties [5, 6]. They have been used as active materials in sensors, as reflective and refractive coatings for optical elements, as protective and decorative films [7-9] and as Fischer-Tropsch catalysts [10]. A variety of approaches have been used to synthesise cobalt films such as thermal evaporation [11-13], electron beam evaporation [14-16], sputtering [17, 18], electro-deposition [19, 20] and chemical vapour deposition (CVD) [21-23]. The CVD technique offers potential for producing films with high uniformity of thickness, high purity, conformal step coverage, minimal substrate damage, high growth rates and the possibility for selected area growth. Several precursors including inorganic precursors (mainly halides) and organometallic precursors have been investigated for the CVD deposition of metallic films [24]. The drawbacks of inorganic precursors are the possible generation of particles and corrosive by-products, as well as halide contamination in the deposited films. Organometallic precursors are typically costly, toxic and highly sensitive to air, moisture and temperature [25, 26]. In addition, the existence of metal-carbon bonds in their structure typically leads to the formation of metal carbides rather than metals [24, 27]. Metal-organic precursors, especially metal acetylacetonates, are less toxic and less costly than the other abovementioned precursors. However, they usually require a strong reducing agent like hydrogen to yield metallic films [28, 29]. Due to the need for safety requirements and handling equipment associated with hydrogen, alternative reducing routes were intensively investigated. High quality nickel and cobalt metallic thin films were deposited using ammonia as a mild reducing agent [30, 31]. However, the required deposition temperatures were relatively high due to the lower reactivity of ammonia as compared to hydrogen.

Recent work of Bahlawane et al. [32-36] has demonstrated CVD of several metals (Ru, Pt, Ag, Cu, Ni, Co) and their alloys using ethanol as unique reducing agent. This approach is characterised by the liquid delivery of commercial metal-organic precursors into the CVD reactor via a pulsed-spray evaporation (PSE) system. These authors [32, 35] studied the reaction mechanisms involved in the PSE-CVD of nickel and copper thin films from an ethanol solution of $Cu(acac)_2$ and $Ni(acac)_2$. The catalytic chemical reduction of the acetylacetonate precursor by ethanol, as shown in Eq. (1), was identified as the reaction pathway that enables the deposition of high-quality films of transition metals:

$$2\,M(acac)_n + n\,C_2H_5OH \rightarrow 2M + 2n\,Hacac + n\,CH_3CHO \qquad (1).$$

In contrast to $Cu(acac)_2$ and $Ni(acac)_2$ precursors, the PSE-CVD of cobalt films from $Co(acac)_2$ was found in this earlier work to be highly sensitive to the nature of the underlying substrate and the deposition temperature. For instance, a transition from cobalt carbide to metallic cobalt was observed upon increasing the substrate temperature from 240°C to 280°C, while an improvement of the growth rate and a decrease of the required deposition temperature were observed when coating a 5 nm-thick nickel seed layer on bare glass [36]. Despite these observations, the role of the nickel seed layer during the film growth is not well understood.

In the present contribution, we evaluate the suitability of $Co(acac)_3$ precursors for the PSE-CVD growth of cobalt metallic films in comparison to $Co(acac)_2$. Cations of transition metals are efficient redox catalysts, and the valence state of the metal centre ($Co^{2+}$ or $Co^{3+}$) of the precursor is expected to influence the catalytic dehydrogenation of ethanol according to Eq.(1) and hence to affect growth kinetics and film quality. To evaluate the influence of the choice of precursor valence state, several *in-situ* characterisation techniques including X-ray photoelectron spectroscopy (XPS) and molecular-beam mass spectrometry (MBMS) were coupled with the PSE-CVD setup to elucidate the role of the nickel seed layer.

## 2. Experimental

### 2.1. Film growth

The growth of metallic films was performed in a CVD reactor employing a pulsed-spray evaporation (PSE) unit for the delivery of the precursor liquid feedstock. $Co(acac)_2$, $Co(acac)_3$, or $Ni(acac)_2$, respectively, were dissolved at a concentration of 5 mM in ethanol. As the growth of cobalt films on bare glass shows serious nucleation difficulties, different quantities influencing the film deposition were comprehensively optimised, including the deposition temperature, pressure, gas flow rate and delivery parameters (Fig. S1). To monitor the effect of the nickel seed layer on the resulting films, both bare glass and Ni-seeded substrates, with a nickel film thickness of ~5 nm, were used for $Co^0$ deposition. The feedstock was injected as a fine spray into a 30-cm long evaporation chamber at 200 °C. The resulting vapour was transported by $N_2$ to the deposition chamber at 220 °C. The deposition of cobalt occurred on the heated substrates (thin glass and silicon wafer with native oxide ($Si/SiO_2$)) in the temperature range of 240-480 °C, while the deposition of the Ni sub-layer was performed at 270 °C. The deposition conditions are summarised in the Supplementary Material (Table S1). Except for the varied substrate temperature during deposition, the same optimised conditions regarding pressure, nitrogen flow rate and liquid feedstock feeding rate were used for the deposition of $Co^0$ films on bare glass from $Co(acac)_2$ precursor as well as from $Co(acac)_3$. The thickness of the deposited films was estimated gravimetrically by measuring the weight change of the substrates before and after deposition with a microbalance (Mettler ME30).

### 2.2. Post-deposition film characterisation

The crystalline phase of the prepared films was identified by XRD using a Phillips X´ Pert Pro MRD instrument equipped with a Cu Kα (λ=0.154056 nm) radiation source and operated at 40 kV and 30 mA. The phases were determined by reference to the powder XRD database (JCPDS). The morphology of the deposited films was ascertained using helium ion microscopy (Carl Zeiss Orion Plus). The helium ion beam was operated at an acceleration voltage of 35 kV with a current between 0.3 and 1.7 pA and a 10 µm aperture at "Spot Control" settings of 4 to 5. Secondary electrons were collected by an Everhart-Thornley detector at 500 V grid voltage. The cross-sectional images were acquired with samples on Si wafer broken directly before inserting them into the vacuum chamber. The chemical composition was determined by XPS (Multiprobe, Omicron Nanotechnology, base pressure about $10^{-10}$ mbar), using a monochromated Al Kα X-ray source (1486.7 eV, 280 W) under an angle of 13° from the surface normal to the electron detector. CasaXPS was used to analyse the spectra with Shirley backgrounds and Scofield cross-sections. The fitting of synthetic components followed the procedures described by Biesinger et al. [37].

### 2.3. *In-situ* diagnostics

*In-situ* monitoring of the reactions occurring under PSE-CVD conditions was performed by coupling a PSE-CVD reactor with electron ionisation time-of-flight (ToF) MBMS. The system (see Fig. S2) consists of a PSE-CVD reactor, a differentially pumped chamber with a molecular-beam sampling system and an electron ionisation chamber with a reflectron time-of-flight mass spectrometer. A quartz cone with an orifice of ~100 µm at the tip was used to sample species from the reaction. The tip of the nozzle was inserted into a hole of the flat heater of the CVD reactor. The sampled species form a molecule beam in the differentially pumped chamber and pass through a copper skimmer into the electron ionisation chamber, where the molecular beam is crossed and ionised by electrons. The produced ions are propelled into a flight tube and reflected to the detector. During the PSE-CVD process, the temperature of the evaporation zone was kept constant (220°C) and only the substrate temperature was increased from 220 to 360°C.

In order to perform XPS analysis at any stage of the thin film growth, a PSE-CVD reactor directly attached to a UHV chamber (a second Multiprobe system, Omicron Nanotechnology, base pressure $10^{-10}$ mbar) for thin film analysis was used with an Al Kα X-ray source without monochromator. The uniquely designed setup provides quick sample transfer between the CVD reactor and XPS without interrupting vacuum. Thereby any sample contamination during the transfer procedure could be avoided [38]. Again, the evaporation and deposition areas of the reactor were heated to 220 °C during deposition to avoid undesirable precursor adsorption on the PSE-CVD reactor walls.

## 3. Results and discussion

### 3.1. Film characterisation

Figure 1 shows the XRD pattern of a 250 nm thick film deposited at 250°C on bare glass using $Co(acac)_2$ precursor. The film appears to be a mixture of hexagonal close packed (hcp) metallic cobalt and orthorhombic cobalt carbide $Co_2C$ phases. This result is in agreement with previous work [36] showing a transition from $Co_2C$ to Co metal by increasing the substrate temperature from 240°C to 270°C. By using

$Co(acac)_3$, neither metallic cobalt nor carbide films could be grown at substrate temperatures below 320°C, even when coating glass or $Si/SiO_2$ substrate with a nickel seed layer. The presence of the nickel seed layer only improves the growth rate in the case of $Co(acac)_3$ but does not decrease the deposition temperature as observed for $Co(acac)_2$ [36]. Considering these observations detailed below, $Co(acac)_2$ appears to be the best precursor to investigate the role of the nickel seed layer.

As shown in Fig. S3, the XRD patterns of the films deposited at 270°C and 280°C on nickel-coated $Si/SiO_2$ substrate using $Co(acac)_3$ clearly indicate the presence of cobalt oxide with poor crystallinity. With and without Ni seed layer, hexagonal close packed (hcp) metallic cobalt (JCPDS no. 05-0727) with a (002) preferred orientation (Fig. 2) is deposited at 320° C. The data for films with thicknesses in the range 200-350 nm show no peaks corresponding to impurity phases such as oxides or carbides. Furthermore, the phase of the metal deposit transforms from hcp to face-centred cubic (fcc) structure (JCPDS no. 15-0806) as the deposition temperature is increased, a behaviour that is visualised by the shift of the most intense diffraction peak, (002), towards lower angle, corresponding to (111) orientation [39, 40]. The calculated lattice spacing for the cobalt deposits grown at 360 °C and 440 °C are 2.022 Å and 2.049 Å, respectively. These values agree with those, 2.023 Å and 2.046 Å, reported in the literature [41] for hcp (002) and fcc (111) of Co phases, confirming a transition from hcp to fcc structure by increasing the substrate temperature from 320 to 480°C. The transformation of hcp to fcc structure was also observed in the same temperature range for the obtained Co films grown on bare glass with a sub-layer of Ni. The presence of a nickel sub-layer improves the growth rate of the films deposited from $Co(acac)_3$ up to a deposition temperature of 360°C. For instance, the calculated growth rate of ~0.7 nm/min on bare glass at 320°C was improved to 2.3 nm/min on

Ni-coated glass. (For comparison: by using Co(acac)$_2$ precursor, the calculated growth rate of 2.8 nm/min on bare glass at 300°C increased to 5 nm/min in the presence of the nickel seed layer [36].) In contrast to substrates with a nickel seed layer, however, we find a steep increase of the growth rate on bare glass substrates as the temperature is raised above 360° C (Fig. 3), resulting in comparable growth rates on both types of substrates at 400-440°C. The effect of the nickel sub-layer will be discussed later.

The surface composition of films deposited at 250 and 400°C on Si/SiO$_2$ substrate using Co(acac)$_2$ and Co(acac)$_3$, respectively, was investigated by means of *ex-situ* XPS (data not shown). Due to contamination arising from the precursor decomposition, the surface oxygen content was found to be about 24 at.% and 10 at.% for the samples deposited using Co(acac)$_2$ and Co(acac)$_3$, respectively. The greater part of the surface oxygen content was bound to carbon as C-O, C=O and in the form of chemisorbed H$_2$O. To probe the bulk properties of the films, the samples were sputtered with Ar ions (1 kV, about 45° incident angle, 15 µA) for 70 min. The XP spectra of the sputtered films and the elemental composition are shown in Fig. 4. The film deposited at 250°C using Co(acac)$_2$ contained ~73 at.% Co and ~25 at.% C, while a small amount of oxygen was still present. The film deposited at 400°C using Co(acac)$_3$, in contrast, only contained 8 at.% Co, showing massive carbon contamination. The Co2p spectra (Fig. 4a,d) for both, the film deposited at 250° C from Co(acac)$_2$ as well as that deposited at 400°C from Co(acac)$_3$, can be fitted with an asymmetric main species at about 778.2 eV and two peaks at 3.0 and 5.0 eV above the main peak which are attributed to origin from a plasmon loss process, indicating metallic cobalt [37]. Both films show ~ 3 at.% oxygen, which is mainly referred to be hydroxides or carbon-bound. In the sample grown from Co(acac)$_2$, about 5 at.% of the oxygen is identified as lattice oxygen (species bound to cobalt, at ~530 eV)[37]. Both films show the presence of alkyl-type carbon at ~284.4 eV as dominant species and a small fraction of oxides (Fig. 4c,f). Only in the film grown from $Co(acac)_2$, more than 30 at.% of the carbon is present in the carbidic type (at 283.4 eV) [16], in agreement with XRD analysis. The massive amount of alkyl-type carbon in the film deposited using $Co(acac)_3$ indicates that decomposition of the precursor and its fragments into volatile species at 400°C is a major problem of using $Co(acac)_3$ in the PSE-CVD process. It is worth mentioning that the carbon content increased as the substrate temperature was raised for films deposited using $Co(acac)_3$, *i.e.*, the formation of the non-volatile carbonaceous species is thermally activated (pyrolysis). In the case of using $Co(acac)_2$ as the precursor, the relatively low deposition temperature of 250° C may help to avoid the formation of these species, leading to comparatively moderate carbon levels of ~25 at.%. The peak near 285 eV in the C1s XP spectrum indicates the presence of C-H and C-C bonds and thus of hydrogen impurities which could not be quantified, however. Again, hydrocarbon fragments from the precursor may contribute to these impurities.

Figure 5 shows the HIM cross section of Co thin films deposited at different substrate temperatures using $Co(acac)_2$ and $Co(acac)_3$. Helium-ion microscopy [42] (HIM) is similar to scanning electron microscopy but it employs helium ions for analysing a sample instead of electrons. In HIM, a focused beam of helium ions with a diameter down to 0.35 nm is scanned over the sample, and the secondary electrons generated by the He+ impact are detected. The resulting images are more surface-sensitive with a higher spatial resolution as compared to scanning electron microscopy. As evident from Fig. 5, compact spherical grains that build a closely packed film are deposited at 250°C using $Co(acac)_2$. The HIM images of Co thin films deposited at 320°C using $Co(acac)_3$ show spherical grains with an island-type growth. The grainy nature of the deposited film indicates that the nucleation step proceeded at low rates. Interestingly, similar growth using the same precursor has been reported by Maruyama et al. [40]. By increasing the deposition temperature to 400°C, the deposited films show an agglomeration of grains with columnar and porous structure, while a fibrous structure was observed at 480°C. As shown in Fig. S4, homogeneous films with a better nucleation were obtained when using a nickel sub-layer during the PSE-CVD process.

### 3.2. Mass spectrometry

The gas sampled after its interaction with the hot glass substrate during the PSE-CVD process was analysed by MBMS. Figure 6 shows the temperature-dependent profiles of the molecular peaks of the $Co(acac)_2$ and $Co(acac)_3$ precursors. The thermolysis of both precursors starts at temperatures above 200°C, and their complete depletion is observed at 280°C and 320°C for $Co(acac)_2$ and $Co(acac)_3$, respectively. Note that the abovementioned temperatures correspond to the minimum temperatures at which entirely metallic cobalt is deposited (no oxides or carbides) using the corresponding metal acetylacetonate precursor. Therefore, it can be concluded that the ethanol-induced depletion of the metal precursor is influenced by the oxidation state of the metal centre. $Co(acac)_2$ is more easily reduced to metallic Co than the $Co(acac)_3$ precursor, which is in agreement with the ex-situ XPS measurements (higher metal content in the films grown using $Co(acac)_2$ than in those obtained from $Co(acac)_3$). The mass spectrometry data do not provide any indication why no cobalt metal or carbide was deposited using $Co(acac)_3$ at temperatures below 320°C. The thermolysis profiles of both precursors show a depletion starting at temperatures below 240°C, but carbide is only obtained when using $Co(acac)_2$ as the precursor. The XRD analysis of the deposited films at 270°C and 280°C using $Co(acac)_3$ (Fig. S3) revealed small amounts of $CoO_x$ oxides while metallic cobalt films are obtained with $Co(acac)_2$ at the same temperature. To understand the formation mechanism of cobalt carbide films, consideration of results reported for related systems such as nickel carbide may help. Leslie-Pelecky et al. [43] reported the synthesis of nickel carbide nano-composites by reducing nickel salts in hydrocarbon solvents using lithium and naphthalene as electron carriers. These authors demonstrated that the formation of the carbide phase proceeded via adsorption of a carbon-containing molecule on the nickel cluster and the subsequent decomposition of the adsorbed molecule during thermal annealing, which then led to incorporation of the carbon atoms into the nickel particle. Coating the nickel cluster with polymers prior to annealing was found to enhance the nickel carbide formation because of the reduction of surface NiO, which blocks the diffusion of carbon atoms. In analogy, one may postulate that the low-temperature formation of cobalt carbide during Co deposition using the Co(acac)$_2$ precursor may result from migration of some "active" carbon species arising from the thermal decomposition of the precursor ligand into cobalt particles. The lack of carbide formation observed in films deposited from Co(acac)$_3$ at higher temperatures may be due to the presence of CoO$_x$ at the surface which hinders the diffusion of carbon into the metal cluster.

### 3.3. Role of the nickel seed layer

To investigate the role of the nickel seed layer, depositions were performed only with Co(acac)$_2$ as the precursor (see Section 3.1.). In the UHV-compatible PSE-CVD reactor directly attached to an XPS system, ultrathin films (of thickness 2-6 nm), representing an early stage of the deposition, were deposited from ethanol solution of Co(acac)$_2$ on Si/SiO$_2$ substrate samples at various temperatures in the range 250-370° C and characterised by XPS. In these experiments, any post-deposition contamination or metal oxidation during sample transfer from the reactor to XPS can be neglected. The results are shown in Fig. 7 for the Co2p, O1s and C1s core-shell spectra. At sample temperatures up to 270° C during deposition, the film surface is composed of carbon, oxygen and oxidised Co, identified by the Co2p XPS peaks at ~782 and ~786 eV binding energy which represent $Co^{2+}$, probably in Co oxide or $Co(OH)_2$. For deposition temperatures of 310°C and higher, metallic Co (Co2p b3/2 peak at ~778 eV) was also found, where the ratio of metallic and oxidised Co increased with temperature. Only at the highest deposition temperature of 370°C, the Co signature of the film was found to be entirely metallic. At this deposition temperature, however, carbon contamination, which increased with deposition temperature, was highest (see Fig. 7c). The C1s binding energy of ~285 eV indicates the prevalence of C-C and C-H bonds, probably due to fragments of decomposed precursor or alcohol on or in the film, which result from pyrolysis of the precursor solution at the hot sample surface. Below 270°C deposition temperature, the C1s peak was found shifted to a binding energy <286 eV, indicating prevalence of carbon in C-O bonds which may be attributed to undecomposed precursor at the surface. The O1s XPS signal is shown only as a reference because it is likely to include significant contributions from the $SiO_x$ substrate due to the thinness of the deposited film. Compared to the XPS data obtained from 250 nm-thick films deposited from $Co(acac)_2$ at 250° C (only metallic Co and Co carbide were found as discussed before), these findings indicate that the growth mode changes as more and more Co is deposited. Probably, the initially deposited cobalt oxide acts as a seed layer and promotes the catalytic decomposition of the precursor at later stages of film growth.

When a nickel seed layer was deposited on the $SiO_x$/Si substrates before depositing Co in the UHV-compatible PSE-CVD reactor, the XPS revealed that 30-nm thin films were composed of entirely metallic cobalt even at temperatures as low as 270° C (see Fig. 8a). Apparently, nickel efficiently catalyses decomposition of the adsorbed precursor and promotes the reduction of $Co(acac)_2$ during the initial stage of deposition. With and without Ni seed layer, carbon contamination at the film surface, as represented by the C1s XPS peak (Fig. 8c), appears to be inherently connected to the formation of metallic Co. Comparison of Figs. 7c and 8c shows that the amount of carbon contamination always increases with deposition temperature. However, at a deposition temperature of 270°C, the amount of carbon at the surface is significantly higher with a Ni seed layer, *i.e.*, when the deposited Co is metallic and not significantly oxidised at the film surface.

To gain more insight into the role of the nickel seed layer during the film growth, the thermolysis of ethanol was performed in a tube flow quartz reactor filled with a stainless steel mesh substrate (SSM) and the exhaust gas was analysed by means of Fourier transform infrared spectroscopy (Nicolet 5700). As shown in Fig. 9, the formation of acetaldehyde in presence of the uncoated mesh substrate requires temperatures exceeding 320°C, indicating that this reaction pathway contributes to the film deposition for temperature above 320°C. The reaction over a nickel-coated SSM and $Ni(acac)_2$ chemisorbed at 200°C on SSM leads to the formation of acetaldehyde at a lower temperature (270°C). This behaviour, in agreement with the *in-situ* XPS measurements, confirms that the presence of a Ni seed layer catalyses the dehydrogenation of ethanol to acetaldehyde and thus, via hydrogen, the decomposition of the precursor. However, as discussed before for films grown from $Co(acac)_3$ at elevated temperature, the presence of carbon impurities in the film indicates that the produced hydrogen does not help to generate entirely volatile fragments from the decomposed ligand.

At a temperature above 370°C, the nickel-coated SSM induces the decomposition of ethanol (Fig. 9) as noticed by the decrease of acetaldehyde, which can be another source of carbon incorporation into the grown films. This might explain the high carbon content observed at 370°C during the *in-situ* XPS measurements.

## Conclusions and perspectives

Metallic cobalt was deposited at lower temperature when using Co(acac)$_2$ than Co(acac)$_3$, a behaviour that is confirmed by the total depletion of Co(acac)$_2$ in ethanol atmosphere at a lower temperature compared to that when using Co(acac)$_3$. Structural characterisations indicated that films deposited with Co(acac)$_3$ contain less cobalt metal and are more porous than those deposited using Co(acac)$_2$. Increasing the deposition temperature for both precursors improved the carbon content as a consequence of the thermal decomposition of the precursor. Enhancement of the growth for both precursors when using a nickel seed layer was ascribed to the improved dehydrogenation of ethanol to acetaldehyde, a process that enables the reduction of the precursor. However, this effect was limited to temperatures below 360°C, above which the thermal decomposition of the precursor is predominant. The decrease of the deposition temperature when using the nickel seed layer was only observed with the Co(acac)$_2$ precursor. *In-situ* monitoring the CVD growth process by means of XPS is an efficient way to control the film quality during the deposition.

Cobalt and cobalt-based thin films have possible applications in microelectronics, especially in the development of digital magnetic data storage devices and magnetic field sensors. One typical example is the development of ferromagnetic/insulator/ferromagnetic junctions such as NiFe/Al$_2$O$_3$/Co trilayers. The aim of this work was to understand the deposition mechanism of metallic cobalt films by means of PSE-CVD from Co(acac)$_n$ precursor in order to contribute to solving the problem of carbon contamination. Using a stronger reducing agent than ethanol will inevitably lower the deposition temperature and hence reduce or suppress the carbon contamination. In the PSE-CVD setup, the presence of voids in the deposited layer generally originates from the film inhomogeneity. Controlling the deposition parameters, such as the pressure of the CVD chamber, the frequency of the liquid delivery and the flow of the carrier gas, can enable improvement of the film packing density.

## Acknowledgements

This work was supported by the Deutsche Forschungsgemeinschaft (DFG) under grants BA 2307/3-1 and BA 1710/20-1. Achraf El Kasmi thanks the German Academic Exchange Service (DAAD) for his fellowship at Bielefeld University. The authors wish to thank Prof. Zhen-Yu Tian and Prof. Armin Gölzhäuser for useful discussions and Udo Mundloch for performing some XRD measurements.

## References

[1] J. Troe, J. Phys. Chem. A **110** (2006) 2831.

[2] J. Troe and V.G. Ushakov, Z. Phys. Chem **228** (2014) 1.

[3] J.A. Miller, M.J. Pilling, and J. Troe, Proc. Combust. Inst. **30** (2005) 43.

[4] H. Karadeniz, C. Karakaya, S. Tischer, and O. Deutschmann, Z. Phys. Chem. **229** (2015) 709.

[5] R. Bashyam and P. Zelenay, Nature **443** (2006) 63.

[6] P. Gambardella, S. Rusponi, M. Veronese, S.S. Dhesi, C. Grazioli, A. Dallmeyer, I. Cabria, R. Zeller, P.H. Dederichs, K. Kern, C. Carbone, and H. Brune, Science **300** (2003) 1130.

[7] V. Bakovets, V.N. Mitkin, and N.V. Gelfond, Chem. Vap. Deposition **11** (2005) 112.

[8] P.A. Lane, P.E. Oliver, P.J. Wright, C.L. Reeves, A.D. Pitt, and B. Cockayne, Chem. Vap. Deposition **4** (1998) 183.

[9] M. Utriainen, M. Kröger-Laukkanen, L.-S. Johansson, and L. Niinistö, Appl. Surf. Sci. **157** (2000) 151.

[10] G.A. Beitel, C.P.M. de Groot, H. Oosterbeek, and J.H. Wilson, J. Phys. Chem. B **101** (1997) 4035.

[11] M.Y. Lee and P.A. Bennett, Phys. Rev. Lett. **75** (1995) 4460.

[12] M. Jergel, I. Cheshko, Y. Halahovets, P. Šiffalovič, I. Mat'ko, R. Senderák, S. Protsenko, E. Majková, and Š. Luby, J. Phys. D: Appl. Phys. **42** (2009) 135406.

[13] W. Szmaja, W. Kozłowski, J. Balcerski, P.J. Kowalczyk, J. Grobelny, and M. Cichomski, J. Alloys Compd. **506** (2010) 526.

[14] V. Scheuch, B. Voigtländer, and H.P. Bonzel, Surf. Sci. **372** (1997) 71.

[15] H. Miura, E. Ma, and C.V. Thompson, J. Appl. Phys. **70** (1991) 4287.

[16] J. Heo and H. Jeon, Thin Solid Films **379** (2000) 265.

[17] D.J. Larson, A.K. Petford-Long, A. Cerezo, and G.D.W. Smith, Acta mater. **47** (1999) 4019.

[18] E. Kondoh, R.A. Donaton, S. Jin, H. Bender, W. Vandervorst, and K. Maex, Appl. Surf. Sci. **136** (1998) 87.

[19] J.D. Lee, T.H. An, H.G. Noh, S.G. Kim, and Y.R. Choi, Jpn. J. Appl. Phys. **49** (2010) 085802.

[20] T.M. Manhabosco and I.L. Müller, J. Mater. Sci. **44** (2009) 2931.

[21] Y.K. Ko, D.S. Park, B.S. Seo, H.J. Yang, H.J. Shin, J.Y. Kim, J.H. Lee, W.H. Lee, P.J. Reucroft, and J.G. Lee, Mater. Chem. Phys. **80** (2003) 560.

[22] M.F. Chioncel, H.S. Nagaraja, F. Rossignol, and P.W. Haycock, J. Magn. Magn. Mater. **313** (2007) 135.

[23] C.F. Powell, J.H. Oxley, and J.M. Blocher (Eds.), Vapor Deposition, John Wiley & Sons, New York, 1966.

[24] T.T. Kodas and M.J. Hampden-Smith (Eds.), The Chemistry of Metal CVD, VCH, Weinheim, 1994.

[25] E.P. Boyd, D.R. Ketchum, H. Deng, and S.G. Shore, Chem. Mater. **9** (1997) 1154.

[26] M.E. Gross, K. Schnoes Kranz, D. Brasen, and H. Luftman, J. Vac. Sci. Technol. B **6** (1988) 1548.

[27] J.E. Gozum, D.M. Pollina, J.A. Jensen, and G.S. Girolami, J. Am. Chem. Soc. **110** (1988) 2688.

[28] B.S. Lim, A. Rahtu, and R.G. Gordon, Nat. Mater. **2** (2003) 749.

[29] J.M. Blackburn, D.P. Long, A. Cabañas, and J.J. Watkins, Science **294** (2001) 141.

[30] H.-B.-R. Lee, W.-H. Kim, J.W. Lee, J.-M. Kim, K. Heo, I.C. Hwang, Y. Park, S. Hong, and H. Kim, J. Electrochem. Soc. **157** (2010) D10.

[31] W.-H. Kim, H.-B.-R. Lee, K. Heo, Y.K. Lee, T.-M. Chung, C.G. Kim, S. Hong, J. Heo, and H. Kim, J. Electrochem. Soc. **158** (2011) D1.

[32] N. Bahlawane, P.A. Premkumar, F. Reilmann, K. Kohse-Höinghaus, J. Wang, F. Qi, B. Gehl, and M. Bäumer, J. Electrochem. Soc. **156** (2009) D452.

[33] P.A. Premkumar, N.S. Prakash, F. Gaillard, and N. Bahlawane, Mater. Chem. Phys. **125** (2011) 757.

[34] N. Bahlawane, P.A. Premkumar, K. Onwuka, K. Rott, G. Reiss, K. Kohse-Höinghaus, Surf. Coat. Technol. **201** (2007) 8914.

[35] N. Bahlawane, P. A. Premkumar, Z. Tian, X. Hong, F. Qi, and K. Kohse-Höinghaus, Chem. Mater. **22** (2010) 92.

[36] P.A. Premkumar, A. Turchanin, and N. Bahlawane, Chem. Mater. **19** (2007) 6206.

[37] M.C. Biesinger, B.P. Payne, A.P. Grosvenor, L.W.M. Lau, A.R. Gerson, and R.St.C. Smart, Appl. Surf. Sci. **257** (2011) 2717.

[38] Th. Weiss, M. Nowak, U. Mundloch, V. Zielasek, K. Kohse-Höinghaus, and M. Bäumer, Rev. Sci. Instrum. **85** (2014) 104104.

[39] A. Rautiainen, M. Lindblad, L.B. Backman, and R.L. Puurunen, Phys. Chem. Chem. Phys. **4** (2002) 2466.

[40] T. Maruyama and T. Nakai, Appl. Phys. Lett. **59** (1991) 1433.

[41] B.X. Gu and H. Wang, J. Magn. Magn. Mater. **187** (1998) 47.

[42] B.W. Ward, J.A. Notte, and N.P. Economou, J. Vac. Sci. Technol. B **24** (2006) 2871.

[43] D.L. Leslie-Pelecky, X.Q. Zhang, S.H. Kim, M. Bonder, and R.D. Rieke, Chem. Mater. **10** (1998) 164.

## Figure captions

**Figure 1:** XRD pattern of a cobalt film deposited on bare glass at 250°C using an ethanol solution of Co(acac)$_2$.

**Figure 2:** XRD patterns of cobalt films grown at different temperatures (a) on bare glass and (b) on Ni layer deposited previously on glass. (PDF numbers refer to the JCPDS database.)

**Figure 3:** Growth rate as a function of temperature of cobalt films deposited using Co(acac)$_3$.

**Figure 4:** XP spectra of cobalt films deposited at 400°C (a, b, c) and 250°C (d, e, f) using Co(acac)$_3$ and Co(acac)$_2$ precursors, respectively.

**Figure 5:** HIM cross-section micrographs of cobalt films deposited at different temperatures, using the precursor Co(acac)$_3$ at 320 °C (a), 400 °C (b) and 480 °C (c), and the precursor Co(acac)$_2$ at 250 °C (d).

**Figure 6:** Left panel: MBMS monitoring of the thermal decomposition of the Co(acac)$_2$ and Co(acac)$_3$ precursors in ethanol atmosphere. The right panel shows spectral intensities for m/z=257 and m/z=356 depending on the substrate temperature.

**Figure 7:** *In-situ* XPS analysis of PSE-CVD cobalt films on SiO$_2$/Si substrate using an ethanol solution of Co(acac)$_2$. Co2p core-shell (a), O1s core-shell (b) and C1s core-shell (c).

**Figure 8:** *In-situ* XPS analysis of PSE-CVD cobalt films on Ni-coated SiO$_2$/Si substrate using an ethanol solution of Co(acac)$_2$. Co2p core-shell (a), O1s core-shell (b) and C1s core-shell (c).

**Figure 9:** Light-off-curves of acetaldehyde formation during the thermolysis of ethanol over uncoated mesh substrate, nickel-coated mesh and Ni(acac)$_2$ chemisorbed on the mesh substrate.

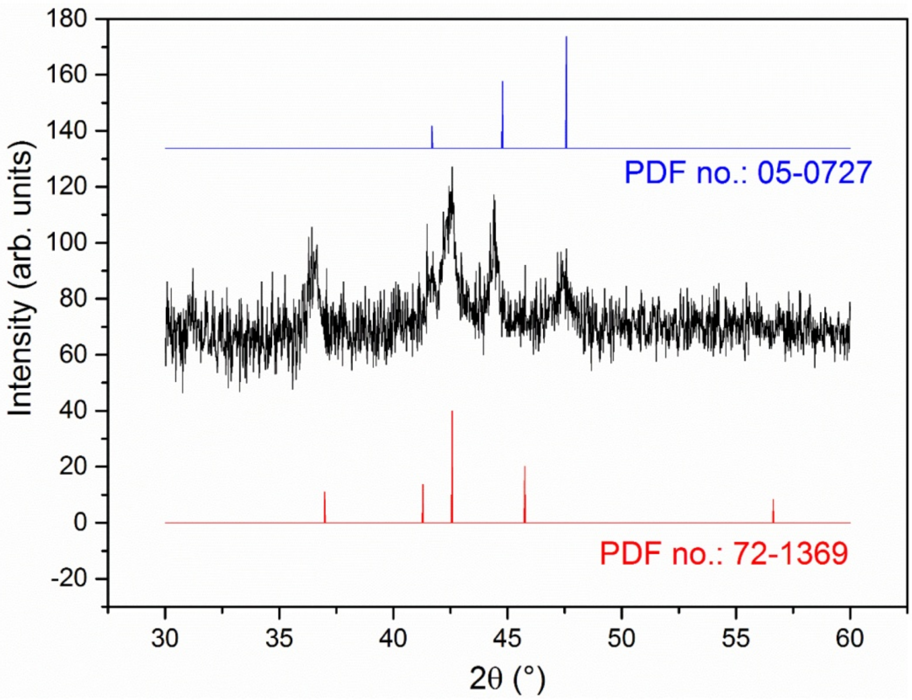

**Figure 1:** XRD pattern of a cobalt film deposited on bare glass at 250°C using an ethanol solution of $Co(acac)_2$.

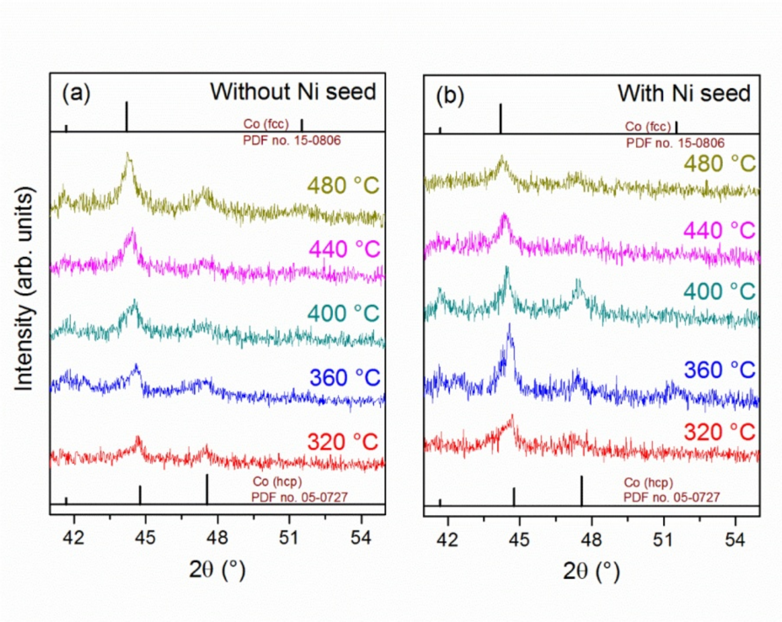

**Figure 2:** XRD patterns of cobalt films grown at different temperatures (a) on bare glass and (b) on Ni layer deposited previously on glass. (PDF numbers refer to the JCPDS database.)

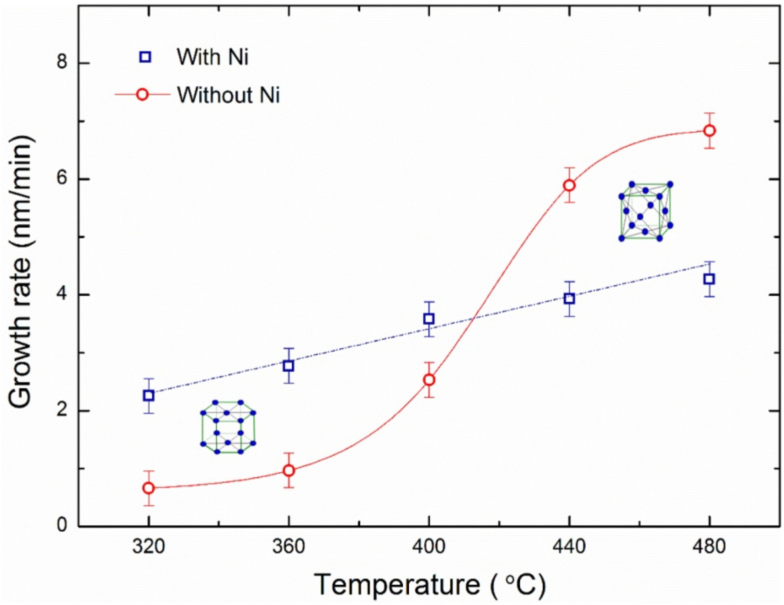

**Figure 3:** Growth rate as a function of temperature of cobalt films deposited using $Co(acac)_3$.

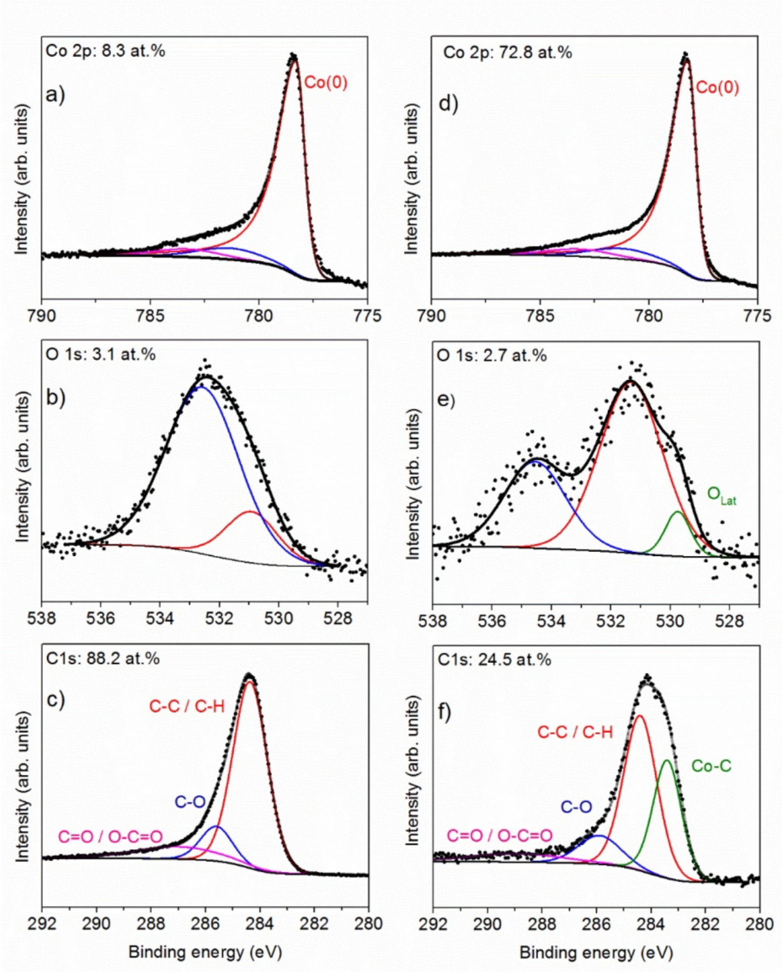

**Figure 4:** XP spectra of cobalt films deposited at 400°C (a, b, c) and 250°C (d, e, f) using $Co(acac)_3$ and $Co(acac)_2$ precursors, respectively.

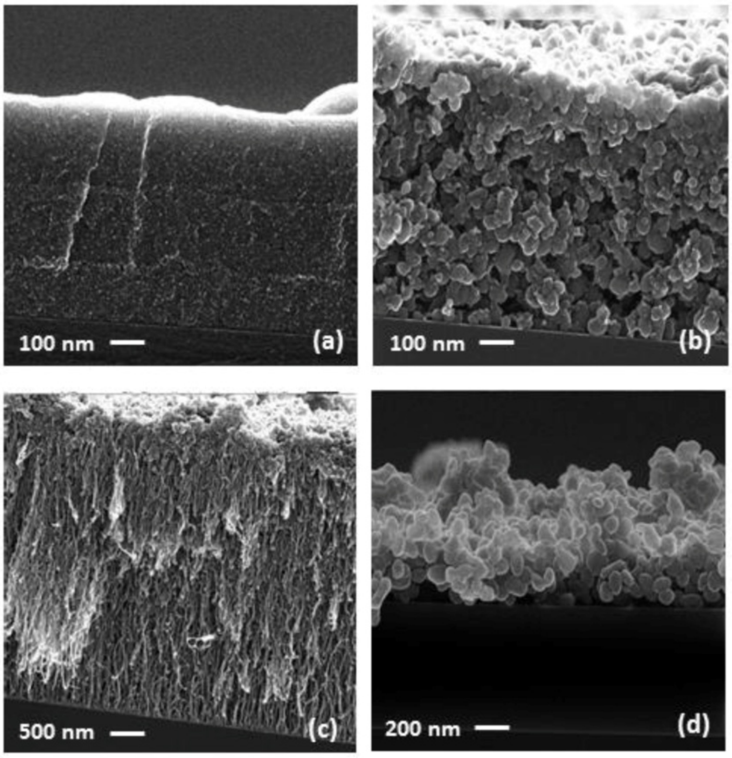

**Figure 5:** HIM cross-section micrographs of cobalt films deposited at different temperatures, using the precursor Co(acac)$_3$ at 320 °C (a), 400 °C (b) and 480 °C (c), and the precursor Co(acac)$_2$ at 250 °C (d).

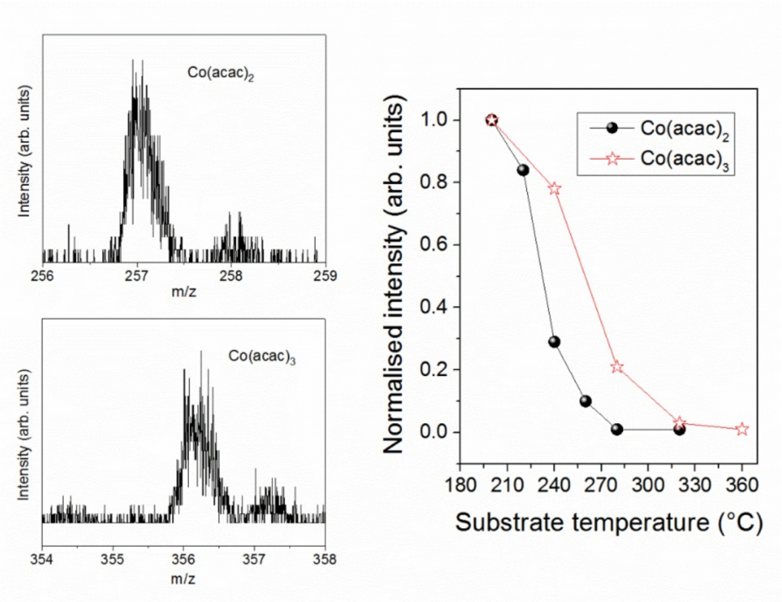

**Figure 6:** Left panel: MBMS monitoring of the thermal decomposition of the Co(acac)$_2$ and Co(acac)$_3$ precursors in ethanol atmosphere. The right panel shows spectral intensities for m/z=257 and m/z=356 depending on the substrate temperature.

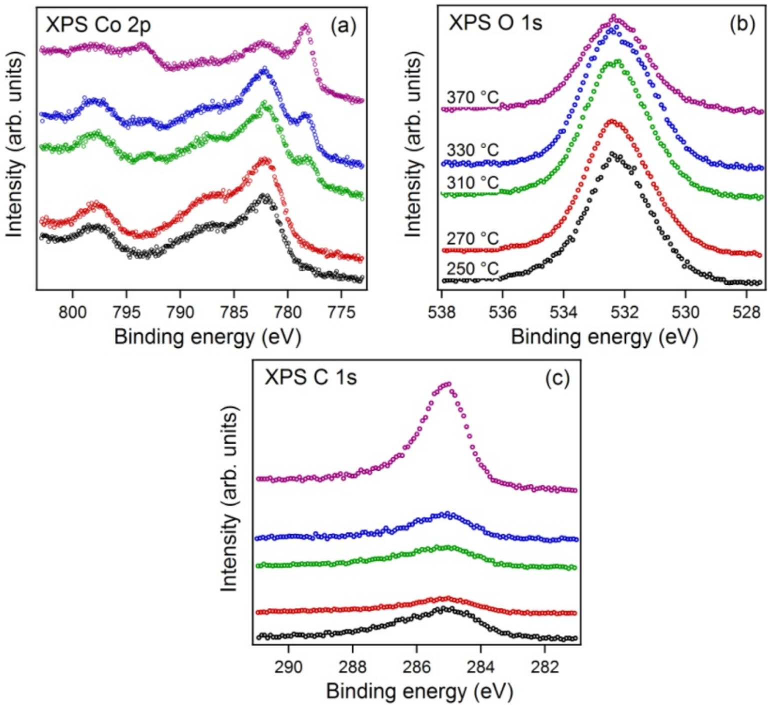

**Figure 7:** *In-situ* XPS analysis of PSE-CVD cobalt films on $SiO_2$/Si substrate using an ethanol solution of Co(acac)$_2$. Co2p core-shell (a), O1s core-shell (b) and C1s core-shell (c).

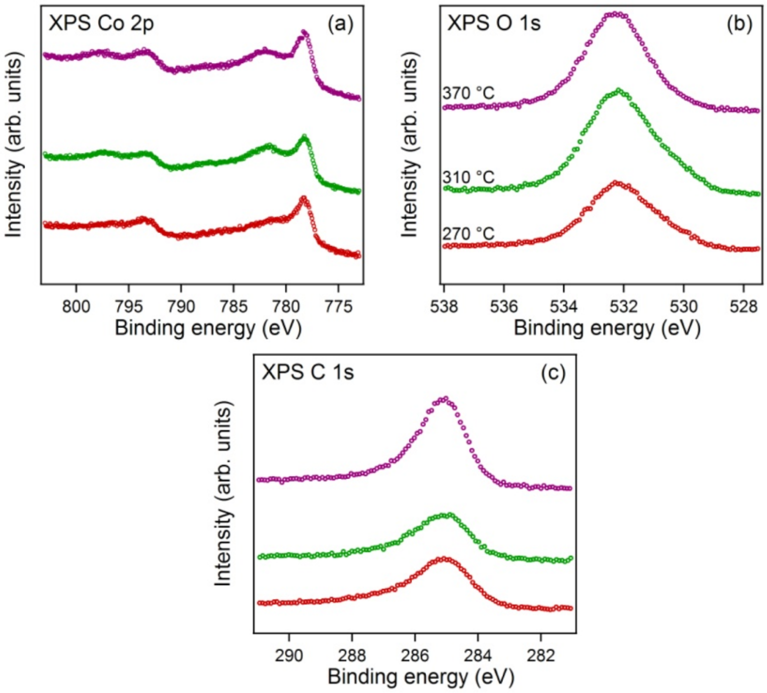

**Figure 8:** *In-situ* XPS analysis of PSE-CVD cobalt films on Ni-coated $SiO_2$/Si substrate using an ethanol solution of $Co(acac)_2$. Co2p core-shell (a), O1s core-shell (b) and C1s core-shell (c).

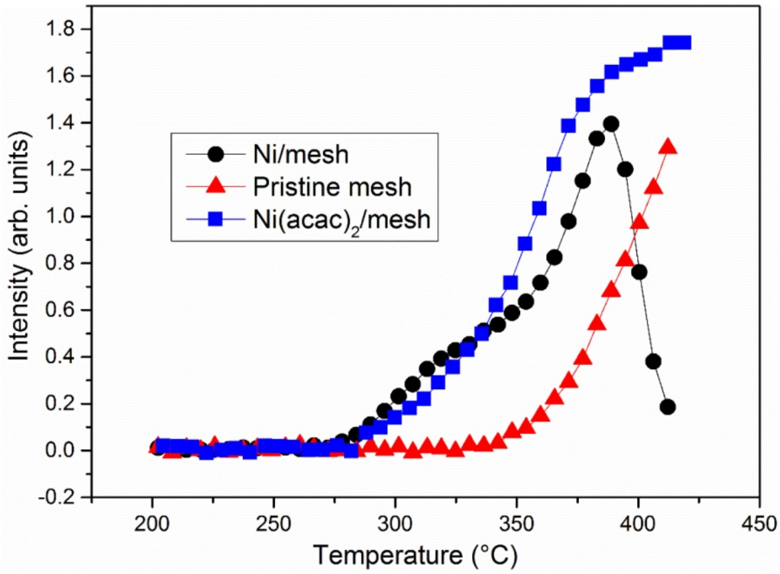

**Figure 9:** Light-off-curves of acetaldehyde formation during the thermolysis of ethanol over uncoated mesh substrate, nickel-coated mesh and Ni(acac)$_2$ chemisorbed on the mesh substrate.

# SUPPLEMENTARY MATERIAL

to

# Investigation of the growth behaviour of cobalt thin films from chemical vapour deposition, using directly coupled X-ray photoelectron spectroscopy

P. H. Tchoua Ngamou[a,1,*], A. El Kasmi[a,b], Th. Weiss[c], H. Vieker[d,2] , A. Beyer[d], V. Zielasek[c], K. Kohse-Höinghaus[a], M. Bäumer[c,*]

[a] Department of Chemistry, Bielefeld University, Universitätsstraße 25, D-33615 Bielefeld, Germany

[b] Laboratory LGCVR, Faculty of Sciences and Techniques, University Abdelmalek Essaadi, B.P. 416 Tangier, Morocco

[c] Institute of Applied and Physical Chemistry, University of Bremen, Leobener Straße UFT, D-28359 Bremen, Germany

[d] Department of Physics, Bielefeld University, Universitätsstraße 25, D-33615 Bielefeld, Germany

* Corresponding authors:

| | |
|---|---|
| Dr. Patrick Hervé Tchoua Ngamou | Prof. Dr. Marcus Bäumer |
| Tel: +49 2461 61 6665 | Tel.: +49 421 218 63170 |
| E-mail: p.tchoua@fz-juelich.de | E-mail: mbaeumer@uni-bremen.de |

---

[1] Now at: Forschungszentrum Jülich GmbH, Institute of Energy and Climate Research, Wilhelm-Johnen-Straße, D-52428 Jülich, Germany

[2] Now at: CNM Technologies GmbH, Herforder Straße 155a, D-33602 Bielefeld, Germany

**Table S1:** Optimised experimental conditions for the deposition of Co metal and Ni seed layer.

| Precursor | $Co(acac)_{2,3}$ | $Ni(acac)_2$ |
|---|---|---|
| Solvent | Ethanol | Ethanol |
| Concentration (mM) | 5 | 5 |
| Substrates | Thin glass, silicon, planar and mesh of stainless steel | |
| Frequency (Hz) | 2-4 | 2-4 |
| Opening time (ms) | 14 | 14 |
| Evaporation temperature (°C) | 200 | 200 |
| Transportation temperature (°C) | 220 | 220 |
| Substrate temperature (°C) | 240 - 480 | 270 |
| System pressure (mbar) | ~ 60 | ~ 60 |
| Carrier gas ($N_2$ ) (slm) | 0.5 - 1.0 | 0.5 - 1.0 |

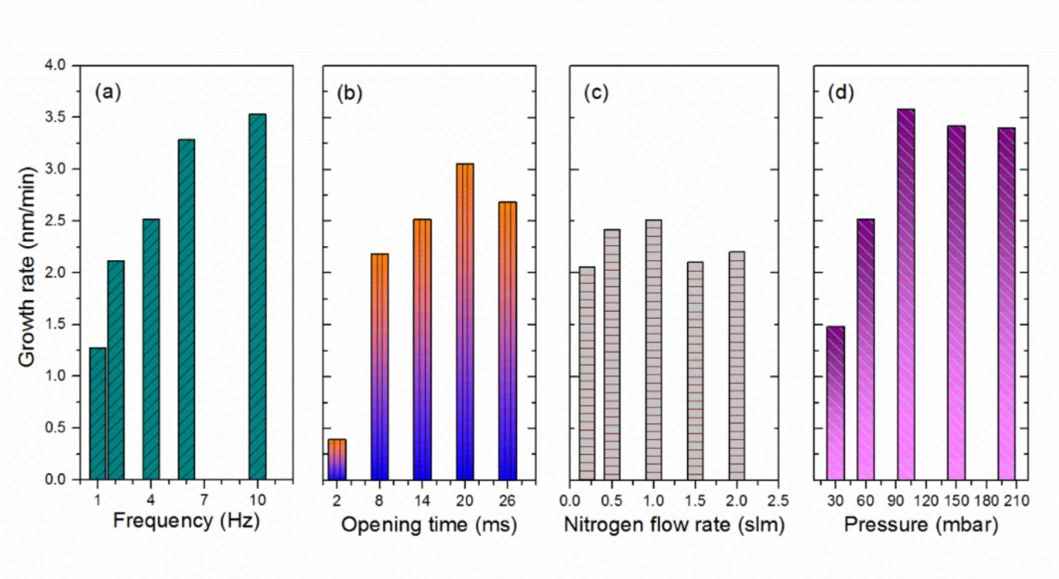

**Figure S1:** Effect of the delivery conditions, the flow rate of $N_2$ and the pressure on the growth of Co films deposited at 400 °C using $Co(acac)_3$ precursor.

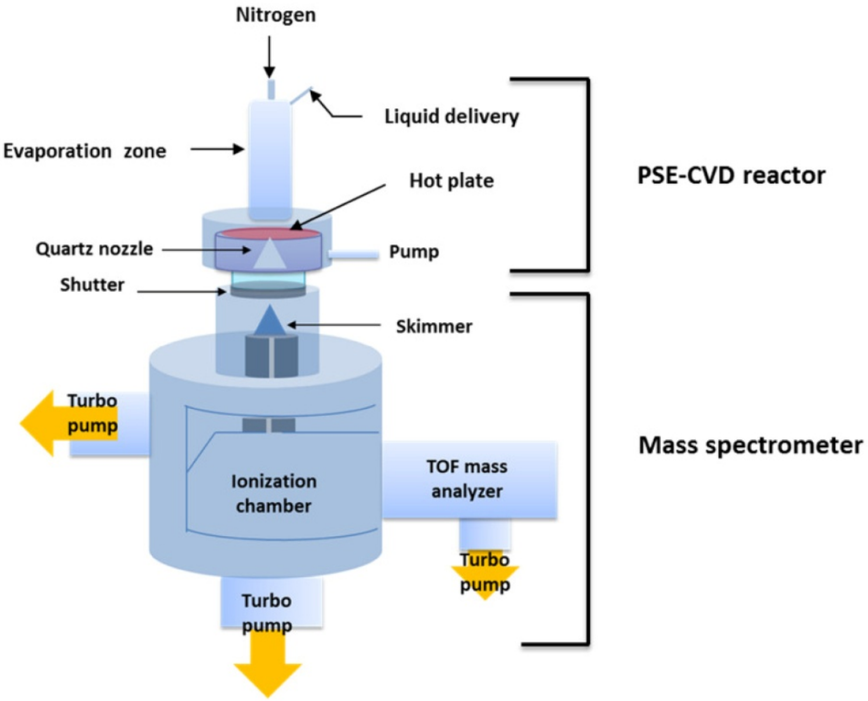

**Figure S2:** Schematic diagram of the PSE-CVD reactor with *in-situ* molecular-beam mass spectrometer.

**Description:** The system consists of the PSE-CVD reactor, a differentially pumped chamber with a molecular-beam sampling system and an electron ionisation chamber with a reflectron time-of-flight mass spectrometer. A quartz cone-shaped nozzle with an orifice of ~100 µm at the tip was used to sample reaction species. The tip of the nozzle was inserted into a hole in the flat heater of the CVD reactor. The sampled species form a molecular beam in the differentially pumped chamber and pass through a copper skimmer into the ionisation chamber, where the molecular beam is crossed and ionised by electrons. The produced ions are propelled into a flight tube and reflected to the detector. During the PSE-CVD process, the temperature of the evaporation zone was kept constant (200°C) and only the temperature of the flat heater was increased from 205 to 360°C. The deposition was performed onto a bare glass substrate with a surface of 50 mm$^2$, negligible to that of the flat heater (19.65 cm$^2$).

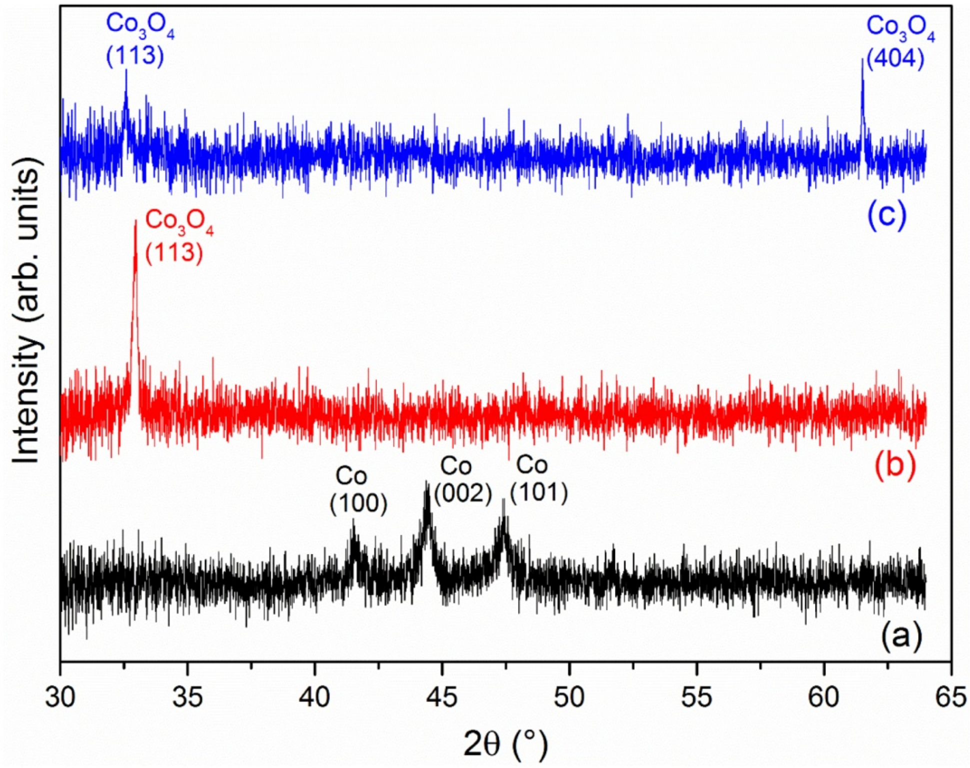

**Figure S3:** XRD patterns of the films grown on nickel-coated Si/$SiO_2$ substrate using ethanol solutions of Co(acac)$_2$ at 250°C (a), Co(acac)$_3$ at 270°C (b) and Co(acac)$_3$ at 280°C (c).

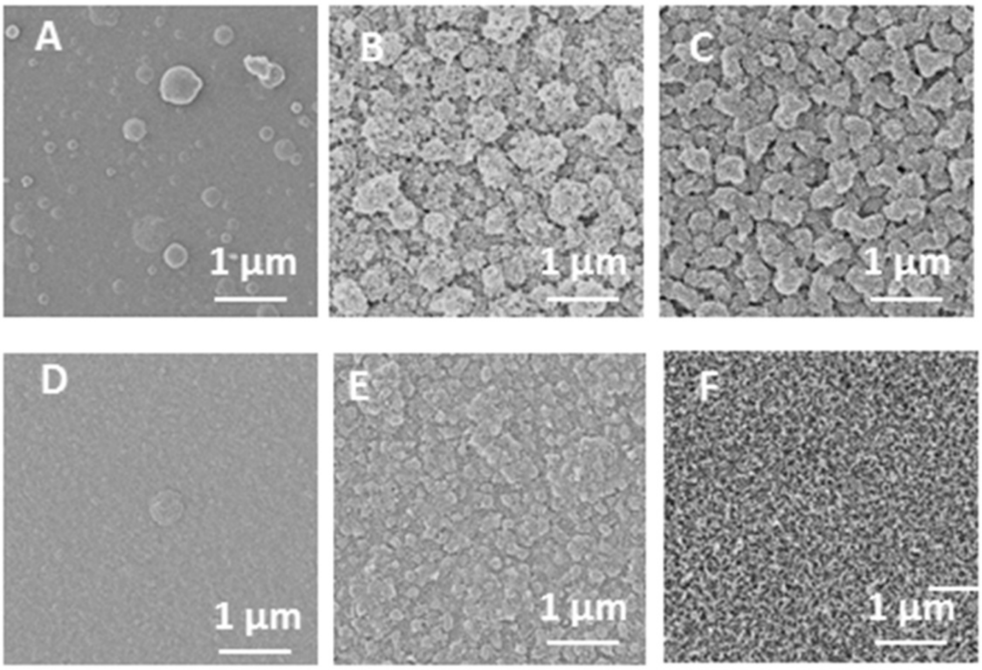

**Figure S4:** HIM micrographs of metallic cobalt films deposited from an ethanol solution of Co(acac)$_3$ at 320°C (A, D), 440°C (B, E) and 480°C (C, F) on bare glass (A, B, C) and nickel-coated glass (D, E, F).

# Paper III

www.nature.com/scientificreports

SCIENTIFIC REPORTS

OPEN

# Influence of Water on Chemical Vapor Deposition of Ni and Co thin films from ethanol solutions of acetylacetonate precursors

Received: 20 May 2015
Accepted: 16 November 2015
Published: 14 December 2015

Theodor Weiss, Volkmar Zielasek & Marcus Bäumer

**In chemical vapor deposition experiments with pulsed spray evaporation (PSE-CVD) of liquid solutions of Ni and Co acetylacetonate in ethanol as precursors, the influence of water in the feedstock on the composition and growth kinetics of deposited Ni and Co metal films was systematically studied. Varying the water concentration in the precursor solutions, beneficial as well as detrimental effects of water on the metal film growth, strongly depending on the concentration of water and the β-diketonate in the precursor, were identified. For 2.5 mM $Ni(acac)_2$ precursor solutions, addition of 0.5 vol% water improves growth of a metallic Ni film and reduces carbon contamination, while addition of 1.0 vol% water and more leads to significant oxidation of deposited Ni. By tuning the concentration of both, $Ni(acac)_2$ and water in the precursor solution, the fraction of Ni metal and Ni oxide in the film or the film morphology can be adjusted. In the case of $Co(acac)_2$, even smallest amounts of water promote complete oxidation of the deposited film. All deposited films were analyzed with respect to chemical composition quasi *in situ* by XPS, their morphology was evaluated after deposition by SEM.**

Chemical Vapor Deposition (CVD) and its variants such as Atomic Layer Deposition (ALD) are key technologies in the industrial production of thin metal films for a broad range of applications[1]. In the CVD family of processes a solid film is deposited from a vapor of precursor molecules by chemical reactions occurring on or in the vicinity of a substrate surface, which is usually heated to thermally stimulate the reaction. Metal CVD can be used to produce fibers, monoliths, foams, and powders of pure metals or alloys with free variation of the composition for catalysis, microelectronic, and optical devices[2,3]. There are two classes of organic precursors which are routinely used in CVD: organometallic (OM) precursors with metal centers mostly bonded to carbon and metal-organic (MO) precursors such as the class of β-diketonate complexes including the acetylacetonates (acac), hexafluoroacetylacetonates (hfac), dipivaloylmethanates (dpm), and alkoxides of different metals, i.e., with metal centers bonded to typically oxygen, nitrogen or sulfur[3,4]. Elucidating the CVD reaction mechanisms for these precursors comprehensively and in detail is prerequisite for process optimization and beneficial for the selection and synthesis of new precursors. In this respect, also boundary conditions may play important roles but often lack systematic studies.

One of the big problems using solid organic precursors in metal CVD is their sensitivity to air and moisture[5–7]. Generally, the hygroscopic nature of many OM and MO precursors promotes the formation of hydrates which leads to significant configuration changes within the precursor depending on the water content. For example, anhydrous $Ni(acac)_2$ forms trimers in order to achieve an octahedral coordination around each nickel atom. When water is present, each $Ni(acac)_2$ prefers to take up position in an octahedral complex with two water molecules for that purpose[7–10]. Such changes may induce strong dependencies of the precursor volatility and thermal stability on the water concentration[7,10,11]. Additionally, water may influence the precursor adsorption selectivity by formation of OH groups on the substrate surface and affect reaction mechanisms thereon[3,9,12–14]. Overall, the sensitivity of the precursor to moisture may render the control of parameters such as nucleation rate, growth rate, or precursor fragmentation difficult and thus affect quality (morphology) and purity (carbon incorporation) of the CV deposits.

Several studies have reported that water affects the reduction mechanisms of β-diketonates, in particular metal (M) $(acac)_x$ precursors, employed in classical CVD and ALD regimes. $M(acac)_x$ as CVD precursors have been in the focus of interest because they are commercially available low-cost products of minor toxicity and exhibit

Institut für Angewandte und Physikalische Chemie, Universität Bremen, Leobener Straße UFT, D-28359 Bremen, Germany. Correspondence and requests for materials should be addressed to V.Z. (email: zielasek@uni-bremen.de)

low evaporation temperatures and easily controllable purity[7,15]. Only few systematic studies on the influence of water on β-diketonates under CVD conditions are available and their results often appear to be contradictory. For instance, it has been reported that CVD with a β-diketonate such as $Cu(hfac)_2$ as precursor in combination with $H_2$ as reducing agent can be area-selective, i.e., copper, in this case, is deposited on metal substrates but not on oxide areas[16–19]. When adding water to the reaction gas mixture, some authors found a loss of the precursor's selectivity to metal substrates[19] while others reported, for apparently similar experiments, that the selectivity is unaffected[20]. Furthermore, there are several reports on an *increase* of carbon contamination due to the presence of water in the gas phase during metaloxide (MOx) deposition on soda lime glass substrates from Cu and Ni β-diketonates such as $M(acac)_2$, $M(dmg)_2$, and $M(hfac)_2$[3,7,9,21]. Using the same β-diketonate precursors for obtaining M, MOx, and metalnitride films on $SiO_2$, $\alpha$-$Al_2O_3$ and polyimide substrates, others found, however, a *decrease* of carbon content when water was added to the CVD reactants mixture[22–24]. Finally, Utraininen *et al*. found as a general trend that $H_2O$ in combination with β-diketonate complexes like Cu/Ni/Pt $(acac)_x$ (deposited on glass, SiOx, AlOx, and TiOx) leads to the deposition of metal oxide films during ALD[9,11]. In accordance with this trend, Borgharkar *et al*. showed for CVD from $Cu(hfac)_2$ on TiN-coated Si(100) substrates that the metal film growth rate and the electrical conductivity of the deposit can be improved by *eliminating* $H_2O$ from the starting precursor[25]. In contrast, several other CVD studies (on many different types of substrates including Kapton) reported that *addition* of water enhanced the metal film nucleation and increased the rate of β-diketonate reduction by $H_2$[16,17,22,26–28].

In practice, controlling water contamination in the entire CVD process is harder than just to care for pure precursor feedstock. As pointed out by Pierson[2], a pure reactant can become contaminated in the distribution system to the reactor by, amongst others, moisture even if gas-tight metal lines are used. Therefore, in order to limit costs it is essential to know what grades of purity of precursors, feed gases and reactor lines have to be maintained for good results. Also, as demonstrated above, water may even have beneficial effects on the composition or growth rate of the deposit. Consequently, in order to make use of these effects purposefully and reach optimal growth conditions with reasonable efforts, systematic studies on the influence of water on CVD processes are, as also noted by others[21], a prerequisite.

In the following we will present a comprehensive study of the influence of water on metal film formation exemplarily in a special field of CVD: the pulsed-spray evaporation (PSE)-CVD from a liquid feedstock of acetylacetonate precursors in ethanol which serves as solvent and reducing agent at the same time[29–32]. The PSE-CVD method offers several advantages compared to the classical gas phase CVD: Metal films can be obtained without employing gaseous hydrogen, there is less demand on the precursor in terms of volatility and stability, and the precursor does not need to be heated for spray evaporation[29,32]. The selection of acetylacetonates as precursor was not only based on low costs, low toxicity, and the commercial availability of a wide variety of different metals (as mentioned above) but acetylacetonates are also readily soluble in ethanol. To a liquid, alcohol-based precursor solution, water is easily added and its amount can be precisely varied, allowing for rigorous studies of the influence of water on the CVD process. By varying systematically and in a broad range the water content in Ni and Co acetylacetonate precursors for PSE-CVD of Ni and Co, we found both, beneficial and detrimental effects of water on the metal film growth, strongly depending on the concentration of water and the β-diketonate in the precursor solution. All deposited films were analyzed with respect to chemical composition quasi *in situ* by x-ray photoelectron spectroscopy (XPS) and their morphology was evaluated after deposition by scanning electron microscopy (SEM).

## Experimental Methods

The deposition experiments were performed in a home-built PSE-CVD reactor described in detail elsewhere[32]. In brief, the reactor is directly attached to an ultra-high vacuum system with XPS (Multiprobe system, Omicron Nanotechnology, base pressure $10^{-10}$ mbar) and allows for contamination-free transfer of a sample from the reactor to the XPS after any stage of deposition. Apart from the water concentration, all experimental deposition parameters (see Supplementary Table S1 available online) were chosen on the basis of previous publications[29,30,33,34]. For all depositions discussed in the following, solutions of commercially available anhydrous 95% $Ni(acac)_2$ and 97% $Co(acac)_2$ (Sigma-Aldrich) in absolute ethanol (VWR Chemicals) were used. In PSE-CVD the concentration of the β-diketonate precursor molecule in the liquid feedstock is an adjustable parameter. To obtain a feedstock with 2.5 mM Ni concentration, 64.2 mg of the Ni precursor was weighed and dissolved in 100 ml alcohol. The solution was ultrasonically shaken to achieve complete dissolution. With double and triple amounts of Ni precursor, also 5.0, and 7.5 mM Ni precursor feedstock were prepared. Using 192.9 mg of $Co(acac)_2$, a 7.5 mM Co precursor feedstock was produced in a similar way. All precursor solutions were prepared freshly directly before PSE-CVD. The purity of the absolute ethanol (>99.9 vol%) was confirmed by an analytical hydrometer. Further tests showed that keeping the absolute ethanol in contact with the atmosphere for one week resulted in absorption of water up to 3 vol%. Therefore, fresh preparation of the precursor solutions directly before PSE-CVD was essential to ensure the purity of our experiments and neutralize the "aging" effect of the precursor feedstock. For a systematic study of the water influence on the CVD process, distilled $H_2O$ was added to the precursor solution to adjust the water concentration. It was varied from 0.0 vol% to 15.0 vol% (1.0 vol% corresponds to 0.555 mol/l) and could be controlled within ± 0.1 vol% as confirmed by the analytical hydrometer.

A piece from a Si(100) wafer was cut as substrate, cleaned with isopropanol in an ultrasonic bath, and dried in air, so that Ni or Co were deposited on top of the native or thermal silicon oxide layer of the wafer. XPS showed that the mild cleaning procedure left, very reproducibly, a level of 9 atom% residual carbon contamination on the substrate surface. In order to keep the substrate preparation simple, neither chemical cleaning steps nor in vacuo thermal treatments were employed to remove all carbon or the SiOx layer from the Si wafer. It should be noted that, depending on CVD applications, typically more vigorous substrate treatments are employed. For precursor delivery via the spray nozzle a solenoid valve pulse frequency of 2 Hz and a spray injection phase of 15 ms were used, meaning that the solenoid valve opened two times per second for 15 ms and a total deposition time of 30 min corresponded to a net precursor solution injection time into the reactor of 54 s. For all experiments shown in the following, the total deposition time was kept constant, resulting in different thicknesses of the deposits for different precursor concentrations, as will be detailed below. During deposition, the pressure in the deposition area as well as the sample surface temperature were adjusted and stabilized (see the previous publication for further details)[32]. The temperature for deposition was chosen equal to the optimal metal deposition temperature with the maximal growth rate determined in previous PSE-CVD experiments as 270 °C and 310 °C for Ni and Co precursors, respectively[29,32,34]. With one exception to be discussed below, higher temperatures were not employed to avoid undesirable decomposition of precursor ligands which would increase contamination of the deposited films. Below 260 °C, cobalt carbide formation was observed[34], leaving a rather narrow temperature range for metal PSE-CVD for both, Ni and Co.

After the deposition process was finished, samples were transferred immediately *in vacuo* into UHV for XPS analysis. For XPS, non-monochromatized Al K$\alpha$ radiation was used for photoelectron generation and a Leybold EA 10 Plus hemispherical energy analyzer with single-channeltron detector was employed. The obtained XP spectra were normalized and then fitted using Igor Pro (from Wave Metrics) and FITT (Seoul National University) software. For the fit a Shirley-type background was taken into account. The morphology of the deposited films was assessed *ex situ* using a Carl Zeiss Ultra Plus Field Emission scanning electron microscope operated at 15.0 keV electron energy.

## Results and Discussion

Conditions for growing (metallic) Ni films by PSE-CVD from Ni(acac)$_2$ dissolved in ethanol had been established in previous work which reported Ni(acac)$_2$ concentrations in the range from 2.5 to 10.0 mM as optimal and the growth rate as increasing linearly with the precursor concentration in that range[29]. Further increase of the Ni(acac)$_2$ concentration is limited by the short lifetime (re-crystallization) of highly concentrated precursor solutions. Below 2.5 mM, film growth becomes impractically sluggish. For our own experiments we selected three different Ni(acac)$_2$ concentrations (2.5, 5.0, and 7.5 mM) with sufficient precursor lifetime within the optimal range and performed PSE-CVD. As noted before, the total deposition time for all Ni films studied in the following was 30 min. The first part of this section will provide a full account of the observed effects of water concentration variation in the precursor solution on composition and morphology of the deposited Ni films. In the second part of this section, the influence of water on films deposited from 7.5 mM Co(acac)$_2$ precursor solution will be demonstrated and discussed. In contrast to PSE-CVD of Cu or Ni, finding parameters for deposition of pure metal Co films from Co(acac)$_2$ has been reported as difficult because cobalt precipitates mainly unreduced as carbide or oxide[35]. Moisture may play a key role here.

**Ni(acac)$_2$ in EtOH on SiOx/Si(100).** The presentation of results and their discussion will be based on a quantitative analysis of XP spectra from the deposited films. Exemplarily, Fig. 1 depicts a selection of O 1s and C 1s XP spectra obtained in the take-off direction normal to the surface after PSE-CVD with 2.5 mM Ni(acac)$_2$ precursor solution and shows the results of the fitting routine including all individual contributions that were considered for the fit. Examples of Ni 2p spectra and their fit by contributions from Ni$^0$ and Ni$^{2+}$ can be found elsewhere[32]. Based on a previous XRD study which found no evidence for Ni$_x$C after PSE-CVD from Ni(acac)$_2$ in ethanol for substrate temperatures in the range from 190 °C to 290 °C[36], the presence of nickel carbide can be ruled out.

The solid (brown) curve labeled "NiOx" in Fig. 1a designates O 1s emissions with a binding energy of 529.9 eV stemming from Ni$^{2+}$O$^{2-}$ [37–39]. It is absent on the clean substrate but can be detected after film deposition and increases with the water concentration in the liquid precursor feedstock. The dotted magenta "C-C/C-H" curve in Fig. 1b (highest intensity at 0.0 vol% water concentration) denotes C 1s emissions from carbon-carbon and hydrocarbon bonds (binding energies 284.8 eV)[40–44] which are also absent on the fresh substrate but can be found after PSE-CVD from Ni(acac)$_2$ solution. Photoemission characteristic for C-O bonds can be found as O 1s signal at a binding energy of 530.9 eV (dashed orange "C-O" curve in Fig. 1a) and as C 1s signal with a binding energy of 286.1 eV (dashed orange "C-O" curve in Fig. 1b)[45–47]. Both show the same trend as the water concentration is increased in the 2.5 mM Ni(acac)$_2$ precursor solution: slight decrease of the intensity up to 0.5 vol% water and then a significant increase at 4.0 vol% and 10.0 vol% water. Contributions of double C=O bonds can be easily distinguished from C-O emissions only by the C 1s signal (Fig. 1b, dash-dotted green "C=O" curve at 287.9 eV)[46]. In the O 1s emission the C=O signal (dash-dotted green" C=O" curve at 532.9 eV in the Fig. 1a) is somehow overlapped by O 1s emissions from SiOx (Dotted magenta "SiOx" curve with the binding energy 532.1 eV), rendering the separation of the C=O from the SiOx contribution within the O 1s signal difficult.

**PSE-CVD from 2.5 mM solutions.** For an interpretation of the XPS results, having an idea of thickness and morphology of the deposits under investigation is instrumental. Supplementary Fig. S1 (online) shows selected SEM data of films deposited from 2.5 mM Ni(acac)$_2$ with 0.0 vol%, 0.5 vol%, 5.0 vol%, and 10.0 vol% water in the precursor feedstock, respectively. Within the SEM resolution, all films appear to be continuous or percolated but composed of grains with diameters on the order of some nanometers in the case of 0.0 vol% and 0.5 vol%. Films obtained from precursor solution with 5.0 vol% water show somewhat bigger grains and those deposited from Ni(acac)$_2$ solution with 10.0 vol% water show an even coarser morphology with more heterogeneously sized grains in the diameter range of some 10 nanometers.

The thickness of the deposited films was estimated from cross sectional images at a cleaved substrate edge. In contrast to Supplementary Fig. S1, the angle of sample rotation was adjusted in order to obtain a projection along the substrate surface plane (viewing angle 90°) so that the metal layer thickness could be directly measured in the SE micrographs. The measured thickness values are 30 nm, 40 nm, 40 nm, and 50 nm (±5 nm), for films deposited from solutions with 0.0%, 0.5%, 5.0%, and 10.0 vol% water, respectively.

Figure 2 provides a comprehensive overview of the XPS data in the binding energy regions of a) Ni 2p, b) O 1s, and c) C 1s obtained for films deposited from 2.5 mM Ni(acac)$_2$ for various water concentrations in the liquid precursor feedstock mixture. Results of a quantitative analysis of these spectra based on the fitting routine sketched

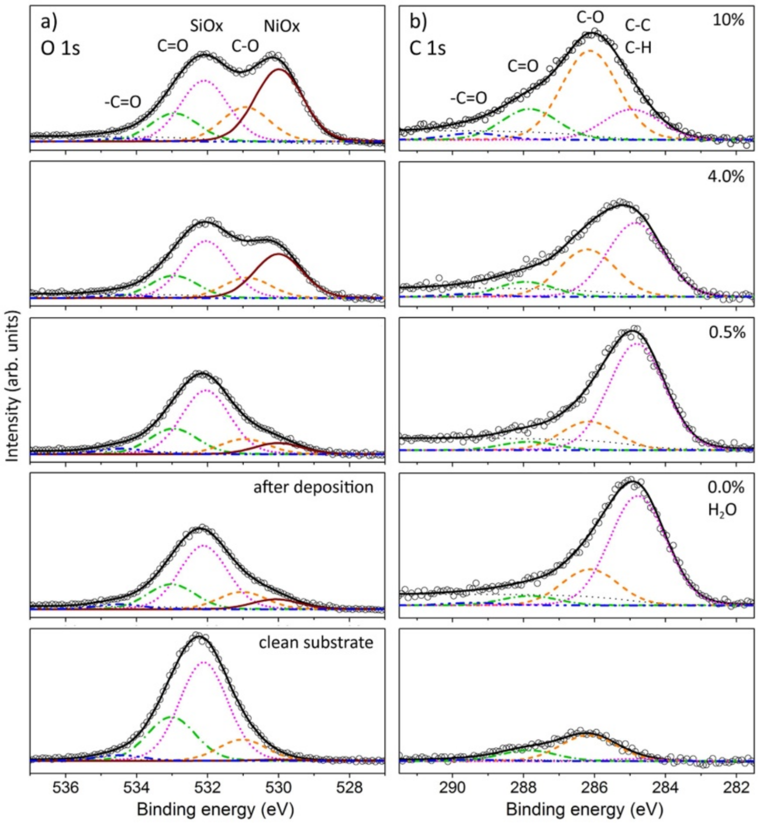

**Figure 1. Fits of the O 1s (a) and C 1s (b) XPS spectra obtained from the SiOx/Si(100) substrate (bottom panels) and Ni/NiOx films grown ontop by PSE-CVD from 2.5 mM Ni(acac)$_2$ in ethanol and with various water concentrations (0.0%, 0.5%, 4.0%, and 10.0 vol%) in the precursor solution at a substrate temperature of 270 °C.**

above are compiled in panels d), e), and f). These show the intensities of major signal contributions depending on the water concentration and allow us to pinpoint trends for the composition of the deposited films. Before, it should be noted that, although the film thickness estimates are large with respect to the typical XPS probing depth of few nm, Si 2p emissions, especially those from SiOx, are still present in XP spectra after film deposition. Given the grainy film structure, we assume that density variations and grain boundaries render fingerprints of the substrate–film interface visible in the XPS spectra. In the following, we will discern the two water concentration regimes 0.0% to 1.0 vol% and 1.0% to 10.0 vol% for the discussion and take the waterless solution as reference.

The Ni 2p XP spectrum (Fig. 2d) of the film deposited from waterless precursor solution (0.0 vol% $H_2O$) indicates the presence of 97% metallic Ni and only 3% oxidized Ni. When the angle of photoelectron detection is changed to 45° off the surface normal, metallic Ni predominates and accounts for >99.5%, indicating that the oxidized Ni may be located close to the substrate-film interface. Therefore we interpret the Ni-oxide signal as related to Si-O-Ni interlayer species probably forming on the native oxide of the Si wafer (which was not removed prior to deposition as mentioned before) and conclude that, on top of that interlayer, PSE-CVD from waterless precursor solution produces only metallic Nickel. In accordance, we interpret that part of the O 1s emission (Fig. 2e) which can be attributed to Ni-oxide (about 3% of the entire O 1s signal) as related to a Si-O-Ni interlayer. Within error bars, both, the NiOx-related Ni 2p and O 1s signals show the same trends.

It has been reported that M(acac)$_x$ precursors are prone to causing relatively high levels of carbon impurities in the deposited films[3,7]. For the film deposited from waterless 2.5 mM Ni(acac)$_2$ precursor we find the atomic ratio

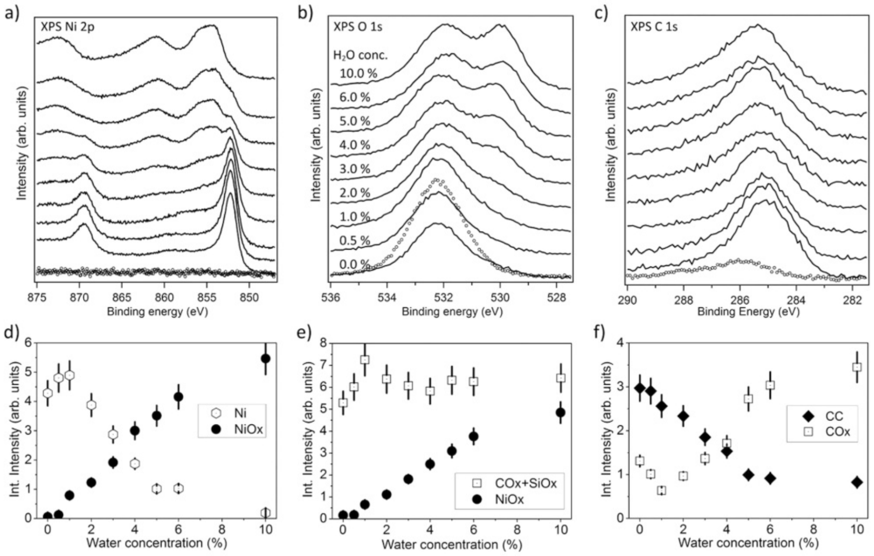

**Figure 2. Top panels: XPS spectra in the binding energy range of (a) Ni 2p, (b) O 1s, and (c) C 1s emissions obtained from the SiOx/Si(100) substrate (dotted curves) and from Ni/NiOx films (thickness 30–50 nm) grown ontop by PSE-CVD from 2.5 mM precursor solution with various water concentrations (from 0.0% to 10.0 vol%) at a substrate temperature of 270 °C (solid lines). Bottom panels: Integral peak intensities determined from fits to the XPS data (see text for details).**

of carbon to nickel ($\frac{n_A}{n_B} = \frac{\frac{I_A}{S_A}}{\frac{I_B}{S_B}}$, where $I_x$ denotes a XPS peak area, and $S_x$ the relative sensitivity factor for element $x$) as about 0.2. This ratio does not change when the polar angle of photoelectron detection is changed to off-normal for higher surface sensitivity. Therefore, we conclude that the carbon is homogeneously distributed within the deposited film. The C 1s photoemission from these carbon impurities is composed of ~70% C-C/C-H and ~30% carbon oxide signals while, in contrast, XPS from intact Cu and Co acetylacetonate precursor clusters had shown a C-C/C-H to COx signal ratio of ~30: 70[48], i.e., the C-C/C-H fragments of the precursor appear to be less volatile.

Adding a small amount of water (about 0.5% – 1.0 vol%) to the liquid feedstock (all other deposition parameters were left unchanged) leads to significant changes. First, an increase of the absolute intensity of the Ni 2p signal by 31% compared to the waterless solution (Fig. 2d) is observed after PSE-CVD. Given the film thickness well beyond the typical XPS probing depth, we interprete the observed variation of the total Ni 2p intensity as related to surface roughness. As demonstrated by others, an increase of surface roughness leads to a decrease of the total photoemission intensity due to shadowing effects and the reduced off-normal yield from inclined surface regions[49–51]. On the nanometer scale which is not resolved in our SEM data, the admission of up to 1.0 vol% of water to the feedstock probably leads to a smoother surface and a denser film, on the average. Concomitantly, the SEM evaluation indicates that the films grown from precursor feedstock with 0.5 vol% and 1.0 vol% water, respectively, are, on average, thicker than the film grown from waterless solution (40 nm vs. 30 nm), indicating an increase of the growth rate. The NiOx component of the Ni 2p signal which we attributed to a Si-O-Ni interlayer remains almost unchanged when 0.5 vol% water is present in the precursor. It increases significantly only at a water concentration of 1.0 vol% in the precursor and then accounts for more than 13% of the entire Ni 2p signal. Concomitantly, the O 1s emissions associated with NiOx (Fig. 2e) increase at 1.0 vol% of water, accounting then for ~8% of the total O 1s intensity. These step-like increases beyond the photoemissions attributed to a Si-O-Ni interlayer indicate the presence of Ni oxide in the film.

The level of carbon contamination in the deposited films decreases as the water concentration in the liquid precursor feedstock is raised to 0.5% and 1.0 vol%, respectively. For 1.0 vol% water the atomic ratio of carbon to nickel is about 0.1, i.e., half of the value observed for waterless precursor solution, while the C-C/C-H to COx ratio changes to 4:1 (Fig. 2f)[48].

The O 1s signal that can be related to both, SiOx and COx, linearly increases with the water concentration in the precursor (Fig. 2e) by up to ~40% compared to the waterless solution. The increase observed for 0.5 vol%

water is probably due to an increase of the SiOx component, only, as confirmed by the Si 2p signal (not shown here) which reveals that emissions from oxidized Si ($Si^{2+}$) (with a binding energy of 103.3 eV) increase as the water concentration in the liquid feedstock is raised from 0.0 to 1.0 vol%. It should be noted that we do not observe a concomitant increase of the $Si^0$ component of the Si 2p signal, indicating that the Si-Ox interlayer grows, probably due to oxidation of the Si substrate by water which, with some caution, may be taken as indicator for the formation of hydroxides at the silica surface upon adsorption of water from the precursor solution[52–55]. The C 1s signal related to COx (Fig. 2f) even decreases (to ~50% of the intensity found for the waterless precursor) as 1.0 vol% water is added to the precursor solution, supporting the conclusion that the observed increase of the O 1s intensity at a binding energy of 532.9 eV is due to oxidation of the substrate.

In summary, for water concentrations in the range 0.0–1.0 vol% we observed the following trends: Water in the liquid precursor feedstock promotes the growth of metallic Ni and reduces carbon contamination of the deposited films. Ni oxide starts to grow only at water concentrations above 0.5 vol%, so that 0.5 vol% water is optimal for the deposition of fully reduced Nickel films, i.e., water at that concentration has a positive influence on PSE-CVD of Ni films from 2.5 mM $Ni(acac)_2$ precursor dissolved in ethanol.

Addition of higher amounts of water (from 1.0% to 10.0 vol%) to the precursor solution causes major changes in the quality and composition of the deposited films. The metallic component in the Ni 2p signal (Fig. 2d) decreases as the water concentration is increased. At the same time the NiOx contribution to the Ni 2p signal and, in accordance, the NiOx contribution to the O 1s signal increase almost linearly with the water concentration. The photoemissions from metallic Ni ($Ni^0$) are less than 3% of the total Ni 2p signal at 10.0 vol% of water in the precursor solution, and from the slope of the NiOx signal in Fig. 2d,e, respectively, we assume that almost completely oxidized Ni films are obtained for water concentrations of 8.0 vol% and higher. The films obtained from precursor solution with 5.0 vol% and 10.0 vol% water shown in Supplementary Fig. S1 contain only ~20% metallic Ni and ~80% of the Ni as oxide according to XPS. The total amount of carbon within the deposited films does not change significantly when more than 1.0 vol% water is added to the precursor solution (within error the total intensity of C 1s emissions remains at the same level), but the ratio of C-C/C-H to COx emissions changes from ~4:1 to ~1:4, as the water concentration is increased from 1.0% to 10.0 vol%. Obviously, excessive amounts of water (>1 vol%) in the precursor feedstock lead to oxidation of the deposited Ni and of the carbon impurities in the film.

Overall, while more than 1.0 vol% water in the liquid 2.5 mM $Ni(acac)_2$/ethanol feedstock is detrimental for the deposition of Ni films, as it leads to oxidation of the deposited metal, small amounts of water (between 0.0% and 1.0 vol%) have positive effects, such as a lower level of carbon contamination and, apparently, a denser and smoother morphology. An improved growth rate may be linked to a promotion of precursor adsorption on the substrate surface by OH-groups forming at the surface upon adsorption of water, as previously reported for various precursors deposited on alumina, soda-lime glass, and $SiO_2$ substrates[4,9,12,14]. On $SiO_2$, surface OH-groups have been demonstrated to be stable up to 800 °C and above[12,56–58]. At the first nucleation steps of the deposited Ni film, OH-groups on the substrate surface may serve as preferable bonding sites for the precursor[12–14]. Enhancing the initial precursor adsorption rate may be very important in the case of relatively low (2.5 mM) precursor concentrations in the liquid feedstock.

Several studies on the interaction of water vapor with Ni surfaces have been reported[59–63]. Oxidation of the Ni surface in presence of water vapor was observed at temperatures as low as 300 °C and even in UHV environment with the oxidation rate increasing as the temperature or the $H_2O$ dose are increased[59,64]. Therefore, as most probable explanation for the onset of Ni oxidation at water concentrations of 1.0 vol% and above we suggest a second decomposition channel of the precursor (where water serves as an oxygen source)[11], initiated by excessive amounts of water (>3 mol% $H_2O$ in ~97 mol% $C_2H_5OH$ with only 0.01 mol% $Ni(acac)_2$ present):

$$\mathrm{M(acac)_2\,(gaseous) + H_2O(gaseous) \rightarrow MOx(solid) + 2H(acac)\ (gaseous)} \qquad (1)$$

This pathway leads to the formation of Ni oxide and will compete with the precursor decomposition by hydrogen which, as previously shown[30,31], is produced by dehydrogenation of ethanol to acetaldehyde and leads to metallic Ni.

To elucidate how the role of water for the Ni deposition process depends on temperature, PSE-CVD from 2.5 mM $Ni(acac)_2$ precursor solution with various water concentrations was also performed at 300 °C substrate temperature which is known to lead to relatively high level of carbon impurities[32]. The analysis of the Ni 2p photoemission spectra is shown in Fig. 3 in direct comparison to the results obtained at 270 °C.

Overall, the integral Ni 2p intensity for the 300 °C deposit is about 50% of that obtained at 270 °C because of carbon contamination which is as high in presence of water as without additional water (data not shown). Similar to the result obtained for 270 °C, a beneficial effect of water on the deposit composition can be identified at 300 °C. There is a maximum of the Ni to NiOx ratio for 2 vol% water which is a four times higher concentration than the optimum for 270 °C. The general trends of the Ni and $NiO_x$ contributions below and above the respective maximum, however, are preserved at elevated temperature. Speculating on a role of surface OH groups as precursor adsorption sites, these OH groups are probably removed from the surface at higher rate at elevated temperature. For compensation, at 300 °C a higher water concentration may be needed than at 270 °C in order to reach optimal growth conditions.

**PSE-CVD from concentrated solutions.** To elucidate the interplay between all three components of the precursor solution, i.e. $Ni(acac)_2$, ethanol and water, PSE-CVD at varying water concentration in the feedstock was also performed starting with 5.0 mM and 7.5 mM concentrations of $Ni(acac)_2$ in ethanol, respectively. As before, the total deposition time was kept constant at 30 min for all deposits.

Qualitatively, the data obtained for 5.0 mM and 7.5 mM solutions show very similar trends when compared to each other while they show significant differences to the data obtained for the 2.5 mM solution. Figure 4 depicts the dependence of XPS in the binding energy regions of a) Ni 2p, b) O 1s, and c) C 1s on water concentration in a

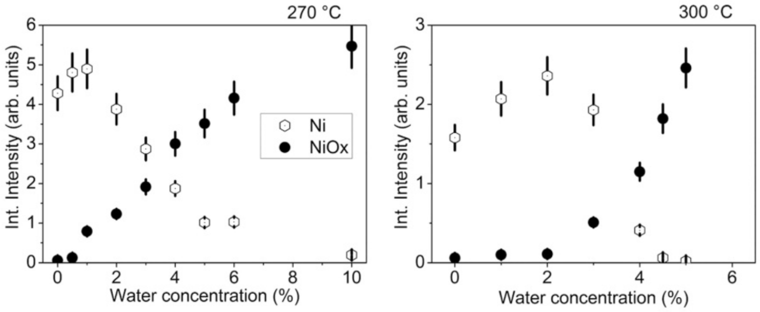

**Figure 3. Integral peak intensities determined from fits to the XPS spectra in the binding energy range of Ni 2p emission obtained from the Ni/NiOx films grown ontop SiOx/Si(100) substrate by PSE-CVD from 2.5 mM precursor solution with various water concentrations (from 0.0% to 10.0 vol%) at a substrate temperature of 270 °C (left) and 300 °C (right).**

liquid feedstock solution of 5.0 mM Ni(acac)$_2$ in ethanol. Similar to Fig. 2, the quantitative analysis of these spectra is condensed into plots d), e), and f), so that the dependence of the deposited Ni film composition on water concentration in the precursor can be followed in detail. For the discussion, the two water concentration ranges 0.0 to 4.0 vol% water and 4.0 to 12.0 vol% water are discerned and, again, the waterless solution is taken as reference.

The Ni 2p photoemission spectrum of a film deposited from waterless 5.0 mM Ni(acac)$_2$ solution (Fig. 4d) shows ~99% metallic Ni and only about 1% oxidized Ni which we attribute to a Si-O-Ni interlayer, in accordance with the results obtained for 2.5 mM precursor solution. Here we take into account that a thicker film has grown from 5.0 mM Ni(acac)$_2$ (60 nm as will be demonstrated below) which should lead to stronger attenuation of the interlayer XPS signal.

In contrast to PSE-CVD with 2.5 mM precursor solution, pure metallic Ni films can be obtained from 5.0 mM Ni(acac)$_2$ precursor dissolved in ethanol only without additional water (0.0 vol%), a positive influence of small amounts of water on the growth rate was not observed. With respect to carbon contamination levels we find C 1s intensities after Ni film deposition from waterless 5.0 mM Ni(acac)$_2$ precursor similar to the deposition from waterless 2.5 mM precursor. The total C 1s to Ni 2p atomic ratio is about 0.2, while carbon impurities (Fig. 4f) consist of ~70% C-C/C-H and 30% C-O/C=O.

When up to 4.0 vol% water are added to the 5.0 mM Ni(acac)$_2$ solution, the film composition significantly changes. The Ni 2p signal representing the metallic fraction of deposited Ni (Fig. 4d) decreases linearly as the $H_2O$ concentration is increased (that also holds for 0.5 vol% water). Instead, a NiOx component becomes evident in O 1s and Ni 2p, accounting for 34% of the entire Ni 2p signal at maximum. Also for PSE-CVD from 5.0 mM Ni(acac)$_2$ precursor solution the addition of water promotes reduction of the carbon impurity level in the film and we found an atomic ratio C : Ni of ~0.14 at minimum by comparing the C 1s an Ni 2p emissions. In contrast to PSE-CVD from 2.5 mM precursor solution, however, the oxidation of carbon impurities sets in already at very low water concentrations as the COx signal in Fig. 4f indicates. The strong singular increase of the combined SiOx and COx components of the O 1s emission upon adding 0.5 vol% water to the waterless precursor solution indicates that, similar to deposits obtained from 2.5 mM precursor, water promotes oxidiation of the Si substrate (Si-Ox interlayer growth).

When the water concentration in the liquid feedstock is increased beyond 4.0 vol%, the Ni oxide content in deposited films does not increase further but even slightly decreases as the water content is raised, so that for water concentrations of ~10 vol% and higher the metallic component of the Ni 2p signal saturates at a level of about 80% of the total nickel emission. As Fig. 4f shows, water in excess of 4.0 vol% in 5.0 mM Ni(acac)$_2$ solution does not change the total level of carbon contamination in the deposited film and, in contrast to the 2.5 mM precursor solution, has no significant influence on carbon oxidation. At water concentrations of 10.0 vol% and higher the ratio between COx and the C-C/C-H contributions to the entire C 1s signal is about 1:1.

The XPS data obtained for PSE-CVD of Ni from 7.5 mM Ni(acac)$_2$ precursor solution are compiled in Fig. 5 and show the same trends within the water concentration ranges 0.0–5.0 vol% and 5.0–15.0 vol%, respectively, as discussed for the deposits from 5.0 mM precursor solution with 0.0–4.0 vol% and 4.0–12.0 vol% water, respectively. Almost metallic Ni films (92% Ni$^0$, Fig. 5d) can be obtained from 7.5 mM precursor solutions only without additional water (0.0 vol%). The Ni oxide content in the film is maximal for 5.0 vol% of water in the feedstock and then accounts for 30% of the total Ni 2p XPS signal. For the waterless 7.5 mM precursor solution carbon impurities in the deposited film (Fig. 5f) consist of ~60% C-C/C-H species and ~40% carbon oxides according to the C 1s signal, with the total amount of contamination (atomic ratio C 1s to Ni 2p is ~0.23) being somewhat higher than in films deposited from 2.5 and 5.0 mM solutions. In contrast to the findings for 2.5 and 5.0 mM precursor solutions, the O 1s signal attributed to SiOx and COx components (Fig. 5e) does not increase as 0.5 vol% water is added to the waterless 7.5 mM precursor solution. Concomitantly, however, the Si 2p substrate signal (not shown here) is not

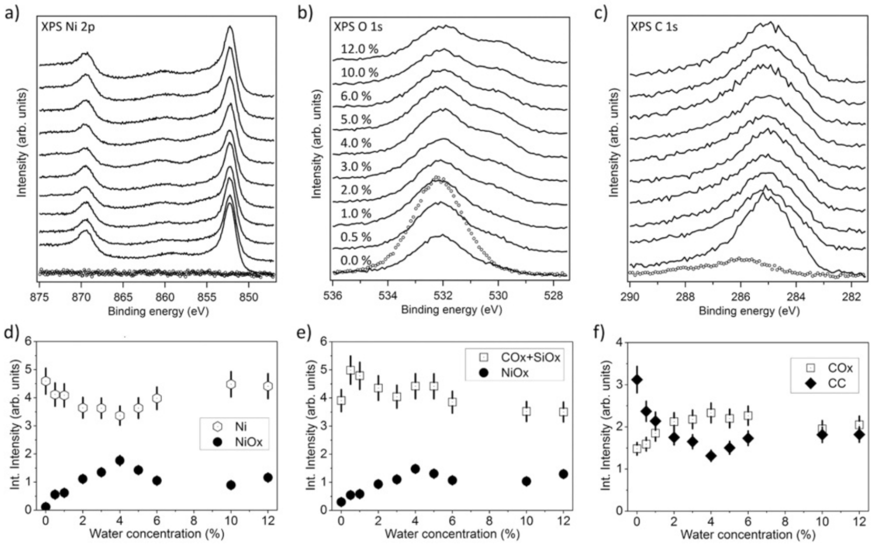

**Figure 4. Top panels: XPS spectra in the binding energy range of (a) Ni 2p, (b) O 1s, and (c) C 1s emissions obtained from the SiOx/Si(100) substrate (dotted curves) and from Ni/NiOx films (thickness 60–120 nm) grown ontop by PSE-CVD from 5.0 mM precursor solution with various water concentrations (from 0.0% to 12.0 vol%) at a substrate temperature of 270 °C (solid lines).** Bottom panels: Integral peak intensities determined from fits to the XPS data (see text for details).

detected on the deposited films due to the large film thickness (>120 nm, see below) so that XPS is not expected to provide any evidence for water-induced oxidation of the Si-Ox interlayer.

SEM images of films deposited from 5.0 mM Ni(acac)$_2$ precursor solution with 0.0 vol% and 12.0 vol% water, respectively, are shown in Supplementary Fig. S2 (online). The film surfaces obtained from the waterless feedstock appear to be continuous and relatively smooth, in contrast to films obtained from solution with 12.0 vol% water (~80% Ni and ~20% NiO), which show a coarse morphology with separate, relatively large and heterogeneously sized grains (grain diameters from some 10 nm up to 150 nm). Compared to the films obtained from 2.5 mM precursor solution, the deposits from 5.0 mM solution have bigger grains and very significant water-induced changes of morphology. The average film thickness measured by SEM is about 60 nm, 70 nm, and 120 nm ($\pm$5 nm) for films deposited from solutions with 0.0%, 5.0%, and 12.0 vol% water, respectively.

Nickel films deposited from waterless 7.5 mM Ni(acac)$_2$ show an even coarser morphology (Supplementary Fig. S3) than the films obtained from waterless 5.0 mM solution, but with homogeneously sized grains. While films obtained from solution with 5.0 vol% water shows somewhat bigger grains, SEM of the film deposited from 7.5 mM solution with 15.0 vol% water reveals a very coarse morphology, with grain diameters from ~50 nm up to 150 nm.

The measured average thickness values are 120 nm, 200 nm, and 220 nm, approximately, for films deposited from solutions with 0.0%, 5.0%, and 15.0 vol% water, respectively. Apparently, the precursor decomposition rate is unaffected by the amount of water within the water concentration range 5.0% to 15.0 vol% as about the same film thickness is obtained. The density of Ni/NiOx nuclei, however, decreases significantly as the water concentration is increased from 5.0% to 15.0 vol% of water, leading to fewer but much bigger grains. Obviously, excessive amounts of water in the precursor limit the nucleation rate of the growing film. At this point we can only speculate that the reportedly low reactivity of $\beta$-diketonate precursors towards surface groups[14] may hinder the initial Si-O-Ni bond formation between precursor and an OH group–saturated substrate, thereby delaying the formation of nuclei which, at high precursor concentrations in the liquid feedstock and on the surface, then quickly grow.

In summary, we observe no positive effect of water on the growth rate or carbon impurity levels of metallic Ni films for 5.0 and 7.5 mM Ni(acac)$_2$ feedstock, in contrast to deposition from 2.5 mM precursor solutions. We presume that any promotional effect of surface OH-groups for the precursor adsorption should be most efficient at lowest precursor concentrations whereas at 5.0 mM and 7.5 mM precursor concentration in the deposited gas phase (spray) the precursor molecule density on the surface may be so high that there is no need to promote adsorption.

An intriguing observation is the fact that at high precursor concentrations (5.0 mM and 7.5 mM) the Ni oxide fraction within the film is maximum for an intermediate water concentration of 4.0% – 5.0 vol% and decreases as the $H_2O$ concentration is further increased. We presume that the morphology of the growing films provides a key to this puzzle: While it seems clear that water promotes the oxidation of Ni, excessive amounts of water do also

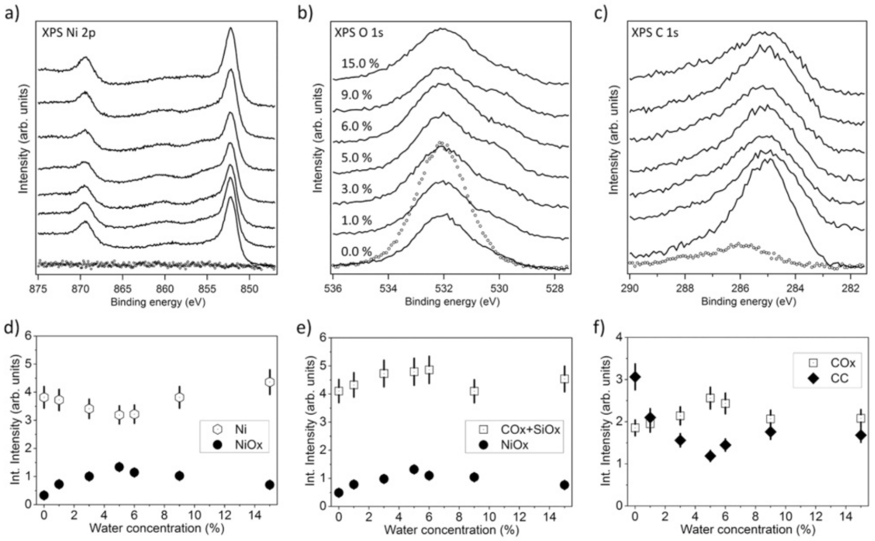

**Figure 5. Top panels: XPS spectra in the binding energy range of (a) Ni 2p, (b) O 1s, and (c) C 1s emissions obtained from the SiOx/Si(100) substrate (dotted curves) and from Ni/NiOx films (thickness 120–220 nm) grown on top by PSE-CVD from 7.5 mM precursor solution with various water concentrations (from 0.0% to 15.0 vol%) at a substrate temperature of 270 °C (solid lines).** Bottom panels: Integral peak intensities determined from fits to the XPS data (see text for details).

limit the nucleation rate and promote the growth of existing nuclei (see above), leading to only few and but larger grains within the film. Due to the lower surface-to-volume ratio, however, large metal grains are presumably less efficiently oxidized than metal films with small grains[65,66], limiting the total oxide fraction in the deposited film. Our observation that films deposited from 2.5 mM solution with small grains (<5 nm) can be completely oxidized in the presence of water while films with larger grains (as deposited from 5.0 and 7.5 mM solutions and high $H_2O$ concentration) can be oxidized only up to a maximum fraction of ~30% is in accordance with this presumption.

Overall, our results show that by tuning the concentrations of Ni(acac)$_2$ and water in the precursor solution, the fraction of Ni metal and Ni oxide in the film or the film morphology can be adjusted. At low (2.5 mM) precursor concentration in the feedstock smoothest morphologies (with grains from 5 to 10 nm) are obtained and the fraction of Ni oxide in the deposit is adjustable from 0 to 100% by varying the water concentration. At high Ni(acac)$_2$ concentrations (5.0 and 7.5 mM) excessive amounts of water strongly affect the film morphology and grain sizes can be varied from 10 to 150 nm. The carbon contamination in deposited films can be minimized to less than 10% when the precursor solution is adjusted to 2.5 mM Ni(acac)$_2$ concentration and 0.5–1.0 vol% water content.

**Co(acac)$_2$ in EtOH on SiOx/Si(100).** XPS data from films obtained by PSE-CVD from 7.5 mM Co(acac)$_2$ in ethanol on SiOx/Si(100) were collected and analyzed in a similar way as shown in the previous section for Ni deposits and compiled into Fig. 6. Co 2p spectra were fitted by contributions from Co$^0$ and Co$^{2+}$ emissions similar to previous reports[67,68]. In contrast to nickel, the deposits from Co(acac)$_2$ contained mainly CoOx, even when waterless precursor solutions were used. With increasing precursor concentration from 2.5 mM (data not shown) to 7.5 mM the Co metal fraction significantly increased, but accounted for only 42% of the Co 2p signal (Fig. 6d).

For the film deposited from waterless 7.5 mM Co(acac)$_2$ precursor we find the atomic ratio of Carbon to Cobalt as 0.18. The C 1s signal (Fig. 6f) is composed of 77% C-C/C-H and 23% COx species. That component of the O 1s signal which can be attributed to CoOx is about 34% of the entire O 1s signal. Because the O 1s signal from SiOx is quite strong, we may assume that Co films are porous. (Supplementary Fig. S4 shows all contributions that were considered for fitting the O 1s spectra.) Adding a small amount of water (about 1.0 vol%) to the precursor solution leads to significant decreases of the metallic component in the Co 2p signal (Fig. 6d): Co$^0$ accounts only for 4% of the entire Co 2p signal (96% Co$^{2+}$) at 1.0 vol% of water in the precursor solution. The Co$^0$: Co$^{2+}$ ratio does not change much at even higher water concentrations (Co 2p accounts for 3% metallic cobalt and 97% cobalt oxide at 6.0 vol% water), i.e., essentially only CoOx is grown. Compared to the films grown from waterless feedstock, the total level of carbon contamination in the film (total C 1s intensity) decreases to ~50–60% as water is added to the precursor solution while the ratio of the COx and C-C/C-H component indicates oxidation of the carbon impurities by water as it increases from ~1:1 at 1.0 vol% water to ~4 : 1 at 6.0 vol% water in the precursor solution (Fig. 6f).

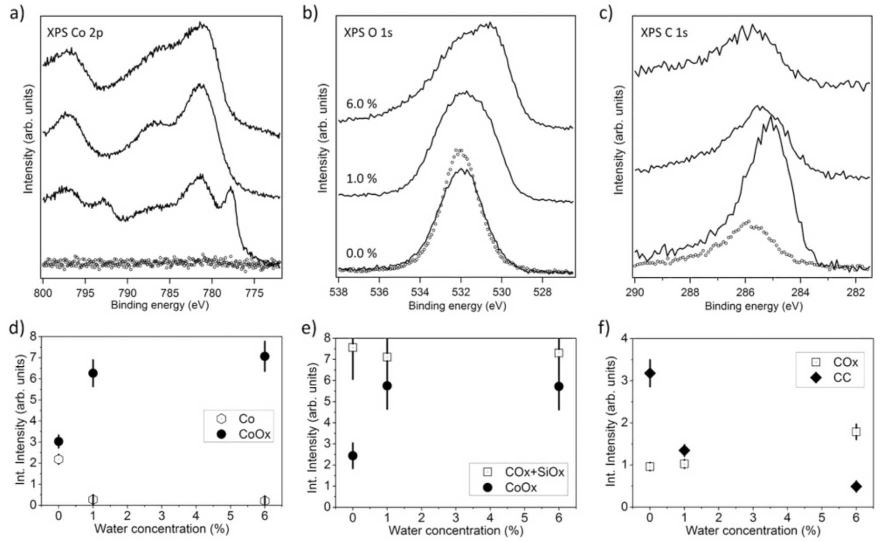

**Figure 6. Top panels: XPS spectra in the binding energy range of (a) Co 2p, (b) O 1s, and (c) C 1s emissions obtained from the SiOx/Si(100) substrate (dotted curves) and from Co/CoOx films (thickness 100–150 nm) grown ontop by PSE-CVD from 7.5 mM precursor solution with various water concentrations (from 0.0% to 6.0 vol%) at a substrate temperature of 310 °C (solid lines).** Bottom panels: Integral peak intensities determined from fits to the XPS data (see text for details).

SEM reveals that the surface of the Co films deposited from waterless 7.5 mM Co(acac)$_2$ (42% Co$^0$, 60% Co$^{2+}$ according to XPS) exhibit a coarse morphology and heterogeneously sized grains. The structure visible in Supplementary Fig. S5 available online (bright grains with diameters of ~10 nm within a greyish matrix) may indicate separation of (metallic) Co particles and Co oxide. In fact, the Co oxide films obtained from solution with 6.0 vol% water do not show clear grains but appear somehow fluffy. The film thickness determined by SEM is about 100 nm and 150 nm for films deposited from 7.5 mM Co(acac)$_2$ solutions with 0.0% and 6.0 vol% water, respectively.

In summary, in contrast to PSE-CVD from Ni(acac)$_2$ even small amounts (1.0 vol%) of water in the 7.5 mM CO(acac)$_2$ precursor feedstock lead to complete oxidation of the deposited Co. A significant fraction of metallic Co$^0$ can be detected in the Co 2p signal only in deposits obtained without water. As well known from recent reports, cobalt is not as good a catalyst for ethanol dehydrogenation as Nickel is[31,34]. Therefore, even small amounts of water in the feedstock probably lead to a high water/hydrogen ratio at the substrate surface, rendering the precursor decomposition and CoOx formation according to Eq. 1 as dominant pathway[11] because Co reduction by hydrogen is expected to be much slower. In accordance with observations made for Ni deposition, we find also water-induced oxidation of carbon impurities when the reaction mechanism changes from M to MOx formation. A significant metallic fraction of deposited Co is observed only for the waterless precursor solution, the observed maximum ratio of Co : CoOx is ~40 : 60.

Because previous studies demonstrated that a Ni interlayer on the SiOx/Si substrate may drastically improve the quality of films deposited from Co(acac)$_2$ on top (almost completely metallic Co, only small amount of CoOx)[31,34], we also included PSE-CVD from 7.5 mM Co(acac)$_2$ on a 40 nm thick Ni layer on SiOx/Si(100) in our experiments. The results obtained for a waterless precursor solution and for 1.0 vol% water in the feedstock are shown in Fig. 7. For deposits from the waterless solution, the Co$^{2+}$ emission (Fig. 7a) accounts for 33% of the entire Co 2p signal which is significantly lower than the oxide fraction detected from films deposited without the Ni interlayer (Fig. 6a). But also with a Ni interlayer, even small amounts (1.0 vol%) of water in the feedstock lead to complete oxidation of the deposited Co, as the Co 2p signal clearly shows. Consequently, in order to benefit from a Ni seed layer for the PSE-CVD of metallic Co from Co(acac)$_2$ in ethanol, care has to be taken that the precursor solution is kept waterless. As mentioned before, previous publications[31,34] suggest that the benefit of a Ni seed layer is catalysis of ethanol dehydrogenation for the formation of hydrogen as reducing agent. Co and in particular CoOx are worse catalysts in this respect. Consequently, while a Ni layer helps to catalyse the formation of an initial metallic Co layer which then may sustain the Co$^0$ formation on top by catalyzing ethanol dehydrogenation, the balance quickly shifts to the precursor decomposition pathway depicted in Eq. 1 as soon as water is present because water oxidizes deposited Co which, in turn, is not available to catalyze ethanol dehydrogenation.

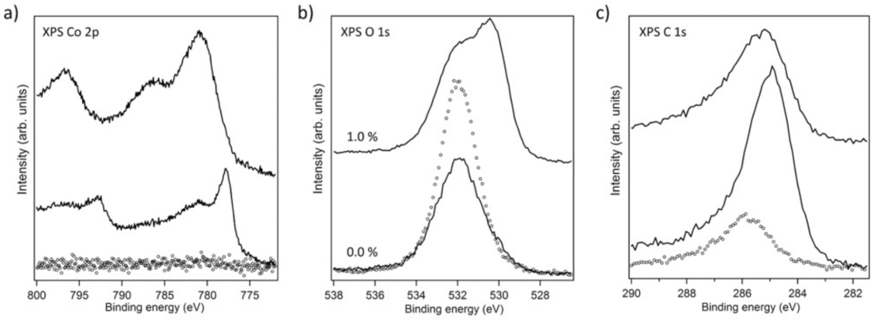

**Figure 7. XPS spectra in the binding energy range of (a) Co 2p, (b) O 1s, and (c) C 1s emissions obtained from the Ni/SiOx/Si(100) substrate (dotted curves) and from Co/CoOx films (thickness 100–150 nm) grown ontop by PSE-CVD from 7.5 mM precursor solution with 0.0% and 1.0 vol% water concentrations at a substrate temperature of 310 °C (solid lines).**

## Summary

Employing PSE-CVD with liquid feedstock of Ni(acac)$_2$ or Co(acac)$_2$ dissolved in ethanol, systematic studies of the influence of water on growth and composition of Ni and Co metal and oxide films were performed. The ethanol-based liquid precursor enabled us to control and vary the water concentration during the deposition process easily and reliably within a range from 0.0 up to 15.0 vol% with an uncertainty of only 0.1%. Using a specially designed CVD reactor directly attached to a UHV system, *in vacuo* transfer of samples after any stage of deposition rendered possible a quasi *in situ* analysis of to film composition by XPS.

Both, beneficial and detrimental effects of water on the growth of metallic films, strongly depending on the concentration of water and the β-diketonate in the precursor solution, were observed. The smoothest morphologies (with grains from 5 to 10 nm) were obtained for metallic Ni films grown from 2.5 mM Ni(acac)$_2$ precursor solution. The film growth could be optimized and the carbon contamination of the deposited Ni films minimized to less than 10% when the water concentration in the precursor solution was adjusted to 0.5 vol%. Only at concentrations of 1.0 vol% and higher water induced significant oxidation of the Ni deposit. From precursor solutions with higher Ni(acac)$_2$ concentrations (5.0. and 7.5 mM), purely metallic films were only obtained when any water in the feedstock was eliminated. Here, the film morphology strongly depended on the water concentration, indicating inhibition of nucleation on the Si/SiOx substrate by excessive amounts of water which lead to the growth of relatively large grains and a coarse film morphology. Overall, the gathered detailed overview over water-induced effects on the PSE-CVD with Ni acetylacetonate precursors dissolved in ethanol shows that by carefully tuning the precursor and water concentration in the feedstock, e.g., the degree of Ni oxidation can be adjusted from 0 to 100% or the size of the grains the film is composed of can be varied from less than 10 to 150 nm.

Compared to Ni(acac)$_2$, an even higher sensitivity for water in the feedstock was observed in the case of Co(acac)$_2$ as precursor. Significant metallic Co fractions within the deposited films on SiOx/Si(100) as well as on Ni/SiOx/Si(100) were obtained only from waterless solutions. The relative sensitivities of Ni- and Co-based precursor solutions on water indicate a strong competition between two precursor decomposition pathways, one probably involving the Ni- or Co-catalyzed dehydrogenation of ethanol and $H_2$-induced reduction of the precursor metal center, the other involving $H_2O$-induced Ni or Co(acac)$_2$ decomposition which leads to Ni or Co oxidation.

## References

1. Martin, P. M. *Handbook of deposition technologies for films and coatings: science, applications and technology*. 3rd edn (Elsevier, 2010).
2. Pierson, H. O. & Pierson, H. O. *Handbook of chemical vapor deposition (CVD): principles, technology, and applications*. 2nd edn (Noyes Publications/William Andrew Pub., 1999).
3. Kodas, T. T. & Hampden-Smith, M. J. *The chemistry of Metal CVD*. (VCH, 1994).
4. Emslie, D. J. H., Chadha, P. & Price, J. S. Metal ALD and pulsed CVD: Fundamental reactions and links with solution chemistry. *Coordination Chemistry Reviews* **257,** 3282–3296, doi: http://dx.doi.org/10.1016/j.ccr.2013.07.010 (2013). (Accessed 13th October 2015)
5. Hubert-Pfalzgraf, L. G. & Guillon, H. Trends in precursor design for conventional and aerosol-assisted CVD of high-Tc superconductors. *Applied Organometallic Chemistry* **12,** 221–236, doi: 10.1002/(SICI)1099-0739(199803)12:3<221::AID-AOC693>3.0.CO;2-O (1998).
6. Boyd, E. P., Ketchum, D. R., Deng, H. & Shore, S. G. Chemical Vapor Deposition of Metallic Thin Films Using Homonuclear and Heteronuclear Metal Carbonyls. *Chem Mater* **9,** 1154–1158, doi: 10.1021/cm9605330 (1997).
7. Brissonneau, L. & Vahlas, C. Precursors and operating conditions for the metal-organic chemical vapor deposition of nickel films. *Ann Chim-Sci Mat* **25,** 81–90, doi: 10.1016/S0151-9107(00)88716-4 (2000).
8. Bullen, G. J., Mason, R. & Pauling, P. The Crystal and Molecular Structure of Bis(acetylacetonato)nickel (II). *Inorganic Chemistry* **4,** 456–462, doi: 10.1021/ic50026a005 (1965).
9. Utriainen, M., Kröger-Laukkanen, M. & Niinistö, L. Studies of NiO thin film formation by atomic layer epitaxy. *Materials Science and Engineering: B* **54,** 98–103, doi: http://dx.doi.org/10.1016/S0921-5107(98)00135-4 (1998). (Accessed 13th October 2015)

10. Lindahl, E., Ottosson, M. & Carlsson, J.-O. Atomic Layer Deposition of NiO by the Ni(thd)2/H2O Precursor Combination. *Chemical Vapor Deposition* **15,** 186–191, doi: 10.1002/cvde.200906762 (2009).
11. Utriainen, M., Kröger-Laukkanen, M., Johansson, L.-S. & Niinistö, L. Studies of metallic thin film growth in an atomic layer epitaxy reactor using M(acac)2 (M=Ni, Cu, Pt) precursors. *Appl Surf Sci* **157,** 151–158, doi: 10.1016/s0169-4332(99)00562-0 (2000).
12. Haukka, S., Lakomaa, E. L. & Root, A. An IR and NMR study of the chemisorption of titanium tetrachloride on silica. *The Journal of Physical Chemistry* **97,** 5085–5094, doi: 10.1021/j100121a040 (1993).
13. Takeda, S., Fukawa, M., Hayashi, Y. & Matsumoto, K. Surface OH group governing adsorption properties of metal oxide films. *Thin Solid Films* **339,** 220–224, doi: http://dx.doi.org/10.1016/S0040-6090(98)01152-3 (1999). (Accessed 13th October 2015)
14. Bernal Ramos, K., Saly, M. J. & Chabal, Y. J. Precursor design and reaction mechanisms for the atomic layer deposition of metal films. *Coordination Chemistry Reviews* **257,** 3271–3281, doi: http://dx.doi.org/10.1016/j.ccr.2013.03.028 (2013). (Accessed 13th October 2015)
15. Maruyama, T. & Tago, T. Nickel thin films prepared by chemical vapour deposition from nickel acetylacetonate. *J Mater Sci* **28,** 5345–5348, doi: 10.1007/BF00570088 (1993).
16. Lecohier, B., Calpini, B., Philippoz, J. M. & van den Bergh, H. Low-pressure chemical vapor deposition of copper: Dependence of the selectivity on the water vapor added to a hydrogen or helium carrier gas. *J Appl Phys* **72,** 2022–2026, doi: http://dx.doi.org/10.1063/1.351630 (1992). (Accessed 13th October 2015)
17. Nobuyoshi, A. & Yoshinobu, A. Accelerated-Deposition Rate and High-Quality Film Copper Chemical Vapor Deposition Using a Water Vapor Addition to a Hydrogen and Cu(HFA) 2 Reaction System. *Jpn J Appl Phys* **32,** 3915 (1993).
18. Kim, D. H., Wentorf, R. H. & Gill, W. N. Selective deposition of copper by chemical vapor deposition using Cu(HFA)2. *Journal of Vacuum Science & Technology A* **12,** 153–157, doi: doi: http://dx.doi.org/10.1116/1.578912 (1994). (Accessed 13th October 2015)
19. Maårtensson, P. & Carlsson, J. O. Atomic Layer Epitaxy of Copper: Growth and Selectivity in the Cu(II)-2,2,6,6-tetramethyl-3,5-heptanedionate/Process. *J Electrochem Soc* **145,** 2926–2931, doi: 10.1149/1.1838738 (1998).
20. See, e.g. Griffin, G.L. & Maverick, A.W. in Kodas, T.T. & Hampden-Smith, M.J. The chemistry of Metal CVD (VCH, Weinheim, New York, 1994) and references therein.
21. Jain, A., Kodas, T. T., Corbitt, T. S. & Hampden-Smith, M. J. Chemical Vapor Deposition of Copper from (hfac)CuL (L=VTMS and 2-Butyne) in the Presence of Water, Methanol, and Dimethyl Ether. *Chem Mater* **8,** 1119–1127, doi: 10.1021/cm950546y (1996).
22. Marzouk, H. A. *et al.* Non-selective copper film growth on Kapton (polyimide) by MOCVD. *Thin Solid Films* **249,** 22–27, doi: http://dx.doi.org/10.1016/0040-6090(94)90080-9 (1994). (Accessed 13th October 2015)
23. Marzouk, H. A. *et al.* Evaluation of copper Chemical-Vapor-Deposition films on glass and Si(100) substrates. *Appl. Phys. A* **58,** 607–613, doi: 10.1007/BF00348173 (1994).
24. Törndahl, T., Ottosson, M. & Carlsson, J.-O. Growth of Copper(I) Nitride by ALD Using Copper(II) Hexafluoroacetylacetonate, Water, and Ammonia as Precursors. *J Electrochem Soc* **153,** C146–C151, doi: 10.1149/1.2160427 (2006).
25. Borgharkar, N. S., Griffin, G. L., Fan, H. & Maverick, A. W. Solution Delivery of Cu ( hfac ) 2 for Alcohol-Assisted Chemical Vapor Deposition of Copper. *J Electrochem Soc* **146,** 1041–1045, doi: 10.1149/1.1391718 (1999).
26. Gelatos, A. V., Marsh, R., Kottke, M. & Mogab, C. J. Chemical vapor deposition of copper from Cu+1 precursors in the presence of water vapor. *Appl Phys Lett* **63,** 2842–2844, doi: doi: http://dx.doi.org/10.1063/1.110304 (1993). (Accessed 13th October 2015)
27. Kim, J.-Y. *et al.* Deposition mechanism of MOCVD copper films in the presence of water vapor. *Thin Solid Films* **330,** 190–195, doi: http://dx.doi.org/10.1016/S0040-6090(98)00597-5 (1998). (Accessed 13th October 2015)
28. Huo, J., Solanki, R. & McAndrew, J. Characteristics of copper films produced via atomic layer deposition. *Journal of Materials Research* **17,** 2394–2398 (2002).
29. Premkumar, P. A., Bahlawane, N. & Kohse-Höinghaus, K. CVD of metals using alcohols and metal acetylacetonates, Part I: Optimization of process parameters and electrical characterization of synthesized films. *Chemical Vapor Deposition* **13,** 219–226, doi: DOI 10.1002/cvde.200606572 (2007).
30. Bahlawane, N. *et al.* Nickel and Nickel-Based Nanoalloy Thin Films from Alcohol-Assisted Chemical Vapor Deposition. *Chem Mater* **22,** 92–100, doi: 10.1021/cm902454w (2009).
31. Bahlawane, N., Kohse-Höinghaus, K., Premkumar, P. A. & Lenoble, D. Advances in the deposition chemistry of metal-containing thin films using gas phase processes. *Chemical Science* **3,** 929–941, doi: 10.1039/C1SC00522G (2012).
32. Weiss, T. *et al.* Design of a compact ultrahigh vacuum-compatible setup for the analysis of chemical vapor deposition processes. *Review of Scientific Instruments* **85,** 104104, doi: http://dx.doi.org/10.1063/1.4897620 (2014). (Accessed 13th October 2015)
33. Premkumar, P. A., Bahlawane, N., Reiss, G. & Kohse-Höinghaus, K. CVD of metals using alcohols and metal acetylacetonates, Part II: Role of solvent and characterization of metal films made by pulsed spray evaporation CVD. *Chemical Vapor Deposition* **13,** 227–231, doi: DOI 10.1002/cvde.200606573 (2007).
34. Premkumar, P. A., Turchanin, A. & Bahlawane, N. Effect of solvent on the growth of Co and Co2C using pulsed-spray evaporation chemical vapor deposition. *Chem Mater* **19,** 6206–6211, doi: Doi 10.1021/Cm701957s (2007).
35. Bahlawane, N. *et al.* Catalytically enhanced H2-free CVD of transition metals using commercially available precursors. *Surface and Coatings Technology* **201,** 8914–8918, doi: http://dx.doi.org/10.1016/j.surfcoat.2007.04.047 (2007). (Accessed 13th October 2015)
36. Bahlawane, N., Antony Premkumar, P., Onwuka, K., Reiss, G. & Kohse-Höinghaus, K. Self-catalyzed chemical vapor deposition method for the growth of device-quality metal thin films. *Microelectron Eng* **84,** 2481–2485, doi: http://dx.doi.org/10.1016/j.mee.2007.05.014 (2007).
37. Galtayries, A. & Grimblot, J. Formation and electronic properties of oxide and sulphide films of Co, Ni and Mo studied by XPS. *Journal of Electron Spectroscopy and Related Phenomena* **98–99,** 267–275, doi: http://dx.doi.org/10.1016/S0368-2048(98)00292-8 (1999). (Accessed 13th October 2015)
38. Marcus, P. & Grimal, J. M. The anodic dissolution and passivation of NiCrFe alloys studied by ESCA. *Corrosion Science* **33,** 805–814, doi: http://dx.doi.org/10.1016/0010-938X(92)90113-H (1992). (Accessed 13th October 2015)
39. Barr, T. L. An ESCA study of the termination of the passivation of elemental metals. *The Journal of Physical Chemistry* **82,** 1801–1810, doi: 10.1021/j100505a006 (1978).
40. Brault, P., Ranson, P., Estrade-Szwarckopf, H. & Rousseau, B. Chemical physics of fluorine plasma-etched silicon surfaces: Study of surface contaminations. *J Appl Phys* **68,** 1702–1709, doi: http://dx.doi.org/10.1063/1.346625 (1990). (Accessed 13th October 2015)
41. Bou, M., Martin, J. M., Le Mogne, T. & Vovelle, L. Chemistry of the interface between aluminium and polyethyleneterephthalate by XPS. *Appl Surf Sci* **47,** 149–161, doi: http://dx.doi.org/10.1016/0169-4332(91)90029-J (1991). (Accessed 13th October 2015)
42. Lascovich, J. C., Giorgi, R. & Scaglione, S. Evaluation of the sp2/sp3 ratio in amorphous carbon structure by XPS and XAES. *Appl Surf Sci* **47,** 17–21, doi: http://dx.doi.org/10.1016/0169-4332(91)90098-5 (1991). (Accessed 13th October 2015)
43. Contarini, S., Howlett, S. P., Rizzo, C. & De Angelis, B. A. XPS study on the dispersion of carbon additives in silicon carbide powders. *Appl Surf Sci* **51,** 177–183, doi: http://dx.doi.org/10.1016/0169-4332(91)90400-E (1991). (Accessed 13th October 2015)
44. Grosvenor, A. P., Biesinger, M. C., Smart, R. S. C. & McIntyre, N. S. New interpretations of XPS spectra of nickel metal and oxides. *Surf Sci* **600,** 1771–1779, doi: http://dx.doi.org/10.1016/j.susc.2006.01.041 (2006).
45. Droulas, J. L., Tran Minh Duc & Jugnet, Y. Etude des propiétés interfaciales des dépôts par évaporation et pulvérisation d' aluminium sur polyéthylène téréphtalate. *Le Vide, les Couches Minces* **258,** 39–41 (1991).
46. Briggs, D. *Handbook of X-ray Photoelectron Spectroscopy C. D. Wanger, W. M. Riggs, L. E. Davis, J. F. Moulder and G. E.Muilenberg Perkin-Elmer Corp., Physical Electronics Division, Eden Prairie, Minnesota, USA, 1979. 190 pp. $195.* Vol. 3 (Heyden & Son Ltd., 1981).

47. Jouan, P. Y., Peignon, M. C., Cardinaud, C. & Lempérière, G. Characterisation of TiN coatings and of the TiN/Si interface by X-ray photoelectron spectroscopy and Auger electron spectroscopy. *Appl Surf Sci* **68,** 595–603, doi: http://dx.doi.org/10.1016/0169-4332(93)90241-3 (1993). (Accessed 13th October 2015)
48. Kodolov, V. I. *et al.* X-ray photoelectron spectroscopic investigation of metallorganic complexes. *Journal of Electron Spectroscopy and Related Phenomena* **88–91,** 977–982, doi: http://dx.doi.org/10.1016/S0368-2048(97)00198-9 (1998).
49. Fadley, C. S. Angle-resolved x-ray photoelectron spectroscopy. *Progress in Surface Science* **16,** 275–388, doi: http://dx.doi.org/10.1016/0079-6816(84)90001-7 (1984). (Accessed 13th October 2015)
50. Fadley, C. S., Baird, R. J., Siekhaus, W., Novakov, T. & Bergström, S. Å. L. Surface analysis and angular distributions in x-ray photoelectron spectroscopy. *Journal of Electron Spectroscopy and Related Phenomena* **4,** 93–137, doi: http://dx.doi.org/10.1016/0368-2048(74)90001-2 (1974). (Accessed 13th October 2015)
51. Wu, O. K. T., Peterson, G. G., LaRocca, W. J. & Butler, E. M. ESCA signal intensity dependence on surface area (roughness). *Applications of Surface Science* **11,** 118–130, doi: http://dx.doi.org/10.1016/0378-5963(82)90058-7 (1982). (Accessed 13th October 2015)
52. Hair, M. L. Hydroxyl groups on silica surface. *Journal of Non-Crystalline Solids* **19,** 299–309, doi: http://dx.doi.org/10.1016/0022-3093(75)90095-2 (1975). (Accessed 13th October 2015)
53. Le Grange, J. D., Markham, J. L. & Kurkjian, C. R. Effects of surface hydration on the deposition of silane monolayers on silica. *Langmuir* **9,** 1749–1753, doi: 10.1021/la00031a023 (1993).
54. Sneh, O. & George, S. M. Thermal Stability of Hydroxyl Groups on a Well-Defined Silica Surface. *The Journal of Physical Chemistry* **99,** 4639–4647, doi: 10.1021/j100013a039 (1995).
55. Yates Jr, J. T. Water interactions with silica surfaces: A big role for surface structure. *Surf Sci* **565,** 103–106, doi: http://dx.doi.org/10.1016/j.susc.2004.06.215 (2004). (Accessed 13th October 2015)
56. Farkas, J., Hampden-Smith, M. J. & Kodas, T. T. FTIR Studies of the Adsorption/Desorption Behavior of Copper Chemical Vapor Deposition Precursors on Silica. 1. Bis(1,1,1,5,5,5-hexafluoroacetylacetonato)copper(II). *The Journal of Physical Chemistry* **98,** 6753–6762, doi: 10.1021/j100078a017 (1994).
57. Farkas, J., Hampden-Smith, M. J. & Kodas, T. T. FTIR Studies of the Adsorption/Desorption Behavior of Copper Chemical Vapor Deposition Precursors on Silica. 2. (1,1,1,5,5,5-Hexafluoroacetylacetonato)(2-butyne)copper(I). *The Journal of Physical Chemistry* **98,** 6763–6770, doi:10.1021/j100078a018 (1994).
58. Haukka, S. & Suntola, T. Advanced Materials Processing by Adsorption Control. *Interface Science* **5,** 119–128, doi: 10.1023/A:1008601024870 (1997).
59. Norton, P. R., Tapping, R. L. & Goodale, J. W. A photoemission study of the interaction of Ni(100), (110) and (111) surfaces with oxygen. *Surf Sci* **65,** 13–36, doi: http://dx.doi.org/10.1016/0039-6028(77)90289-8 (1977). (Accessed 13th October 2015)
60. Benndorf, C., Nöbl, C. & Thieme, F. Interaction of H2O with a clean and oxygen precovered Ni(110) surface studied by XPS. *Surf Sci* **121,** 249–259, doi: http://dx.doi.org/10.1016/0039-6028(82)90041-3 (1982). (Accessed 13th October 2015)
61. Carley, A. F., Rassias, S. & Roberts, M. W. The specificity of surface oxygen in the activation of adsorbed water at metal surfaces. *Surf Sci* **135,** 35–51, doi: http://dx.doi.org/10.1016/0039-6028(83)90208-X (1983). (Accessed 13th October 2015)
62. Heras, J. M. & Albano, E. V. Interaction of water molecules with polycrystalline films of Fe, Co and Ni with different surface roughness: I. Water adsorption on clean films. *Applications of Surface Science* **17,** 207–219, doi: http://dx.doi.org/10.1016/0378-5963(83)90034-X (1983). (Accessed 13th October 2015)
63. Heras, J. M. & Albano, E. V. Interaction of water molecules with polycrystalline films of Fe, Co and Ni with different surface roughness: II. Water adsorption on water pretreated and passivated films. *Applications of Surface Science* **17,** 220–230, doi: http://dx.doi.org/10.1016/0378-5963(83)90035-1 (1983). (Accessed 13th October 2015)
64. Payne, B. P., Biesinger, M. C. & McIntyre, N. S. The study of polycrystalline nickel metal oxidation by water vapour. *Journal of Electron Spectroscopy and Related Phenomena* **175,** 55–65, doi: http://dx.doi.org/10.1016/j.elspec.2009.07.006 (2009). (Accessed 13th October 2015)
65. Van Steen, E. *et al.* Stability of Nanocrystals: Thermodynamic Analysis of Oxidation and Re-reduction of Cobalt in Water/Hydrogen Mixtures. *The Journal of Physical Chemistry B* **109,** 3575–3577, doi: 10.1021/jp045136o (2005).
66. Fischer, N., Clapham, B., Feltes, T., van Steen, E. & Claeys, M. Size-Dependent Phase Transformation of Catalytically Active Nanoparticles Captured *In Situ*. *Angewandte Chemie International Edition* **53,** 1342–1345, doi: 10.1002/anie.201306899 (2014).
67. McIntyre, N. S. & Cook, M. G. X-ray photoelectron studies on some oxides and hydroxides of cobalt, nickel, and copper. *Analytical Chemistry* **47,** 2208–2213, doi: 10.1021/ac60363a034 (1975).
68. Yang, J., Liu, H., Martens, W. N. & Frost, R. L. Synthesis and Characterization of Cobalt Hydroxide, Cobalt Oxyhydroxide, and Cobalt Oxide Nanodiscs. *The Journal of Physical Chemistry C* **114,** 111–119, doi: 10.1021/jp908548f (2010).

## Acknowledgements

Assistance with scanning electron microscopy by Petra Witte (Geosciences department of the University of Bremen) and valuable discussions with Patrick H. Tchoua Ngamou and Katharina Kohse-Höinghaus (University of Bielefeld) are gratefully acknowledged. The project has been funded by the German Research Foundation.

## Author Contributions

T.W. performed all experiments and data analysis. V.Z. and M.B. supervised this work. T.W. and V.Z. wrote the main manuscript text and T.W. prepared all figures. All authors reviewed the manuscript.

## Additional Information

**Supplementary information** accompanies this paper at http://www.nature.com/srep

**Competing financial interests:** The authors declare no competing financial interests.

**How to cite this article**: Weiss, T. *et al.* Influence of Water on Chemical Vapor Deposition of Ni and Co thin films from ethanol solutions of acetylacetonate precursors. *Sci. Rep.* **5**, 18194; doi: 10.1038/srep18194 (2015).

# Supplementary Information

# Influence of Water on Chemical Vapor Deposition of Ni and Co thin films from ethanol solutions of acetylacetonate precursors

Theodor Weiss, Volkmar Zielasek*, Marcus Bäumer

Institut für Angewandte und Physikalische Chemie, Universität Bremen, Leobener Straße UFT,
D-28359 Bremen, Germany

*) corresponding author

## Experimental Parameters

Supplementary Table S1. PSE-CVD reactor parameters for Ni and Co metal films deposition

| Precursor: | $Ni(acac)_2$ | $Co(acac)_2$ |
|---|---|---|
| Solvent: | Ethanol | |
| Concentration of the precursor [mmol/l] | 2.5, 5.0, 7.5 | 7.5 |
| Water concentration [vol%] | 0.0 – 15.0 | |
| Spray pulse frequency [Hz] | 2 | |
| Spray pulse width [ms] | 15 | |
| Deposition area pressure [Pa] | $5 \cdot 10^3$ | |
| Carrier gas flow rate [sml/min] | 500 | |
| Substrate temperature [° C] | 270 | 310 |
| Total duration of deposition [min] | 30 | |

## **Scanning Electron Micrographs of Ni deposits**

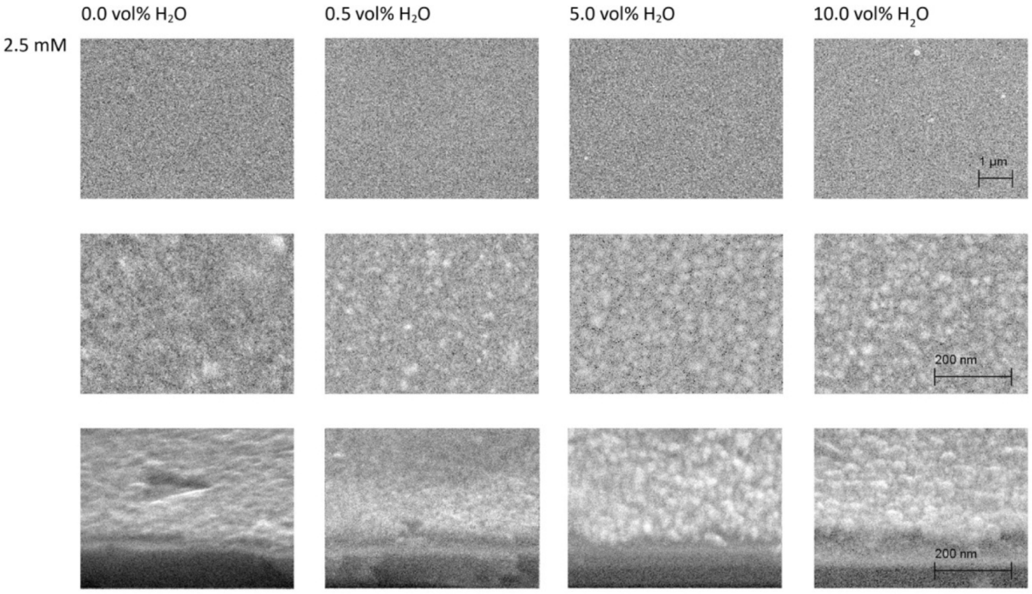

Supplementary Figure S1. SEM of films deposited on a SiOx/Si(100) substrate from 2.5 mM $Ni(acac)_2$ in ethanol with 0.0 %, 0.5 %, 5.0 %, and 10.0 vol% water, respectively. First row: plane view on the substrate surface (scale bar 1 μm); second row: enlarged plane view on substrate surface (scale bar 200 nm); third row: enlarged view (scale bar 200 nm) at a viewing angle of ~ 60° with respect to surface normal, showing a cleaved sample edge with the substrate (bottom) and deposits on top. Film thicknesses estimated by SEM: 30 nm, 40 nm, 40 nm, and 50 nm for films obtained from solutions with 0.0 %, 0.5 %, 5.0 % and 10.0 vol% of water, respectively.

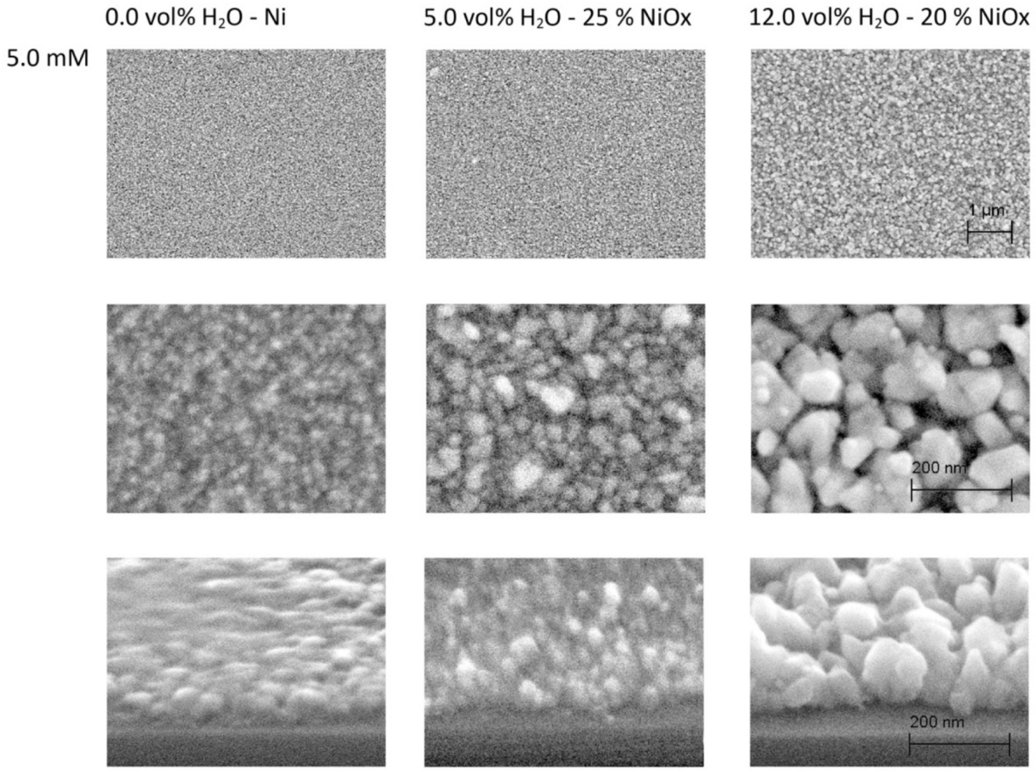

Supplementary Figure S2. SEM of Ni/NiOx films deposited on a SiOx/Si(100) substrate from 5.0 mM Ni(acac)$_2$ in ethanol with 0.0 % and 12.0 vol% water, respectively. First row: plane view on the Ni-covered substrate surface (scale bar 1 µm); second row: enlarged plane view on the Ni-covered substrate surface (scale bar 200 nm); third row: enlarged view (scale bar 200 nm) at a viewing angle of ~ 60° with respect to surface normal, showing a cleaved sample edge with the substrate (bottom) and Ni deposits on top. Film thicknesses estimated by SEM: 60 nm, 70 nm, and 120 nm for Ni/NiOx films obtained from solutions with 0.0 %, 5.0 %, and 12.0 vol% of water, respectively.

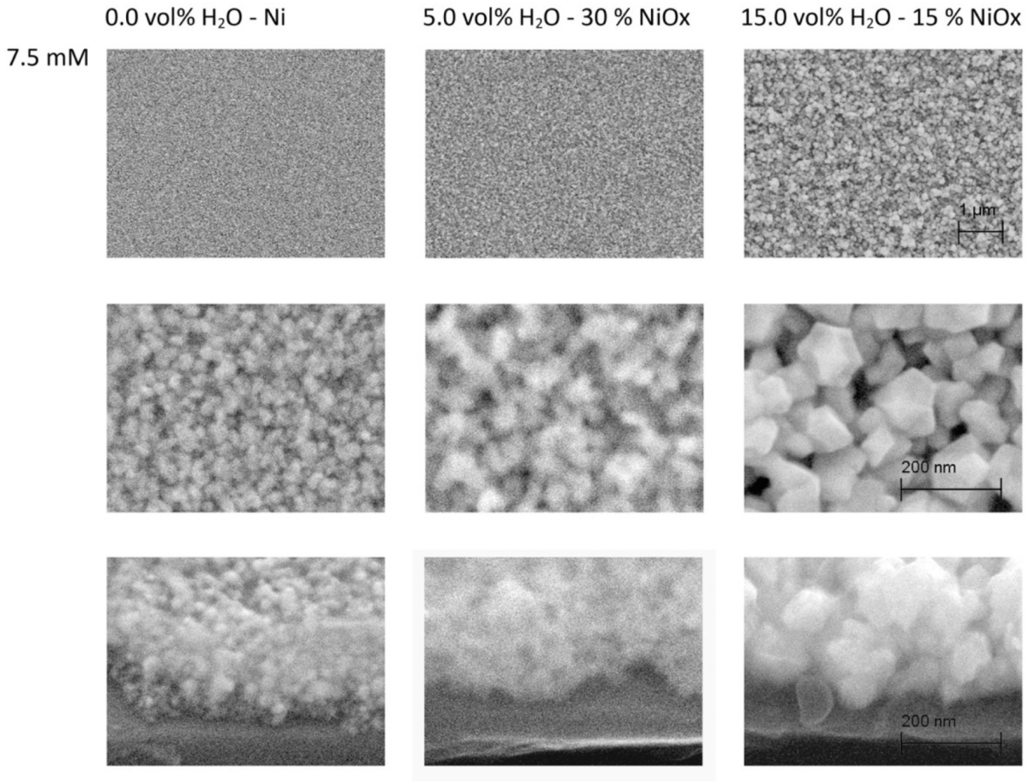

Supplementary Figure S3. SEM of Ni/NiOx films deposited on a SiOx/Si(100) substrate from 7.5 mM Ni(acac)$_2$ in ethanol with 0.0 %, 5.0 %, and 12.0 vol% water, respectively. First row: plane view on the Ni-covered substrate surface (scale bar 1 µm); second row: enlarged plane view on the Ni-covered substrate surface (scale bar 200 nm); third row: enlarged view (scale bar 200 nm) at a viewing angle of ~ 60° with respect to surface normal, showing a cleaved sample edge with the substrate (bottom) and Ni deposits on top. Film thicknesses estimated by SEM: 120 nm, 200 nm, and 220 nm for Ni/NiOx films obtained from solutions with 0.0 %, 5.0 %, and 12.0 vol% of water, respectively.

## X-ray Photoelectron Spectra of Co deposits

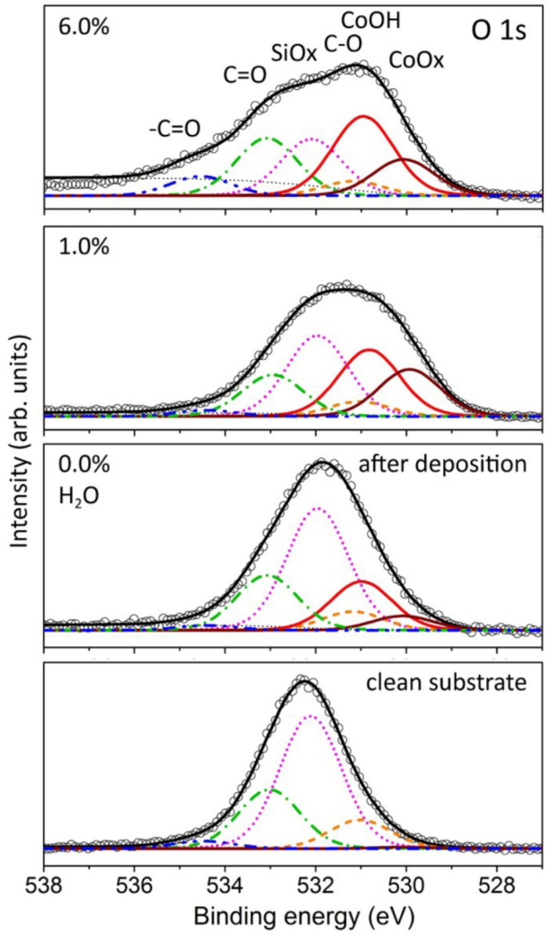

Supplementary Figure S4. Fits of the O 1s XPS spectra obtained from the SiOx/Si(100) substrate (bottom panel) and Co/CoOx films grown ontop by PSE-CVD from 7.5 mM Co(acac)$_2$ in ethanol and various water concentrations (0.0 %, 1.0 %, and 6.0 vol%) in the precursor solution at a substrate temperature of 310 °C.

## Scanning Electron Micrographs of Co deposits

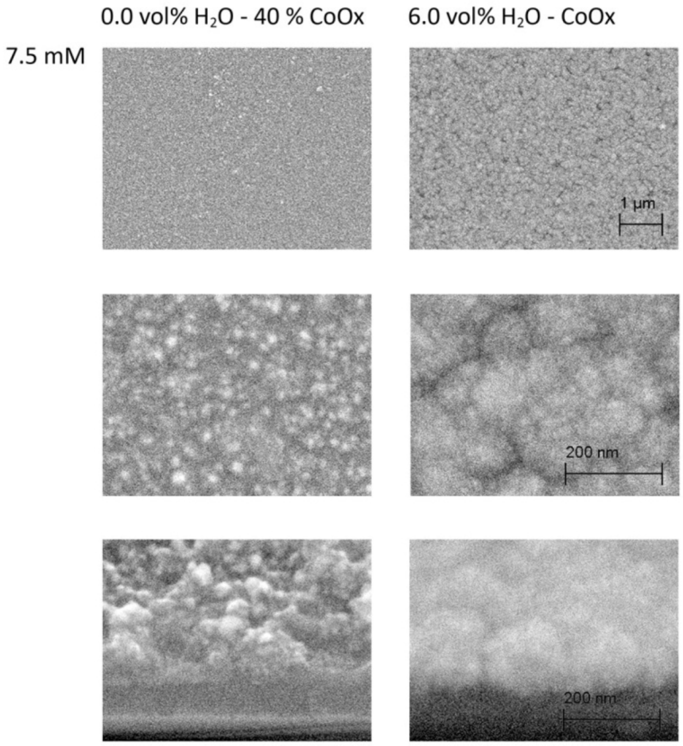

Supplementary Figure S5. SEM of Co/CoOx films deposited on a SiOx/Si(100) substrate from 7.5 mM Co(acac)$_2$ in ethanol with 0.0 % and 6.0 vol% water, respectively. First row: plane view on the Co-covered substrate surface (scale bar 1 μm); second row: enlarged plane view on the Co-covered substrate surface (scale bar 200 nm); third row: enlarged view (scale bar 200 nm) at a viewing angle of ~ 60° with respect to surface normal, showing a cleaved sample edge with the substrate (bottom) and Co deposits on top. Film thicknesses estimated by SEM: 100 nm and 150 nm for Ni/NiOx films obtained from solutions with 0.0 % and 6.0 vol% of water, respectively.

# Paper IV

## XPS study of thermal and electron-induced decomposition of Ni and Co acetylacetonate thin films for metal deposition

Theodor Weiss, Jonas Warneke, Volkmar Zielasek*, Petra Swiderek, Marcus Bäumer
*Institut für Angewandte und Physikalische Chemie, Universität Bremen, Postfach 330440,*
*D-28334 Bremen, Germany*

**Abstract**

Optimizing thin metal film deposition techniques from metal-organic precursors such as ALD, CVD, or EBID with the help of surface science analysis tools in ultrahigh vacuum requires a contamination-free precursor delivery technique, especially in the case of the less volatile precursors. For this purpose the preparation of layers of undecomposed Ni(acac)$_2$ and Co(acac)$_2$ was tried via pulsed spray evaporation of a liquid solution of the precursors in ethanol into a flow of nitrogen on a CVD reactor. Solvent-free layers of intact precursor molecules were obtained when the substrate was held at a temperature of 115 °C. A qualitative comparison of thermally initiated and electron-induced precursor decomposition and metal center reduction was carried out. All deposited films were analyzed with respect to chemical composition quasi *in situ* by XPS. Thermally initiated decomposition yielded higher metal-to-metal oxide ratios in the deposit than the electron-induced process for which ratios of 60:40 and 20:80 were achieved for Ni and Co, resp.. Compared to continuous EBID processes, all deposits showed low levels of carbon impurities of ~10 at.%. Therefore, post-deposition irradiation of metal acetylacetonate layers by a focused electron beam and subsequent removal of intact precursor by dissolution in ethanol or by heating is proposed as electron beam lithography technique on the laboratory scale for the production of the metal nanostructures.

*corresponding author, e-mail address: zielasek@uni-bremen.de

**Keywords:** Electron beam-induced deposition, Chemical vapor deposition, Ultrahigh vacuum, XPS, Metal acetylacetonate, Thin film

**Abbreviations**

EBID: Electron beam-induced deposition
CVD: Chemical vapor deposition
ALD: Atomic layer deposition
PSE: Pulsed spray evaporation
UHV: Ultrahigh vacuum
XPS: X-ray photoelectron spectroscopy
LEED: Low Energy Electron Diffraction
FWHM: Full Width at Half Maximum
acac: Acetylacetone
hfac: Hexafluoroacetylacetone

## 1. Introduction

Electron beam-induced deposition (EBID) is a low vacuum deposition technique that uses a focused electron beam to produce micro- and nanometer sized 3D deposits by decomposing precursor molecules from a feed gas adsorbed on the substrate surface.[1-3] It is standard practice in such gas-phase EBID processes to use precursors designed for thermal processes, such as chemical vapor deposition (CVD).[4] Correspondingly, also the volatile metal β-diketonates such as acetylacetonates were suggested for EBID of metals.[1, 5] One of the major limitations of EBID is the typically high levels of organic contamination in the supposedly metallic nanostructures deposited from organometallic precursors which adversely affect the material's properties by often unacceptable levels.[6, 7] Therefore, fundamental research in order to understand electron-induced decomposition mechanisms in detail and optimize the EBID precursors is urgently needed.

Another severe limitation of current gas-phase EBID processes is the typically low speed of deposition. This is related to the low precursor surface densities achieved when relying on the adsorption equilibrium under low precursor flux conditions. As an alternative, condensed-phase EBID processes have recently been proposed.[8] These approaches not only enhance the efficiency of the deposition process as anticipated from the much larger surface precursor density.[9] They also widen the range of potential precursors to non-volatile materials that can, for instance, be applied in solution via a spraying technique.[8] However, detailed insight into the electron-induced reactions of non-volatile EBID precursors is so far virtually non-existent. This is even more the case regarding the contribution of the solvent to the electron-induced reduction of the precursor to elementary metal.

Surface-sensitive analytical tools in ultrahigh vacuum (UHV) are optimally suited for model studies on electron-induced reactions relevant for EBID.[10, 11, 6, 12] These UHV tools and model studies require, however, a precursor delivery technique compatible with the clean UHV environment and suitable for producing a layer of intact precursor on the substrate. So far, the most common approach has been leaking the precursor into the chamber through a UHV-compatible leak valve.[7] Also, molecule flux delivery by a nozzle-based gas injection system was tried.[13] These techniques have been demonstrated to work at acceptable deposition rates only for vapour from liquid or very volatile solid precursors such as Cu(hfac)$_2$ or Me$_2$Au(acac), and they require sample substrate cooling far below typical processing temperature to condense the volatile precursors onto the substrate. This same problem has so far restricted fundamental studies of electron-induced fragmentation to precursors of type M(hfac)$_2$ [14] while, due to their lower volatility, equivalent experiments on non-fluorinated acetylacetonates so far have not been published.

As an alternative delivery method, in particular for the injection of less volatile solid precursors, such as, e.g., Cu, Ni, or Co(acac)$_2$, the pulsed spray evaporation (PSE) of liquid feedstocks of the precursor dissolved in adequate solvents (such as ethanol in the case of acetylacetonates) has been demonstrated for applications in CVD (PSE-CVD). The spray injection method offers several advantages compared to the classical leak valve or nozzle-based gas delivery systems: the precursor does not need to be heated for thermal evaporation and there is less demand on the precursor in terms of volatility and stability.[15, 16]

Having available a PSE-CVD reactor directly connected to a UHV system with surface science tools such as x-ray photoelectron spectroscopy (XPS), we generated solvent-free layers of undecomposed Ni or Co(acac)$_2$ precursor for fundamental surface science studies of the EBID process in UHV. The precursor layers obtained by our approach were used for a qualitative comparison of thermally initiated and electron-induced precursor decomposition and metal reduction, based on XPS data. Thermal treatments in connection with EBID are particularly interesting because they have demonstrated the ability to improve the EBID purity.[17, 7] We focused on Ni and Co precursors, taking into account wide applicability and permanent industrial interest in deposits of Ni, Co and their alloys,[18-22] as well as our previous experience with PSE-CVD of Ni and Co.[23]

## 2. Material and methods

The deposition was performed in a home-built PSE-CVD reactor described in detail elsewhere.[16] In brief, the reactor is directly attached to an ultra-high vacuum system with XPS (Multiprobe system, Omicron Nanotechnology, base pressure $10^{-10}$ mbar) and allows for contamination-free transfer of a sample from the reactor to the XPS after the precursor deposition.

For all depositions discussed in the following, solutions of commercially available anhydrous 95 % $Ni(acac)_2$ or 97 % $Co(acac)_2$ (Sigma-Aldrich) in absolute ethanol (VWR Chemicals) were used. The concentration of the $\beta$-diketonate precursor molecule in the liquid feedstock was chosen on the basis of previous publications.[15, 24, 23] To obtain a feedstock with 5.0 mM concentration, 128.4 mg $Ni(acac)_2$ or 128.6 mg $Co(acac)_2$, respectively, was weighed and dissolved in 100 ml alcohol. The solution was ultrasonically shaken to achieve complete dissolution. All precursor solutions were freshly prepared directly before PSE deposition. A piece of a Si(100) wafer was cut as substrate, cleaned with isopropanol in an ultrasonic bath, and dried in air, after that annealed under UHV conditions at 700 °C and transferred *in vacuo* into PSE-CVD reactor, so that Ni or Co precursors were deposited on top of the native or thermal silicon oxide layer of the wafer.

For precursor delivery via the spray nozzle, a solenoid valve pulse frequency of 2 Hz and a spray injection phase of 15 ms were used, meaning that the solenoid valve opened two times per second for 15 ms and a total deposition time of 1 min corresponded to a net precursor solution injection time into the reactor of 1.8 s. The film thickness after 1.8 s CVD of 5.0 mM $Ni(acac)_2$ can be estimated as ~2 nm, in comparison to our previous report, where thickness was found as ~60 nm after 54 s deposition.[23] For all experiments shown in the following, the total precursor deposition time was kept constant. During precursor deposition, the pressure in the deposition area as well as the sample surface temperature were adjusted and stabilized.

The electron-induced precursor decomposition was performed in the UHV chamber via the electron gun of a conventional LEED system (Omicron). The electron beam had a spot size of 3 mm on the sample surface (FWHM of the intensity profile) and was centered to ensure that the entire sample surface area was irradiated. The kinetic energy of the electrons ($E_0$) was set to 25 eV (low-energy electron exposure regime) first, and then increased to 500 eV (high-energy electron exposure regime). Beam currents in μA range were measured using a Keithley Instruments Model 610C Solid State Electrometer. The beam current densities on the 0.25 $cm^2$ sample surface area were varied in such a way, that electron exposures of 0.125 and 2.5 mC $cm^{-2}$ at $E_0$=25 eV were achieved first, and then increased to 12.5 and 50 mC $cm^{-2}$ at $E_0$=500 eV (in case of Co precursor the final electron exposure was increased to 150 mC $cm^{-2}$ at $E_0$=500 eV).

The temperature for thermal decomposition of the Ni- and Co-containing precursor films was chosen equal to the optimal deposition temperature determined in our previous PSE-CVD experiments as 270 and 310 °C for Ni and Co precursors, respectively (see the previous publication for further details).[15, 24, 23] Higher temperatures were not employed to avoid undesirable decomposition of precursor ligands which would increase contamination of the deposited films.[16, 23]

After the decomposition process was finished, samples were transferred immediately *in vacuo* into UHV for XPS analysis. For XPS, non-monochromatized Al Kα radiation was used for photoelectron generation and a Leybold EA 10 Plus hemispherical energy analyzer with single-channeltron detector was employed. The obtained XP spectra were normalized and then fitted using Igor Pro (from Wave Metrics) and FITT (Seoul National University) software. Atomic ratios of elements at the surface were calculated from XPS intensities as

$$\frac{n_A}{n_B} = \frac{I_A/S_A}{I_B/S_B}, \tag{1}$$

where $I_x$ denotes the total XPS peak area of an individual emission from element $x$ and $S_x$ the relative sensitivity factor[25, 26] for that emission and element $x$.

## 3. Results and discussion

### 3.1. Deposition of the precursor layer via PSE

Experimental characterization of the deposits and of electron-induced or thermally initiated changes was based on XP spectra in the range of C 1s, O 1s, Si 2p, Ni 2p, and Co 2p binding energies. The C 1s emissions may provide information on the type of carbon species on the surface. For example, the alkyl group of acetylacetonate as well as traces of hydrocarbon contamination contribute to emissions from carbon-carbon and hydrocarbon bonds at binding energies of ~284.8 eV.[27-31] These are absent or negligibly small on freshly prepared substrate samples. Photoemission characteristic for C-O bonds is found as C 1s signal with a binding energy of ~286.1 eV and as O 1s signal at a binding energy of ~530.9 eV.[32-34] As fingerprint from the double C=O bonds of acetylacetone a C 1s signal at ~287.9 eV can be easily distinguished from C-O emissions[33, 35] and is expected to appear after precursor layer deposition. As previously demonstrated,[23] the O 1s emission from C=O bonds and from COx species is partly overlapped by the strong O 1s emissions from SiOx (data not shown), rendering their separation difficult. In the Ni 2p and Co 2p spectra, contributions from $M^0$ and $M^{2+}$ emissions (M=Ni or Co) can be distinguished as demonstrated in previous reports.[23, 36, 37] NiO and CoO can be identified by their O 1s emissions at around 529.9 eV[38, 39, 36, 37, 40] as well.

To obtain a solvent-free layer of undecomposed Ni or Co acetylacetonate precursor molecules via PSE of the liquid feedstock, the substrate temperature should be kept higher than the ethanol desorption temperature from silica surfaces (peak at ~90 °C)[41] and below the desorption temperature of $M(acac)_2$ (thermogravimetric studies[42] indicated that $M(acac)_2$ precursors volatilized completely between 150 and 200 °C). To test that concept, first pure solvent was spray-evaporated on the surface at three different temperatures: at 30° for reference, at 115°, i.e., somewhat above the reported desorption temperature of ethanol, and at 270 °C, i.e., at that temperature at which the CVD process is initiated.

The C1s spectra in Fig. 1 a) reveal reduction of the level of carbon contamination as the benefit of annealing the freshly prepared SiOx/Si substrate to 700 °C in vacuum. The atomic ratio of C to Si is reduced from 0.09 on the native SiOx/Si substrate to 0.01 after annealing. Subsequent injection of ethanol at 115 or 270 °C leads to similarly minor increases of the C 1s emission only by a factor of ~2 compared to the substrate annealed at 700 °C. Clear indication of ethanol adsorption was observed only at 30 °C by an increase of the C 1s emission at 286 eV binding energy by a factor of ~15-20 compared to the annealed substrate, corresponding to an atomic ratio of C to Si at the surface of 0.29. Concomitantly, the Si 2p emission decreases while we find the O 1s emission due to Si oxide increasing (data not shown) with a small binding energy shift of ~0.5 eV, probably due to the formation of Si-$OC_2H_5$ bonds. Overall, any residues from ethanol at 115 °C are as negligibly small as observed at 270 °C substrate temperature, i.e., a deposition temperature of 115 °C is high enough to safely get rid of the solvent.

When Ni(acac)$_2$ precursor solution is injected at 270 °C sample temperature, the acetylacetonate decomposes and a film containing only metallic Ni (100 % $Ni^0$) and some carbon inclusions is formed (CVD process[15, 23]). By XPS we determined the atomic ratio of Carbon to Nickel as 0.19. A shift of the C 1s emission from C=O to C-O and C-C shows that acetylacetonate precursor ligands have decomposed upon reduction of carbon. In contrast, during injection of Ni(acac)$_2$ precursor solution at 115 °C substrate temperature adsorption of intact Ni(acac)$_2$ molecules predominates. The ratio between C 1s peak intensities at ~286 eV (C-O) and ~288 eV (C=O) is 1.8 to 1, i.e., close to 2:1 as expected for pure acetylacetonate precursor adsorption.[35, 43] The Ni 2p signal indicates that there is only $Ni^{2+}$ present on the sample surface, similar to deposition at 30 °C. Overall, we conclude that a solvent-free layer of intact Ni(acac)$_2$ precursor molecules forms during deposition at 115 °C. At this temperature, the total intensity of the C 1s emission is lowest compared to injection at 270 or 30 °C. After injection of Ni(acac)$_2$ precursor solution at 30 °C, we found evidence for joint adsorption of ethanol and Ni(acac)$_2$ in the C 1s spectrum. Both, C-O and C=O bonds are prevalent on the surface, the C-O signal, however, dominates by far (ratio between C 1s peak intensities at ~286 eV and ~288 eV is 3.4 to 1), due to contributions from acetylacetonate and ethanol (comparison with the ratio of 1.8 to 1 observed at 115 °C indicates that almost half of the C-O signal can be attributed to ethanol). Comparison of the absolute C 1s intensities observed after injection of pure solvent and the precursor solution (Fig. 1 a) and b)) shows that the total amount of adsorbed ethanol is reduced with Ni(acac)$_2$ precursor as co-adsorbate.

Similar to nickel, injection of Co(acac)$_2$ precursor solution at 30 °C leads to joint adsorption of ethanol and Co(acac)$_2$, while at 310 °C substrate temperature the Co precursor decomposes on the surface and forms a deposit of Co oxide and metallic Co (only 25 % Co$^0$), with some C-O-C and C-C inclusions (CVD process[23]). The atomic ratio of carbon to cobalt was found as 0.07 in the CVD deposits. Notably, in contrast to CVD from Ni(acac)$_2$, a shift of the C 1s emission to C-C was not observed, indicating that the acetylacetonate ligands are not fragmented during precursor decomposition. Also the smaller amount of carbon impurities as compared to the Ni PSE-CVD indicates that, during Co-PSE CVD, the Co precursor decomposes more easily into the metal center and unfragmented, volatile acetylacetone, which is in accordance with the observation that Co(acac)$_2$ is less stable than Ni(acac)$_2$.[44-46] After injection of Co(acac)$_2$ dissolved in ethanol at 115 °C substrate temperature the XPS data indicate that, similar to Ni(acac)$_2$ injection at that temperature, adsorption of intact Co(acac)$_2$ precursor molecules predominated. The ratio between C 1s peak intensities at ~286 eV and ~288 eV (cf. Fig. 1c) is 2.1 to 1. Thus we propose that selecting a substrate temperature of 115 °C during PSE of metal(M) acetylacetonate precursors is well suited for the preparation of solvent-free layers of undecomposed M(acac)$_x$ precursor.

### 3.2. Electron beam-induced and thermally induced decomposition of M(acac)$_2$ precursors

Precursor layers produced by PSE of the liquid feedstock onto an annealed SiOx/Si substrate at 115 °C were transferred into UHV and then either irradiated by electrons at room temperature (22 °C, heating power by the electron beam can be neglected) or heated up to 270 or 310 °C (using a filament from behind). XPS data obtained after electron irradiation of Ni(acac)$_2$ layers are shown in Fig. 2. They reveal that irradiation in the low-energy electron exposure regime (at $E_0$=25 eV) for 15 min/0.125 mC cm$^{-2}$ (red curve) and 375 min/2.5 mC cm$^{-2}$ (green) did not lead to any significant changes (1 mC cm$^{-2}$ corresponds to ~$6.25 \cdot 10^{15}$ e cm$^{-2}$). Only after switching to the high-energy electron exposure regime (at $E_0$=500 eV) electron induced reduction of the metal from Ni$^{2+}$ to Ni$^0$ can be observed after 15 min/12.5 mC cm$^{-2}$ (blue). After 90 min irradiation at 50 mC cm$^{-2}$ (purple) the final film contained 59 % of Ni$^0$ with some carbon inclusions. The final atomic ratio of Carbon to Nickel was calculated as 0.13 which is ~30 % lower than after ethanol-assisted CVD. A shift of the C 1s emission from C=O to

C-O and C-C indicates reduction of carbonyl groups, as also observed during the PSE-CVD process. After a Ni precursor layer was heated up to 270 °C for 1 min, XPS (Fig. 2 b) revealed reduction of 86 % of the metal ions to $Ni^0$ and only residual amounts of carbon inclusions. The level of carbon contamination in the film (atomic ratio of C/Ni = 0.13) was similar to electron-induced decomposition and a shift in C 1s emission from C=O to C-O and C-C indicating acetylacetonate fragmentation was observed as well. While the thermal decomposition of the $Ni(acac)_2$ layer did not reach 100% reduction of the deposited Ni as the ethanol-assisted CVD process did, it was more efficient in this respect than electron-induced decomposition.

Similar to the $Ni(acac)_2$, also $Co(acac)_2$ layers did not show significant changes in XPS after electron irradiation at room temperature in the low-energy electron exposure regime ($E_0$=25 eV) for 15 min/0.125 mC $cm^{-2}$ (red curve) and 375 min/2.5 mC $cm^{-2}$ (green)). Unlike for $Ni(acac)_2$, however, even the high-energy electron exposure regime ($E_0$=500 eV, 15 min at 12.5 mC $cm^{-2}$ (blue), 90 min at 50 mC $cm^{-2}$ (lila) and 210 min at 150 mC $cm^{-2}$ (orange)) did only reduce minor amounts of $Co^{2+}$ precursor ions to $Co^0$. Only 21 % of Co was metallic after irradiation, compared to 25% obtained with CVD, as described above. A shift of the C 1s emission from C=O to C-O and C-C indicates reduction and fragmentation of the precursor ligands over the time of electron irradiation. The final atomic ratio of carbon to cobalt was found as 0.08. Also heating a $Co(acac)_2$ film to 310 °C lead to precursor decomposition and fragmentation, a shift in C 1s emission to C-O and C-C was observed as well. Compared to electron irradiation and, in particular, the ethanol assisted CVD at 310 °C, we found an unexpectedly high fraction of metallic $Co^0$ (41 % of the entire Co) and preferably CoOx with some carbon inclusions (atomic ratio of carbon to cobalt is about 0.11) after heating. In strong contrast to the results obtained for Ni, ethanol-asstisted CVD of $Co(acac)_2$ leads to a lower amount of metallic Co in the deposit than plain thermal treatment of a $Co(acac)_2$ layer at the same temperature.

In the present work, the level of carbon impurities (summarized in Tab. 1) compared to reports for continuous EBID processes is relatively low (for some MO precursors it may reach even 80-90 %at).[5, 1, 6] The relatively low level of carbon impurities may be explained as follows: In our experiments, post-deposition electron beam-induced decomposition of the precursor is performed in good vacuum conditions while usually in EBID electron irradiation is performed during exposure of the substrate to the precursor gas. Therefore, any accumulation of carbonaceous species from electron beam-induced decomposition of precursor in the gas phase and adsorption of the produced fragments is avoided, in contrast to "real" EBID. The temperature range of EBID is often so low that dissociation fragments remain adsorbed and immobile on the substrate[1] while classical CVD operates at temperatures above the precursor decomposition temperature in order to increase the probability of rapid desorption of ligands or other undesired precursor fragments.

The temperature difference results in different ways in which adsorbed metal-ligand species are processed by either electrons or thermal reactions. Under EBID deposition conditions, experimental evidence suggests that ligand *decomposition* rather than *desorption* dominates. In the CVD reaction pathway thermal reactions are often characterized by ligand *desorption* as opposed to ligand *decomposition*.[4] A comparison of the metal contents in the deposited films achieved by PSE-CVD of Ni or Co(acac)$_2$ and by thermal or electron-induced *post-deposition* decomposition of solvent-free Ni or Co(acac)$_2$ layers is summarized in Tab. 2. As pointed out before, ethanol-asstisted CVD of Co(acac)$_2$ leads to a lower amount of metallic Co in the deposit than plain thermal treatment of a Co(acac)$_2$ layer at the same temperature.

Possibly, the high sensitivity of cobalt to oxidizing agents plays a major role here. Ethanol is added for the CVD process because hydrogen is formed upon the decomposition of ethanol and acts as a reducing agent. However, also water is a product of EtOH decomposition (and may be also be present as contamination in the precursor solution) and acts as oxidizing agent.[23, 42, 47] The observation that thermal decomposition of the ethanol-free precursor layer produces higher metal contents than obtained during CVD indicates that oxidation reactions by the presence of water dominate over the reduction of $Co^{2+}$ by protons delivered by catalytic ethanol decomposition at Co.[23]

On SiOx, reaction between surface OH-groups could lead to the formation of siloxane bonds and molecular water.[48] However, according to a study by L.T. Zhuravlev[48] there is neither physisorbed nor chemisorbed $H_2O$ on top of SiOx in vacuum at temperatures above 190 °C and only a low density of free single or geminal OH-groups is stable at and above 400 °C. Therefore, we assume that in our experiments at the temperature regime of precursor layer deposition (115 °C) and in particular when the substrate is heated to 310 °C in UHV for the thermal decomposition of the precursor film, the amount of water on the substrate surface is reduced to such low levels that oxidation of precursor metal centers is negligible.

## 4. Conclusions

The injection of liquid precursors using pulsed spray evaporation into a flow of nitrogen as carrier gas was successfully applied for preparation of solvent-free layers of undecomposed $M(acac)_2$ precursor on a SiOx substrate heated to 115° C. This method opens up $M(acac)_2$ layers to qualitative and quantitative analysis by a variety of UHV-based surface science tools. A qualitative comparison of thermally initiated and electron beam-induced precursor decomposition and metal center reduction was carried out. For both, Ni and Co, thermally initiated decomposition leads to higher concentration of $M^0$ in deposited films compared to electron beam-induced decomposition. In the case of $Co(acac)_2$ precursor, thermally initiated reduction was even more efficient than that observed in PSE-CVD from $Co(acac)_2$.

In our experiments, EBID showed acceptable results only in the high-energy electron exposure regime, i.e., for electron energies of 500 eV, where, in part, reduction of Ni ions from $Ni^{2+}$ to $Ni^0$ could be observed. Unlike nickel, however, $Co^{2+}$ could not be reduced to $Co^0$ by electron irradiation in significant amounts, even after switching to high-energy electron exposure regime and extensive irradiation. The level of carbon impurities compared to reports for continuous EBID processes was notably low in our experiments of post-deposition electron-induced precursor decomposition. Therefore, we suggest that at least in the laboratory the metal acetylacetonate deposition followed by post-deposition irradiation with a focused electron beam and subsequent removal of intact precursor by dissolution in ethanol or by heating may constitute an interesting electron beam lithography technique for the production of the metal nanostructures. Furthermore, our solution-based approach offers the perspective to also investigate the fundamentals of EBID processes in the presence of remaining solvent.

This kind of research is urgently needed for the further development of condensed-phase EBID processes.

## Acknowledgements

Funding by the Deutsche Forschungsgemeinschaft under contract Ba 1710/20-1 and inspiration from COST Action CM1301 (CELINA) is gratefully acknowledged.

## References

1. Utke I, Hoffmann P, Melngailis J. Gas-assisted focused electron beam and ion beam processing and fabrication. J Vac Sci Technol B. 2008;26(4):1197-276. doi:10.1116/1.2955728.
2. van Dorp WF, Hansen TW, Wagner JB, De Hosson JTM. The role of electron-stimulated desorption in focused electron beam induced deposition. Beilstein Journal of Nanotechnology. 2013;4:474-80. doi:10.3762/bjnano.4.56.
3. Silvis-Cividjian N, Hagen CW, Kruit P, v.d. Stam MAJ, Groen HB. Direct fabrication of nanowires in an electron microscope. Applied Physics Letters. 2003;82(20):3514-6. doi:10.1063/1.1575506.
4. Spencer J, Rosenberg S, Barclay M, Wu Y-C, McElwee-White L, Howard Fairbrother D. Understanding the electron-stimulated surface reactions of organometallic complexes to enable design of precursors for electron beam-induced deposition. Appl Phys A. 2014;117(4):1631-44. doi:10.1007/s00339-014-8570-5.
5. Warneke J, Van Dorp WF, Rudolf P, Stano M, Papp P, Matejcik S et al. Acetone and the precursor ligand acetylacetone: distinctly different electron beam induced decomposition? Physical Chemistry Chemical Physics. 2015;17(2):1204-16. doi:10.1039/C4CP04239E.
6. Wnuk JD, Rosenberg SG, Gorham JM, van Dorp WF, Hagen CW, Fairbrother DH. Electron beam deposition for nanofabrication: Insights from surface science. Surface Science. 2011;605(3–4):257-66. doi:10.1016/j.susc.2010.10.035.
7. Rosenberg SG, Landheer K, Hagen CW, Fairbrother DH. Substrate temperature and electron fluence effects on metallic films created by electron beam induced deposition. Journal of Vacuum Science &amp; Technology B. 2012;30(5):051805. doi:10.1116/1.4751281.
8. Fisher JS, Kottke PA, Kim S, Fedorov AG. Rapid Electron Beam Writing of Topologically Complex 3D Nanostructures Using Liquid Phase Precursor. Nano Letters. 2015;15:8385.
9. Bresin M, Toth M, Dunn KA. Direct-write 3D nanolithography at cryogenic temperatures. Nanotechnology. 2013;24:035301.
10. Lafosse A, Bertin M, Azria R. Electron driven processes in ices: Surface functionalization and synthesis reactions. Progress in Surface Science. 2009;84(5–6):177-98. doi:10.1016/j.progsurf.2009.03.001.
11. Arumainayagam CR, Lee H-L, Nelson RB, Haines DR, Gunawardane RP. Low-energy electron-induced reactions in condensed matter. Surface Science Reports. 2010;65(1):1-44. doi:10.1016/j.surfrep.2009.09.001.
12. Böhler E, Warneke J, Swiderek P. Control of chemical reactions and synthesis by low-energy electrons. Chemical Society Reviews. 2013;42(24):9219-31. doi:10.1039/C3CS60180C.
13. Friedli V, Utke I. Optimized molecule supply from nozzle-based gas injection systems for focused electron- and ion-beam induced deposition and etching: simulation and experiment. Journal of Physics D: Applied Physics. 2009;42(12):125305.
14. Engmann S, Ómarsson B, Lacko M, Stano M, Matejčík Š, Ingólfsson O. Dissociative electron attachment to hexafluoroacetylacetone and its bidentate metal complexes M(hfac)2; M = Cu, P. The Journal of Chemical Physics. 2013;138:234309. doi:10.1063/1.4810877.
15. Premkumar PA, Bahlawane N, Kohse-Höinghaus K. CVD of metals using alcohols and metal acetylacetonates, Part I: Optimization of process parameters and electrical characterization of synthesized films. Chemical Vapor Deposition. 2007;13(5):219-26. doi:10.1002/cvde.200606572.
16. Weiss T, Nowak M, Mundloch U, Zielasek V, Kohse-Höinghaus K, Bäumer M. Design of a compact ultrahigh vacuum-compatible setup for the analysis of chemical vapor deposition processes. Review of Scientific Instruments. 2014;85(10):104104. doi:10.1063/1.4897620.
17. Roberts NA, Fowlkes JD, Magel GA, Rack PD. Enhanced material purity and resolution via synchronized laser assisted electron beam induced deposition of platinum. Nanoscale. 2013;5(1):408-15. doi:10.1039/C2NR33014H.

18. Kodas TT, Hampden-Smith MJ. The chemistry of Metal CVD. Weinheim; New York: VCH; 1994.
19. Deng W-Q, Xu X, Goddard WA. A Two-Stage Mechanism of Bimetallic Catalyzed Growth of Single-Walled Carbon Nanotubes. Nano Letters. 2004;4(12):2331-5. doi:10.1021/nl048663s.
20. Bakovets VV, Mitkin VN, Gelfond NV. Mechanism of Ni film CVD with a Ni(Ktfaa)(2) precursor on a silicon substrate. Chemical Vapor Deposition. 2005;11(8-9):368-74. doi:10.1002/cvde.200506376.
21. Elbuken C, Yavuz M, Khamesee MB. Development of crystalline magnetic thin films for microlevitation. Journal of Applied Physics. 2008;104(4):044905. doi:10.1063/1.2969832.
22. Zhang Z, Nenoff TM, Huang JY, Berry DT, Provencio PP. Room Temperature Synthesis of Thermally Immiscible Ag−Ni Nanoalloys. The Journal of Physical Chemistry C. 2009;113(4):1155-9. doi:10.1021/jp8098413.
23. Weiss T, Zielasek V, Bäumer M. Influence of Water on Chemical Vapor Deposition of Ni and Co thin films from ethanol solutions of acetylacetonate precursors. Sci Rep. 2015;submitted.
24. Bahlawane N, Premkumar PA, Tian Z, Hong X, Qi F, Kohse-Höinghaus K. Nickel and Nickel-Based Nanoalloy Thin Films from Alcohol-Assisted Chemical Vapor Deposition. Chemistry of Materials. 2009;22(1):92-100. doi:10.1021/cm902454w.
25. Wagner CD, Davis LE, Zeller MV, Taylor JA, Raymond RH, Gale LH. Empirical atomic sensitivity factors for quantitative analysis by electron spectroscopy for chemical analysis. Surface and Interface Analysis. 1981;3(5):211-25. doi:10.1002/sia.740030506.
26. Briggs D, Seah MP, Sherwood PMA. Practical Surface Analysis. Volume 1. Auger and X-ray Photoelectron Spectroscopy. Chichester, UK: John Wiley & Sons; 1990.
27. Brault P, Ranson P, Estrade-Szwarckopf H, Rousseau B. Chemical physics of fluorine plasma-etched silicon surfaces: Study of surface contaminations. Journal of Applied Physics. 1990;68(4):1702-9. doi:10.1063/1.346625.
28. Bou M, Martin JM, Le Mogne T, Vovelle L. Chemistry of the interface between aluminium and polyethyleneterephthalate by XPS. Applied Surface Science. 1991;47(2):149-61. doi:10.1016/0169-4332(91)90029-J.
29. Lascovich JC, Giorgi R, Scaglione S. Evaluation of the sp2/sp3 ratio in amorphous carbon structure by XPS and XAES. Applied Surface Science. 1991;47(1):17-21. doi:10.1016/0169-4332(91)90098-5.
30. Contarini S, Howlett SP, Rizzo C, De Angelis BA. XPS study on the dispersion of carbon additives in silicon carbide powders. Applied Surface Science. 1991;51(3–4):177-83. doi:10.1016/0169-4332(91)90400-E.
31. Grosvenor AP, Biesinger MC, Smart RSC, McIntyre NS. New interpretations of XPS spectra of nickel metal and oxides. Surface Science. 2006;600(9):1771-9. doi:10.1016/j.susc.2006.01.041.
32. Droulas JL, Tran Minh Duc, Jugnet Y. Etude des propiétés interfaciales des dépôts par évaporation et pulvérisation d' aluminium sur polyéthylène téréphtalate. Le Vide, les Couches Minces. 1991;258:39-41.
33. Briggs D. Handbook of X-ray Photoelectron Spectroscopy C. D. Wanger, W. M. Riggs, L. E. Davis, J. F. Moulder and G. E.Muilenberg Perkin-Elmer Corp., Physical Electronics Division, Eden Prairie, Minnesota, USA, 1979. 190 pp. $195. Surface and Interface Analysis, vol 4. Heyden & Son Ltd.; 1981.
34. Jouan PY, Peignon MC, Cardinaud C, Lempérière G. Characterisation of TiN coatings and of the TiN/Si interface by X-ray photoelectron spectroscopy and Auger electron spectroscopy. Applied Surface Science. 1993;68(4):595-603. doi:10.1016/0169-4332(93)90241-3.
35. Chao J, Wang H-T, Xia B, Liu H-B, Xiao Z-D, Xiao S-J. Metal Acetylacetonate Domains Grown on H-Terminated Porous Silicon at Room Temperature and Their Specific I−V Behavior. The Journal of Physical Chemistry B. 2006;110(48):24565-70. doi:10.1021/jp0628481.
36. McIntyre NS, Cook MG. X-ray photoelectron studies on some oxides and hydroxides of cobalt, nickel, and copper. Analytical Chemistry. 1975;47(13):2208-13. doi:10.1021/ac60363a034.

37. Yang J, Liu H, Martens WN, Frost RL. Synthesis and Characterization of Cobalt Hydroxide, Cobalt Oxyhydroxide, and Cobalt Oxide Nanodiscs. The Journal of Physical Chemistry C. 2010;114(1):111-9. doi:10.1021/jp908548f.
38. Galtayries A, Grimblot J. Formation and electronic properties of oxide and sulphide films of Co, Ni and Mo studied by XPS. Journal of Electron Spectroscopy and Related Phenomena. 1999;98–99(0):267-75. doi:10.1016/S0368-2048(98)00292-8.
39. Barr TL. An ESCA study of the termination of the passivation of elemental metals. The Journal of Physical Chemistry. 1978;82(16):1801-10. doi:10.1021/j100505a006.
40. Dupin J-C, Gonbeau D, Vinatier P, Levasseur A. Systematic XPS studies of metal oxides, hydroxides and peroxides. Physical Chemistry Chemical Physics. 2000;2(6):1319-24. doi:10.1039/A908800H.
41. Noller H, Ritter G. Temperature-programmed desorption of methanol, ethanol, propan-1-ol and propan-2-ol on silica-magnesia mixed oxides. Journal of the Chemical Society, Faraday Transactions 1: Physical Chemistry in Condensed Phases. 1984;80(2):275-83. doi:10.1039/F19848000275.
42. Utriainen M, Kröger-Laukkanen M, Johansson L-S, Niinistö L. Studies of metallic thin film growth in an atomic layer epitaxy reactor using M(acac)2 (M=Ni, Cu, Pt) precursors. Applied Surface Science. 2000;157(3):151-8. doi:10.1016/s0169-4332(99)00562-0.
43. Kodolov VI, Tchirkova EI, Bystrova SG, Shabanova IN, Popova OV, Babushkina SN. X-ray photoelectron spectroscopic investigation of metallorganic complexes. Journal of Electron Spectroscopy and Related Phenomena. 1998;88–91(0):977-82. doi:10.1016/S0368-2048(97)00198-9.
44. Gentile PS, Dadgar A. Stability constants of some metal chelates in mixed solvent systems. Journal of Chemical & Engineering Data. 1968;13(2):236-8. doi:10.1021/je60037a030.
45. Barabanov VA, Davydova SL, Plate NA. Zhur Fiz Khim. 1968;42(4):990-2.
46. Pilipenko AT, Savransky LI. Selectivity and sensitivity of metal determination by co-ordination compounds. Talanta. 1987;34(1):77-86. doi:10.1016/0039-9140(87)80011-5.
47. Utriainen M, Kröger-Laukkanen M, Niinistö L. Studies of NiO thin film formation by atomic layer epitaxy. Materials Science and Engineering: B. 1998;54(1–2):98-103. doi:10.1016/S0921-5107(98)00135-4.
48. Zhuravlev LT. The surface chemistry of amorphous silica. Zhuravlev model. Colloids and Surfaces A: Physicochemical and Engineering Aspects. 2000;173(1–3):1-38. doi:10.1016/S0927-7757(00)00556-2.

## Figures

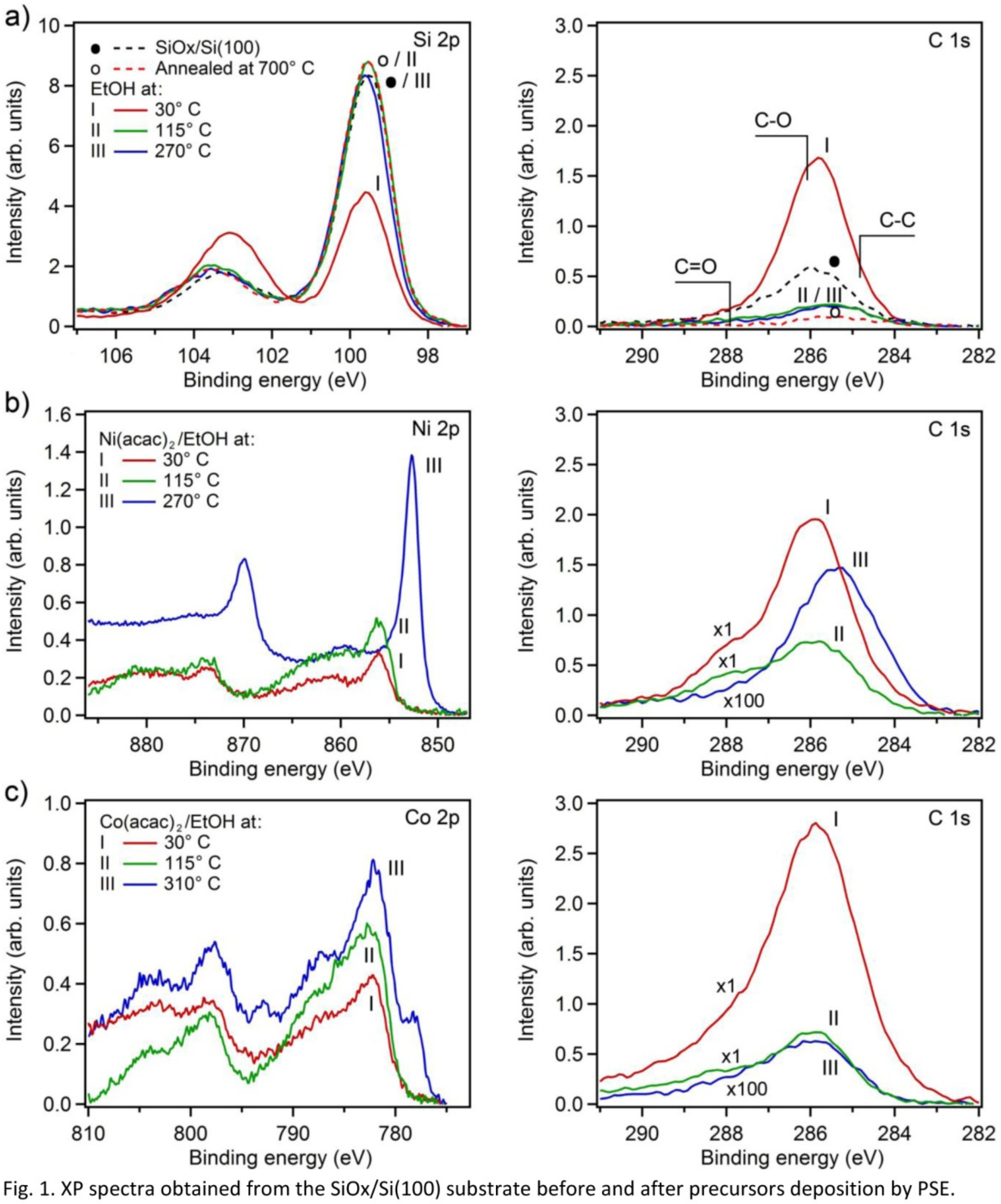

Fig. 1. XP spectra obtained from the SiOx/Si(100) substrate before and after precursors deposition by PSE.

a) (top row): XP spectra in the binding energy range of Si 2p (left) and C 1s (right) emissions obtained from the native SiOx/Si(100) substrate (●), annealed at ~700 °C (○), and after ethanol deposition on the substrate at 30 °C (I), 115 °C (II), and 270 °C (III). b) (center row): XP spectra in the binding energy range of Ni 2p (left) and C 1s (right) emissions obtained after deposition of Ni(acac)$_2$/ethanol by PSE on annealed SiOx/Si(100) substrate from 5.0 mM precursor at a substrate temperature of 30 °C (I), 115 °C (II), and 270 °C (III). c) (bottom row): XP spectra in the binding energy range of Co 2p (left) and C 1s (right) emissions obtained after deposition of Co(acac)$_2$/ethanol by PSE on annealed SiOx/Si(100) substrate from 5.0 mM precursor at a substrate temperatures of 30 °C (I), 115 °C (II), and 310 °C (III). Please note the different scaling factors of the C 1s spectra (spectra III scaled by factor 100 to allow for better comparison with I and II).

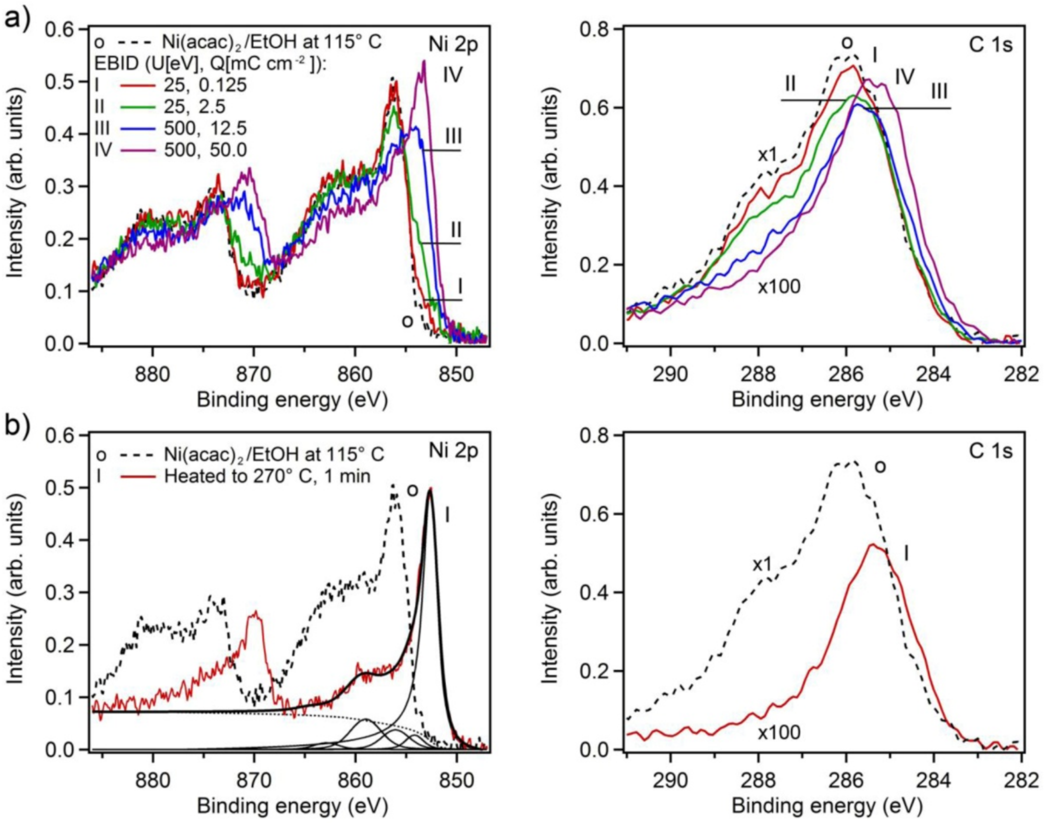

Fig. 2. XP spectra obtained from deposited Ni(acac)$_2$ after thermal and electron-induced precursor decomposition. a) (top row): XP spectra in the binding energy range of Ni 2p (left) and C 1s (right) emissions obtained after deposition of Ni(acac)$_2$ by PSE on annealed SiOx/Si(100) substrate from 5.0 mM precursor at a substrate temperature of 115 °C (○), and after Ni/NiOx formation by electron-induced decomposition of Ni(acac)$_2$ precursor with electron exposure of 0.125 (I) and 2.5 mC cm$^{-2}$ (II) at $E_0$=25 eV provided first, and then increased to 12.5 (III) and 50 mC cm$^{-2}$ (IV) at $E_0$=500 eV. b) (bottom row): XP spectra in the binding energy range of Ni 2p (left) and C 1s (right) emissions obtained after deposition of Ni(acac)$_2$ by PSE on annealed SiOx/Si(100) substrate from 5.0 mM precursor at a substrate temperatures of 115 °C (○), and after Ni/NiOx formation by thermal decomposition of Ni(acac)$_2$ precursor heated to 270 °C (I) for 1 min. Please note the different scaling factors of the C 1s spectra (spectra o scaled by factor 1, all other spectra scaled by factor 100 to allow for better comparison).

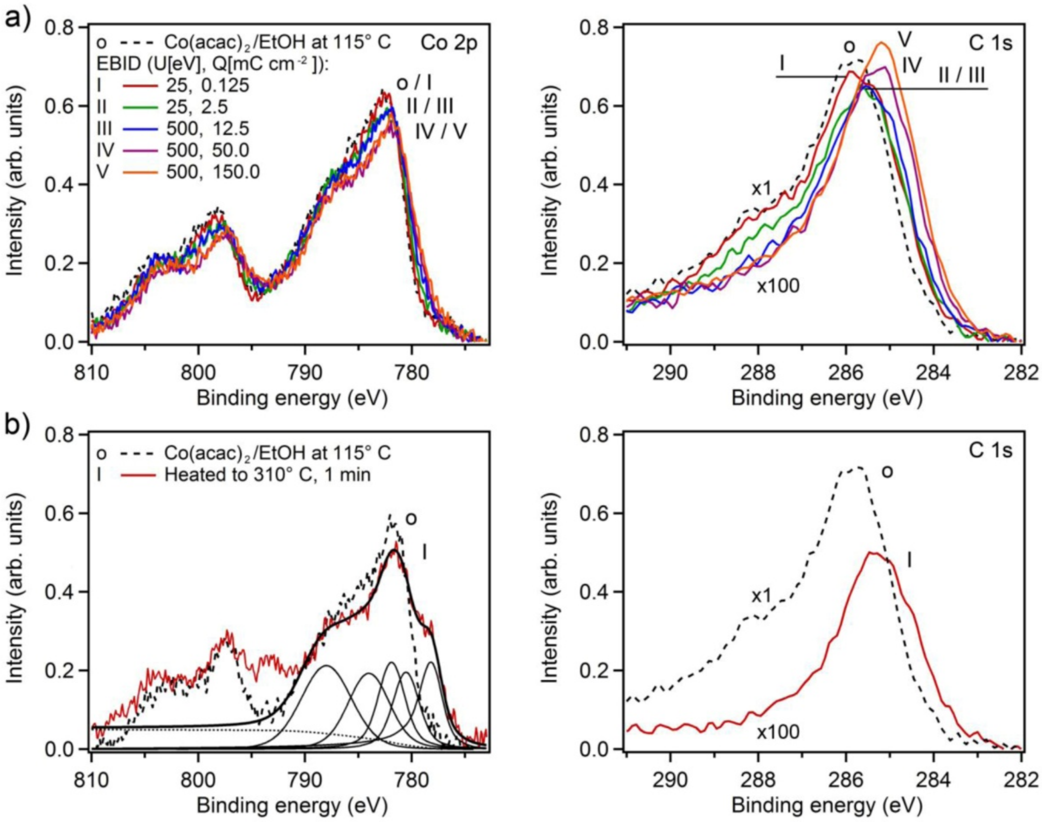

Fig. 3. XP spectra obtained from deposited Co(acac)$_2$ after thermal and electron-induced precursor decomposition. a) (top row): XP spectra in the binding energy range of Co 2p (left) and C 1s (right) emissions obtained after deposition of Co(acac)$_2$ by PSE on annealed SiOx/Si(100) substrate from 5.0 mM precursor at a substrate temperatures of 115 °C (○), and after Co/CoOx formation by electron-induced decomposition of Co(acac)$_2$ precursor with electron exposure of 0.125 (I) and 2.5 mC cm$^{-2}$ (II) at $E_0$=25 eV provided first, and then increased to 12.5 (III), 50 mC cm$^{-2}$ (IV), and 150 mC cm$^{-2}$ (V) at $E_0$=500 eV. b) (bottom row): XP spectra in the binding energy range of Co 2p (left) and C 1s (right) emissions obtained after deposition of Co(acac)$_2$ by PSE on annealed SiOx/Si(100) substrate from 5.0 mM precursor at a substrate temperatures of 115 °C (○), and after Co/CoOx formation by thermal decomposition of Co(acac)$_2$ precursor heated to 310 °C (I) for 1 min. Please note the different scaling factors of the C 1s spectra (spectra o scaled by factor 1, all other spectra scaled by factor 100 to allow for better comparison).

## Tables

Tab. 1. Atomic ratio C to M in the films.
They were obtained by various ways from Ni and Co acetylacetonate precursors.

| | Ni precursor | Co precursor |
|---|---|---|
| **Ethanol assisted CVD** | 0.19 | 0.07 |
| **Thermal decomposition** | 0.13 | 0.11 |
| **Electron beam-induced decomposition** | 0.13 | 0.08 |

Tab. 2. Percentage amount of metallic Ni or Co (of all deposited Ni or Co) in films.
They were obtained by PSE-CVD or by thermal treatment or electron irradiation of Ni and Co acetylacetonate precursor layers.

| | Ni precursor | Co precursor |
|---|---|---|
| **Ethanol assisted CVD** | 100 | 25 |
| **Thermal decomposition** | 86 | 41 |
| **Electron beam-induced decomposition** | 59 | 21 |

# Lebenslauf

***Theodor Weiss***
*(geb. Strigunov)*

13.12.1983, Charkow

Im Bleeke 47
30826 Garbsen
post@theoweiss.de

## MEILENSTEINE DES LEBENS

| | |
|---|---|
| Apr 2011 – heute | **Promotion in Physikalischer Chemie**<br>Universität Bremen, Institut für Angewandte und Physikalische Chemie |
| Aug 2008 – Okt 2010 | **Wissenschaftlicher Mitarbeiter / EU-Gastwissenschaftler**<br>Universität Ulm, Institut für Elektrochemie |
| Nov 2005 – Jul 2008 | **Forschungs- und Entwicklungsingenieur**<br>Institut der Bioorganischenchemie und Petrolchemie, Kiew, UA |
| Sep 2005 – Mär 2007 | **Diplomabschluss** (Note 1,6)<br>Ingenieur für Chemieingenieurwesen und Verfahrenstechnik<br>Studienrichtung - Elektrochemie<br>Nationale Technische Universität der Ukraine „KPI“, Kiew, UA |
| Sep 2001 – Jul 2005 | **Bachelorabschluss** (Note 2,1)<br>Chemische Technologie und Chemieingenieurwesen<br>Nationale Technische Universität der Ukraine „KPI“, Kiew, UA |

## AUSZEICHNUNGEN & STIPENDIEN

| | |
|---|---|
| 2009 | DAAD Stipendium<br>Deutscher Akademischer Austausch Dienst, Bonn, Deutschland |
| 2008 | ELCAT Surface Electrochemical Reactivity in Electrocatalysis Initial Training Network finanziert durch das Marie Curie-Programm der EU |

***Bremen, November 2015***

Th. Weiss